

Design of Distributed Wireless Power Transmission System

by:

Telnaz Zarifi Dizaji

A thesis submitted in partial fulfillment of the requirements for the degree of

Master of Science

in

Electromagnetics and Microwaves

Department of Electrical and Computer Engineering

University of Alberta

© Telnaz Zarifi Dizaji, 2016

Abstract

Wireless power transmission technology offers a wide range of industrial and biomedical applications and could lead to clean sources of electricity for a variety of users. In this technique, conventional power sources are replaced with power transmission devices, such as coils, and electric power storage devices, such as capacitors. Electronic devices, equipped with wireless power transmission systems, can operate for longer periods without the malfunctions caused by their low battery capacity.

One of the main objectives in wireless power transfer is to obtain high efficiency in the system. Several parameters can affect the efficiency, such as the coil's structure, distance between coils, load on the receiver side, number of simultaneous loads connected to one transmitter, and electric properties of WPT environment. Some of these parameters can be determined initially and properly be treated; other parameters such as load, distance between coils and environment change are more chaotic and require real-time and *in situ* treatment.

The main purpose of this dissertation is to address the power efficiency enhancement techniques, such as real-time matching configuration and methods to increase the efficiency of the transmitted power. This thesis presents a novel-matching approach and dynamic impedance matching using capacitor matrix for real-time impedance matching. Additionally, a unique approach is presented for transmitting the RF power through an arbitrary medium and using open ended coils to locally perform the power distribution to the load nodes. A comprehensive study on the WPT subsystems has presented in FEM and circuit model simulations.

Dedication

Family is the best thing you could ever wish for. They are there for you during the ups and downs and love you no matter what.

Dedicated to My Beloved Family

Acknowledgements

I would like to express my deepest gratitude to my advisors, Professor Pedram Mousavi, Professor Kambiz Moez for their excellent guidance, support, patience and encouraging my research to grow as a research scientist. Your advice on both research as well as on my career have been priceless.

I also want to acknowledge my evaluation committee members, Professor Masum Hossain and Professor S. Ali Khajehoddin. In addition, I would like to thank Ms. Pinder Bains for organizing the defense session.

My dearest brother I take this opportunity to thank you for giving your little sister big bundles of advice which helped me take the big steps towards my goals in life. You are wonderful brother and one of most inspiring person in my life. And my most heartfelt thanks to my dear family and my beloved Behzad for their endless love and courage which always make my dreams come true.

Lastly, thanks to my wonderful friends here in Edmonton and also back home who have helped me stay sane through these difficult years away from home. I deeply appreciate their friendships and warm sympathies.

Table of Contents

List of Tables	viii
List of Figures	ix
List of Symbols	xv
List of Abbreviations	xvi
Chapter 1- Introduction	1
1.1 Review	1
1.2 Motivation	2
1.3 Aim and Objective.....	7
1.4 Thesis structure.....	8
Chapter 2- Transmitter and Receiver Design	10
2.1 Motivation	10
2.2 Introduction to RIC Method and Coil Design for WPT Systems.....	11
2.3 Resonant Inductive Coupling Method.....	12
2.3.1 Definition	12
2.3.2 Inductive link	12
2.3.3 Circuit Model Analysis	13
2.4 Conventional Coil Design	15
2.4.2 Circular Spiral Coil Design.....	17
2.5 Design Procedure and Electromagnetic Simulation of the Conventional Coils.....	19
2.6 Coupling effect of conventional transmitter and receiver coils on power transmission efficiency	21

2.7 Measurement Results for the fabricated Coil Structures.....	24
2.8 Open-ended Coil structure for WPT systems.....	27
2.9 Studying the ground plane size on S_{11} parameter.....	33
2.10 Measurement results for Ground Eliminated Open-ended Coil.....	34
2.11 Tunability and Matching of a Ground Eliminated Open-ended Resonator Coil structure	39
2.12 Conclusion.....	41
Chapter 3- AC to DC Power Converters in WPT	43
3.1 Introduction.....	43
3.2 Voltage Doubler Operation.....	44
3.3 Rectifier Design.....	46
3.3.1 Dickson Doubler Analysis.....	50
3.3.2 Multistage Dickson Rectifier.....	50
3.3.3 Multi-stage Rectifiers.....	53
3.4 Implementation and Measurement Results.....	54
3.5 Conclusion.....	56
Chapter 4- Dynamic Real Time Matching and Tuning System	58
4.1 Motivation.....	58
4.2 Introduction.....	59
4.3 Study of Matching Effect of Power efficiency.....	60
4.4 Motivation for Implementing an Intelligent Algorithm.....	69
4.4.2 Genetic Algorithm Operation.....	71
4.5 GA Algorithm Analysis and Implementation for Dynamic Matching Network.....	72
4.5.1 Processing Unit and Intelligent Algorithm Implementation.....	79
4.5.2 Analog Switches.....	80

4.6 Circuit implementation and Fabrication of the dynamic matching technique for WPT system.....	81
4.7 Conclusion.....	83
Chapter 5- Conclusion and Future Directions	85
5.1 Conclusions	85
5.2 Directions for future Research.....	86
Bibliography	88

List of Tables

Table 1.1 : Commercially available WPT systems	5
Table 1.2 : Maximum permitted transmitted signal in US and Europe.....	6
Table 2.1 : Inductor's values for operation frequency at 13.56 MHz for long-range and short-range distances	16
Table 2.2 : Values for K_1 and K_2	18
Table 2.3 : Implemented coils geometries.....	18
Table 3.1 : Summarizes prior reported designs on the rectifier-multiplier structure	44
Table 4.1 : Comparison of different microcontrollers with potential application for WPT systems	79

List of Figures

Figure 1.1 : Antenna Field Regions	4
Figure 1.2 : System level architecture of Wireless Power Transmission (WPT)	7
Figure 2.1 : AC model of typical series resonant circuit	13
Figure 2.2 : Spiral shape inductance for WPT systems.	17
Figure 2.3 : Electromagnetic field distribution around the transmitter coil.....	20
Figure 2.4 : (a) Magnetic field distribution on a distance of (50 mm) from the coil surface and (b) perpendicular to coil surface.....	20
Figure 2.5 : (a) Configuration of the Tx and Rx coils in WPT system at $d=40$ cm, (b) magnetic field in vector for over the plotting plane perpendicular to the surface of the structure, (c) smith chart of the transmitter and receiver impedance, (d) S-Parameter of the Tx and Rx coils, demonstrates the transmitted power.....	21
Figure 2.6 : (a) Configuration of the WPT system with coil distances of $d=7$ cm, (b) Magnetic field in vector over the plotting plane perpendicular to the surface of the structure, (c) smith chart of the transmitter and receiver impedance, (d) S-Parameter of the system considering Tx and Rx coils demonstrates the transmitted power.....	22
Figure 2.7 : (a) Configuration of the WPT system with coil distances of $d=2$ cm, (b) magnetic field in vector over the plotting plane perpendicular to the surface of the structure, (c) smith chart of the transmitter and receiver impedance, (d) S-parameter of the system considering Tx and Rx coils demonstrates the transmitted power.....	23
Figure 2.8 : (a) EM simulation results for S_{21} parameter for a Tx/RX WPT system in air for different distances at operation frequency of 13.56 MHz. (b) circuit model and S_{21} -	

simulation analysis for different coupling factor, the results of this model are confirmed by HFSS analysis.....	24
Figure 2.9 : (a) WPT system for unmatched transmitter/receiver coils, (b) output DC voltage versus Tx to Rx distance for, square shape planar coil, (c) Spiral, (d) Concentric rings coil.....	25
Figure 2.10 : (a) Resonant frequency versus transmitter coil to receiver coil distances, (b) measurement setup.....	26
Figure 2.11 : Experimental setup, using a single Tx coil to drive multiple Rx units.....	26
Figure 2.12 : A metallic structure used for delivering electrical power to several power transmitter nodes	27
Figure 2.13 : Three different antenna structures, (a) Hertz, (b) Marconi, (c) Tesla.	28
Figure 2.14 : (a) The structure of the coil and simulated system in HFSS, (b) magnetic field in vector for over the plotting plane perpendicular to the surface of the structure at matched frequency, (c) smith chart of the structure and (d) S-parameter phase and magnitude which demonstrate the resonance at 13.56 MHz.	29
Figure 2.15 : (a) The structure of the coil and simulated system in HFSS, (b) magnetic field in vector for over the plotting plane perpendicular to the surface of the structure at matched frequency, (c) smith chart of the structure and (d) S-parameter phase and magnitude which demonstrate the resonance at 13.56 MHz.	30
Figure 2.16 : (a) The structure of the coil and simulated system in HFSS, (b) magnetic field in vector for over the plotting plane perpendicular to the surface of the structure at matched frequency, (c) smith chart of the structure and (d) S-parameter phase and magnitude which demonstrate the resonance at 13.56 MHz.	31
Figure 2.17 : Amplitude of S_{11} parameter at 13.56 MHz for different distances between ground and the coil.....	32
Figure 2.18 : (a) The simulated WPT structure in HFSS, (b) magnetic field in vector form in between the coils at the operation frequency, (c) smith chart of the coupling coils, (d)	

S-parameter of the coupled coils, where S_{21} shows an acceptable level of transmitted power from Tx to Rx coil.....	33
Figure 2.19 : (a) Simulated GE open-ended coil with a distance of 70 cm from the ground and $A_{\text{Ground}} / A_{\text{Coil}} = 5$, (b) phase and amplitude profile of the S_{11} parameter for the configuration presented in (a), (c) comparison of S_{11} -profile for different area size of the ground plane at distance of 150 cm above ground plane, (d) S_{11} for different distances between the ground plane and coil and different ratios of area between the ground plane to the coil plane.....	34
Figure 2.20 : (a) Implemented $\lambda/4$ coil resonator at 13.56 MHz, (b) different distance between open-ended coil and ground, (c) S_{11} parameter of open-ended coil for different distances.....	35
Figure 2.21 : Experimental results for open-ended transmitter coil after implementation of the matching circuit.....	36
Figure 2.22 : Power delivering to two independent loads with different distances from an open-ended spiral coil, the metallic arbitrary structure is the main signal carrier in the environment.....	37
Figure 2.23 : (a) Matching network design for an arbitrary structure connected to Tx coil with a power load, (b) schematic of the matching network and its practical implementation.....	37
Figure 2.24 : (a) Comparison of matched and unmatched S-parameters in ADS software, Smith chart, (b) magnitude of the transmitted to reflected power, S_{21} , (c) smith chart of the measured S_{11} parameter for matched condition considering the load, transmitter and arbitrary structure impedance, (d) measured magnitude of the S_{11} for matched condition from power source port.....	38
Figure 2.25 : (a) Schematics of a coil with associated voltage propagation profile along the wire for first and second harmonics, (b) transient response of the voltage signal at selected nodes on the coil wire.....	39

Figure 2.26 : (a) Matching network using virtual ground for open-ended coil, (b) S_{11} parameters for matched and unmatched open-ended coil.	40
Figure 2.27 : (a) Measured S-parameters for open ended Tx and conventional Rx resonant coils in unmatched condition, (b) S-parameter of the system in matched condition (coils have distance of 6 cm and open-ended coil has 79 cm distance from the ground plane).	41
Figure 3.1 : (a) The rectifier system with matching network and load, (b) diode small signal combined with packaging model.	45
Figure 3.2 : Comparison between (a) unmatched and (b) matched conditions for doubler rectifier.....	48
Figure 3.3 : S_{11} simulation for various load resistances, (a) smith chart, (b) log chart, (c) matching efficiency analysis versus load change at 13.56 MHz in the doubler structure, (d) transient simulation results for different input voltages.....	49
Figure 3.4 :(a) Circuit schematic of the two stages Dickson rectifier, (b) matching efficiency analysis for load range of 1 to 10 k Ω	51
Figure 3.5 : Transient response of the output voltage in a 2-stage Dickson rectifier for different input signal amplitudes.	51
Figure 3.6 : Simulated circuit Schematic for a 3-stage Dickson rectifier with matching network.....	52
Figure 3.7 : (a) Smith chart of S_{11} parameter, (b) magnitude of the S_{11} at matching state, (c) matching efficiency analysis versus different resistance load, (d) transient analysis of the rectifier circuit for variable inputs.....	53
Figure 3.8 : (a) Output voltage versus input signal amplitude at 13.56 MHz for different numbers of rectifiers, (b) matching efficiency analysis and comparison of 1, 2 and 3-stage rectifiers versus output load	54
Figure 3.9 : (a) Circuit implementation for 3-stage rectifier circuit, (b) comparison for the matched and unmatched condition of rectifier circuit for 4.7 k Ω and open-load, (c) smith chart	

of S_{11} parameter for different loads, (d) effect of output load variation of the rectifier on matching efficiency.....	55
Figure 3.10 : Measured S_{11} parameters for different available power at the rectifier input.	56
Figure 4.8 : (a) S_{21} for Tx to Rx for matching on Tx or Rx (b) matching performance results for Tx or Rx side.....	66
Figure 4.9 : S-parameter simulation with post-matching for a single transmitter WPT system with two independent receiver loads with different coupling factors of $K=0.1$ and $K=0.5$. Post-matching study on Tx coil or R_{x1} and R_{x2} coils, (a) matching analysis, (b) S_{21} and S_{31} analysis for post-matching on Tx coil or post-matching on R_{x1} and R_{x2} coils. ...	68
Figure 4.10 : System level description for the receiver unit of a WPT system with dynamic matching and tuning capabilities.....	69
Figure 4.11 : Location of the different families of evolutionary algorithms	70
Figure 4.12 : One-point cross-over schematic	71
Figure 4.13 : Two-point cross-over schematic.....	72
Figure 4.14 : Mutation schematic	72
Figure 4.16 : Cost-function versus number of iteration in Binary search algorithm for two different runs.....	74
Figure 4.18 : Statistical analysis on Binary search algorithm over 200 runs.....	75
Figure 4.19 : Flow chart for the algorithm implemented in the processing unit for real time dynamic matching.....	77
Figure 4.20 : Simulation environment for the digitally implemented algorithm, and the simulated hardware realization.....	78
Figure 4.22 : (a) PCB layout of the controller circuit which is designed using top and bottom layer of the board, (b) fabricated circuit board and (c) implemented controller board operating in the system.	81

Figure 4.23 : Experimental setup for WPT using dynamic, real-time matching network, the processor utilizes intelligent algorithm for fast and assured convergence.....82

Figure 4.24 : (a) Measured results of output DC voltage versus different distance between Tx and Rx coils before and after real-time matching, (b) Measured output DC voltage for a sinusoidal signal with a constant amplitude of 1 V at different frequencies for unmatched and post-matched states.....83

List of Symbols

Symbol	Definition
λ	Free space wavelength
c	Speed of light in free space
ω	Angular frequency
Z_0	Characteristic impedance of free space
ϵ_r	Relative permittivity
μ_0	Magnetic permeability of free space
M	Mutual inductance between coils

List of Abbreviations

Abbreviation	Description
WPT	Wireless P ower T ransmission
SCMR	Strongly Coupled M agnetic R esonance
IC	Inductive Coupling
RIC	Resonant Inductive Coupling
NFC	Near F ield C ommunication
FEM	Finite E lement M ethod
HFSS	High Frequency Structural Simulator
ADS	Advance D esign C ircuit
LED	Light-Emitting D iode
EFM	Electromotive force
ERP	Effective R adiative P ower
EIRP	Effective I sotropic R adiated P ower
VNA	Vector Network Analyzer
PCB	Printed C ircuit B oard
Tx	Transmitter
Rx	Receiver
AC	Alternating Current

DC	Direct Current
RF	Radio Frequency
dBm	Decibel-milliwatts
ME	Matching Efficiency
LSSP	Large Signal S-parameter
CMOS	Complementary Metal–Oxide–Semiconductor
GA	Ground Eliminated
EA	Evolutionary Algorithms
GA	Genetic Algorithm
EC	Evolutionary Computation
EP	Evolutionary Programming
ES	Evolutionary Strategies
GP	Genetic Programming
CS	Classifier Systems
RBS	Rules Based Systems
PGA	Parallel Genetic Algorithm
MIPS	Million Instructions Per Second
ALU	Arithmetic Logic Unit
PPM	Parts Per Million

Chapter 1

Introduction

1.1 Review

The demand for electric power is increasing in vast variety of applications from industrial to biomedical, and from military to everyday-life purposes. This enormous interest on electric power forces technology developers to consider a replacement for conventional power sources, such as batteries. Many recent researches have been performed on improvement of batteries capacity and life-time, while reducing the physical size and weight of them to increase the reliability and mobility of the carrier electronic device. New battery technologies increase the cost-per-watt without reducing the dependency to portable power sources [1].

The worldwide battery market is about \$50 billion USD, of which roughly \$5.5 billion is allocated to rechargeable batteries. An estimated incremental rate of at 6% per year has been expected through 2006. Developing countries such as China, India, Brazil, the Czech Republic and South Korea are some of the strongest market gains. The demand for primary batteries is increasing about 1000 million USD per decade. Looking to global demand on batteries, cellular devices, power tools and personal computers have first, second and third rank in battery market, respectively [2].

This massive amount of batteries is threatening the human health and environment and has been considered as a dangerous, environment pollutant for the next centuries. Government of Canada, under the environment pollution and waste, has dedicated a section to batteries and considered all batteries as an environmental hazard. Under the same section, replacement of conventional batteries with rechargeable ones is recommended [3].

Transmission of electric power to a portable or non-portable device can be an alternative energy source to eliminate battery for future electronic devices. Power transmission is more effective if wires, as the power transmission medium, are eliminated by wireless techniques. Wireless Power Transmission (WPT) is an effective and powerful technique to deliver the electric power to energy consumers by eliminating the wires or physical connectors [4],[5].

1.2 Motivation

In this era of technology where automatization and intelligent systems are not a luxury but a demand in different applications, sensors are playing an inevitable role. These sensors which ten years ago mostly belonged to industrial environments are now integrated with humans' daily life.

Although new technologies bring the advantages of miniaturizations and enhancement on efficiency, the demand of energy for powering these systems remains, furthermore with more complicated structures, this demand is getting more serious than before. In a short view, providing continuous amount of power which is necessary for proper operation of complicate sensor structures, without interruption in their performance for battery replacement or charger connection is still a challenge. Scientists and large companies are trying to produce batteries with a long life time or finding the technique to avoid utilizing batteries in their devices by integrating newborn nanotechnology based techniques with the conventional structures. In a single word, the main goal of the new products is to avoid seeing the message of "Low Battery"!

Wireless Power Transfer (WPT) is a method of transferring the electric energy from a power source to several electrical load nodes without using cords. Wireless transmission is useful in cases which connecting lines are inconvenient, hazardous or impossible. Wireless power transmission can perform based on three main principles: a) electric field in the near-field, b) magnetic field in near field and c) electromagnetic field in far field. WPT systems generally can be divided to near

field and far-field systems based on their operation principal. Generally, if the distance between the transmitter and receiver coils is less than $\lambda/2\pi$, where λ is the wavelength of the operation frequency, system operates in near field regime if the size of antenna is comparable to the wavelength, the far-field regime is established [6],[7]. In near-field transmission, magnetic and electric fields are not linked, they are very strong in the near vicinity of the transmitter coil but decrease rapidly in long distances (-60 dB/decade) [8].

History of wireless power transfer goes back to early 1889 when Nikola Tesla, who had invented the famous Tesla-coils to transfer power wirelessly [9]. William C. Brown proposed a point-to-point wireless power transfer scheme on the basic of microwave beams in 1964 [10]. In 1968 a concept of a space solar power station, and further conceived that solar energy could be converted into electric energy first and then transmitted to the Earth in the form of microwaves was presented by American engineer Peter Glaser [11]. In November 2006, the research team headed by Professor Marin Soljacicb from MIT brought novelty to wireless power transfer by introducing Strongly Coupled Magnetic Resonance (SCMR). They transferred 60 watts wirelessly with ~40% efficiency over distances in excess of 2 meters. Subsequently, Intel and Qualcomm also demonstrated their wireless power transfer systems, which indicated that this novel technology would rapidly appear in human daily life [12].

As mentioned above, WPT systems can be divided to near-field and far-field methods. Near-field dominant methods are Inductive Coupling (IC) and Resonant Inductive Coupling (RIC). These methods use the non-radiative portion of the electromagnetic field. They closely resemble a transformer with primary windings separated from the secondary by an air gap. The transferred power efficiency of inductive devices decreases dramatically with increasing separation distances or resonant frequency splitting phenomena. However, the advantage of resonant induction relies on the quality factor of the resonator, which generally improves with higher frequency, at least up to a point. Therefore, in resonant inductive coupling method frequency of operation is in a range of 10 kHz to 10 MHz [13]. The most common and efficient form of near-field wireless power transmission is via direct induction followed by resonant magnetic induction. Other methods like Electrostatic induction, Electrical conduction are rarely used since the power efficiency has proven to be low [14]. The operating region of an Antenna based on signal wavelength was demonstrated in **Figure 1.1** [15].

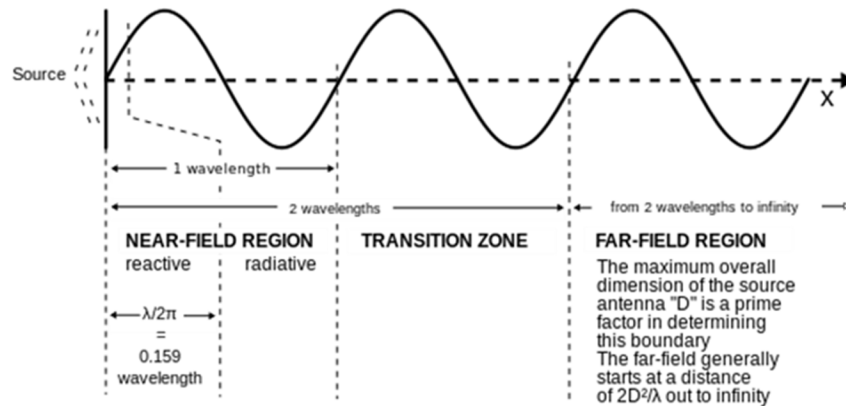


Figure 1.1 : Antenna Field Regions

The near-field electromagnetic induction technology is used at distances of up to about one-sixth the wavelength [15]. This approach is suitable for universal wireless charging pads for portable electronic devices such as cell phones and supply of equipment with no batteries such as passive RFID patches and contactless smartcards. This has been utilized as part of the Qi wireless charging standard [14].

In recent years, attempts have been increased to develop improved wireless non-radiative power-transfer systems with increased efficiency for a range of distances, or equivalently, mutual coupling. The resonant based WPT structure demonstrates relatively high efficiency compared to other methods. However, this method is susceptible to distance or angle variation between the coils. Since, RIC method is highly dependent to resonance frequency and its effect on mutual coupling, several techniques have been applied to compensate the efficiency drops such as tuning the frequency of operation, employing impedance-matching networks [16],[17],[18], transponder, coil arrays [19], and the use of a super-lens to enhance coupling [20]. In [21],[22] constant efficiencies were maintained by tuning a wireless non-radiative power-transfer system's operating frequency while the transmitting and receiving resonators were strongly coupled.

NFC's (Near Field Communications) or wireless charging became hot topics of this decade and almost all cellular carriers require charge their device within near-field region that performs inductive charging method. Though, far-field charging is still not widely used and capacitive charging is the basic requirement for far field charging. Renowned NFC devices which are currently available in market, Nokia's wireless charging plate and JBL Power-up Wireless

Introduction

Charging Speaker and Nexus 4 wireless charger from Google. In summary, microwaves and lasers are dominant methods in the long-range wireless power transfer applications, and electromagnetic induction is more popular in the short-range wireless power transfer systems. As a novel and burgeoning technology, Strongly Coupled Magnetic Resonant (SCMR) demonstrates rising potential for the mid-range wireless power transfer applications.

Table 1.1[23] summarizes the commercially available systems and standards for WPT systems. Traditional magnetic induction coils with operating frequencies between 100-300 kHz, and Class E, F and S amplifier converter topologies have been used in many wireless charging products. Recently, organizations such as the Consumer Electronics Association and A4WP (Alliance for Wireless Power) have proposed a higher frequency standard (6.78 MHz) for wireless power transmission systems. At higher frequencies, switching capability of old-fashion silicon-based power transistors (MOSFETs) limits their applications in the new standards. This can be resolved by altering the fabrication process and design of solid state electronics with ability of operating efficiently at high frequency, high voltage, and large amount of power. EPC and WiTricity are two pioneer companies in WPT systems, and have jointly, revealed a WPT system at 6.78 MHz with power delivering capability of 15 W. The demonstrated system includes all the critical components in a single system for powering of a device with wireless energy transfer [24]. Since WPT systems are getting more popular and integrated to human daily life, regulations and operation frames have been drawn to ensure their minimum impact on the human health and safety.

Table 1.1 : Commercially available WPT systems

Name	Organization	Frequency	Comments
Qi	Wireless power Con-sortium (WPC)	100-205 kHz	Commercial chip solutions available
Powermat	Power Matters Alliance(PMA)	277-357 kHz	Commercial charging station available
A4WP	Alliance for Wireless Power	6.78 MHz	Up to 50mm transmission distance
NFC Charging	Renesas	13.56 MHz	One-chip solution NFC and charging
Air Voltage	Murata	unknown	Displacement tolerance
Powercast	Powercast	850-950 MHz	Dedicated power transmitter optional

Table 1.2 [23] presents the maximum permitted transmitted signal amplitude in United State of America and Europe. These regulations can effectively limit the maximum transferable power

Introduction

in WPT systems. Oil & Gas companies are an important source of asset in the province of Alberta and there is an increasingly demand for using different types of sensors for different applications to optimize the production of natural gas or oil resources. Introducing a technique to power up this huge amount of sensors network is inevitable. Since, wireless power transmission based on RIC technique has shown potential capability to power up the small portable device as well as industrial instruments and machines such as charging the industrial vehicles. This method can also be applied to power up the sensors in harsh environments.

Table 1.2 : Maximum permitted transmitted signal in US and Europe

Wireless Power transmission limit in US	
Frequency (MHz)	Power Density (W/m²)
0.1-1.0	9000
1.0-30	9000/f ²
30-300	10
300-3000	f/30
3000-300000	100
Wireless Power transmission limit in Europe	
Frequency band	Power Density/Magnetic Field Strength
90-119 kHz	5.93e-6 W/m ²
119-135 kHz	1.49e-3 W/m ²
135-140 kHz	5.93e-6 W/m ²
13.553-13.567 MHz	5.93e-6 W/m ²
865.6-867.6 MHz	2 W e.r.p.
2446-2454 MHz	500 mW e.i.r.p.

In oil extractor environments most sensors are in the vicinity of metal structures such as oil-rigs, oil-racks or pipes. These metal structures can be used as the signal carrier in that environment utilizing electromagnetic induction method to deliver the electric power to receiver nodes wirelessly. These metal structures acting as signal carriers' medium can extend the distance between the source of the energy and the target loads.

According to the described potential of WPT systems to be applied in industrial and everyday life, increasing the efficiency of the WPT system can have extensive advantages and be profitable for next generation of technologies and human life, consequently.

1.3 Aim and Objective

Here in this thesis, the design and implementation of a WPT system will be studied and reported in details with more focus on the receiver design. The reported WPT system is less application-specific; therefore, the size, power consumption and voltage across the load can be customized per application. WPT system is shown in Figure 1.2, has 3 main subcomponents.

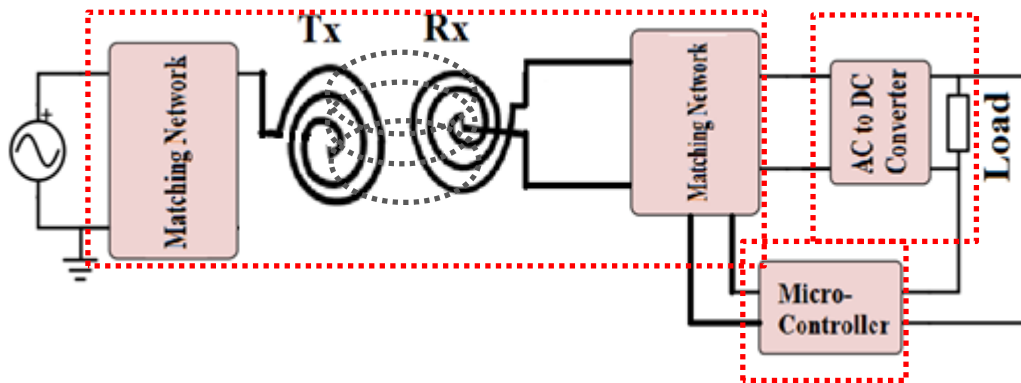


Figure 1.2 : System level architecture of Wireless Power Transmission (WPT)

Coupling coils are the heart of the wireless power transmission systems which transmits electric power from the transmitter to receiver node. An analytical study on conventional resonant coils needs to be performed in Finite Element Method (FEM) model. The effect of variant distance between the transmitter and receiver coils will be examined on the power efficiency of the coupled-coil structures in FEM simulations and measurements. A new method of delivering electric power to transmitter coils using a metallic arbitrary structure will be investigated to increase the power transmission range and to multiply the number of receiver nodes in different locations. This new method, needs ground eliminated coils in the transmitter side because, only the signal is provided to the structure and ground node is unreachable. Having ground signal on the transmitter coils is possible but can be expensive and increases the complexity of the system. Open-ended resonant coils with length of $\lambda/4$ will be studied to prevail this issue. Open-ended resonant coils eliminate the required electric ground signal on the coil but demonstrate sensitivity to distance variation

between the coils and ground planes. FEM analysis for variant distance between coil to ground plane in open-ended coil structure is necessary to gain a better understanding of the open-ended coil behavior in various situations. Practical experiments and measurement results will be performed to confirm the FEM analysis. A design procedure for signal transmission through an unknown structure is needed to be studied.

To reduce the ambient loss on the transmitted electric signal in WPT systems and create electromagnetic signal in the receiver coil, periodic waveform is mostly used as a power-signal. This form of transmitted power is not suitable to be considered as the supply voltage for electronic devices and requires a conversion to DC form factor. AC to DC conversion is performed by a voltage doubler, and rectifier block in a WPT system on the receiver node. Rectifier design and implementation is important to study since its power conversion efficiency can affect the efficiency of the overall system. Design of AC to DC converter with different number of stages needs to be studied for variant load and using discrete components. One of the design constraints is to guarantee a minimum transmitted to reflected power ratio of -20 dB in the rectifier input. Additionally, the robustness of the implemented rectifier to load variation of one order of magnitude (from 1 k Ω to 10 k Ω) needs to be investigated.

The main contribution of this thesis is implementing a feedback system on the receiver node to realize a dynamic matching network for power efficiency enhancement. This feedback system needs a processor unit; analog to digital converter and a switch array to samples the analog DC voltage across the load and use intelligent algorithm as the processing algorithm while performing the readjustment on impedance matching network utilizing analog switches. A capacitor bank associated with analog switches should be considered to control and adjust the impedance matching network in real-time fashion. Extensive simulations and measurements should be provided to illustrate the dynamic matching effect on frequency splitting phenomena and loss compensation for different coupling conditions between coils.

1.4 Thesis structure

This thesis is organized into five chapters. The operation principal of conventional and open-ended coils is presented in chapter 2. Additionally, coupling effect and related equations are

explained and comprehensive simulations are reported in FEM based software such as HFSS and circuit models are simulated in ADS. Explanation of the design, fabrication process and experimental results of conventional and open-ended coils concludes this chapter.

Chapter 3 explains the concept of AC to DC conversion. Circuit simulations for different structures of AC to DC converters using SPICE model, which is provided by the manufacturer company, are reported in this chapter. An impedance matching network is designed for final converter structure using lumped element components. This chapter is concluded by presenting the measurement results of the fabricated rectifier with a high efficiency on AC to DC conversion.

Chapter 4 discusses the design of a WPT system with a dynamic matching network utilizing a feedback loop. More clarification on definitions of “real-time”, “online” and “offline” systems are provided at Chapter 4. This chapter presents the study of mutual inductance variation between transmitter and receiver coils and its effect on the power efficiency of the WPT system. The frequency splitting phenomena is discussed in detail in this chapter and the importance of having a dynamic impedance matching system is described. Moreover, a comparison between having a dynamic matching network on transmitter or on the receiver side is studied and the significance of having dynamic matching network on the receiver node is demonstrated. A search algorithm for capacitor values to attain the maximum power efficiency is presented and full WPT system implementation is reported in this chapter.

The final chapter discusses conclusions drawn from the research, simulations, and experimental analyses. It describes strength and weakness of WPT systems with dynamic matching and highlights future progress that could stem from these ideas.

Chapter 2

Transmitter and Receiver Design

2.1 Motivation

In this chapter, coil design for transmitter and receiver nodes in WPT systems will be studied in detail. This chapter has been divided to two sections. Conventional two port coils and coupling inductors will be studied in the first part. Finite element method simulation (FEM) is used as a powerful simulation tool to study different structures and scenarios of coupling coils. Effect of coupling variation between Tx and Rx coils have been studied by changing the distance between the coils and an optimum distance between coils have been extracted where maximum power efficiency is achieved at that distance. Measurement results for different coil structures for different distances will conclude the first part of this chapter. In the second part, open-ended coil structures are studied in details for quarter and half lambda coil structures. Open ended coils are considered as one input devices with no ground wire. They can have a unique application to deliver the power to local receiver nodes while using an arbitrary structure as a feeding line to the transmitter coils. In the second part of the chapter, ground effect on the open-ended coils is studied in simulation in detail by varying the distance and comparing the power efficiency parameter. The measurement results for the open-ended structure will conclude the second part. A brief conclusion on the achieved results is also included this chapter.

2.2 Introduction to RIC Method and Coil Design for WPT Systems

RIC is a new concept in wireless energy transmission which is the combination of both inductive coupling and resonance phenomena. RIC makes two objects to interact with each other very strongly.

The RIC has some remarkable differences in comparison to conventional magnetic induction method, which is the widely used for the transmission of wireless power. In magnetic coupling, varying current in primary coil produces magnetic field in the near ambient of the coil and flow of electric inductive current in the secondary coil in its vicinity, consequently.

In magnetic coupling technique, presence of permanent inductance creates reactive power in the system. This reactive power is never delivered to the load and bounces back and forth between the inductance and the power source. This can generate imaginary power in the systems and reduces the efficiency of the system. While in RIC concept, having a capacitor operating in the resonance condition, leads to imaginary power compensation and enhance the power delivering efficiency toward the load [25].

This non-radiative energy transfer technology utilizes the stationary fields around the coils to transfer the power, therefore this method has low radiation loss since it does not spread the energy in all directions and it is just concentrated toward the device at identical resonant frequency. Additionally, RIC method has low loss and interference with other environmental objects while demonstrating a promising performance in the midrange (twice the coil diameter) power transmission applications [26],[27].

According to the advantages of RIC method, which is mentioned above, this method is employed to establish the coupling between the transmitter (Tx) and receiver (Rx) coils in this work. Also, operation frequency of 13.56 MHz is selected according to NFC standard which demonstrates less heating effect and smaller geometries of the coupling coils in comparison to low frequency operation [28].

2.3 Resonant Inductive Coupling Method

2.3.1 Definition

In electromagnetic induction technique, electric current flow through a primary coil which is a winding conductor and induce a magnetic field that acts on the secondary coil to generate a current therein. Coupling has to be in order to achieve high efficiency. In this configuration primary and secondary circuit of a transformer are not directly connected therefore energy transfers through a process known as mutual inductance.

2.3.2 Inductive link

In circuit theory, induction is modeled by $u = L \frac{di}{dt}$ for a single inductor, and for two coupled inductors with a negligible resistance and parallel capacitance, both induction effects always act simultaneously. Therefore, emf has two contributions: one from the current in the coil itself and the other from the current in the mutually coupled coil. The model can be mathematically described as:

$$\begin{bmatrix} u_1 \\ u_2 \end{bmatrix} = \begin{bmatrix} L_1 & M_{21} \\ M_{12} & L_2 \end{bmatrix} \begin{bmatrix} \frac{di_1}{dt} \\ \frac{di_2}{dt} \end{bmatrix} \quad (2.1)$$

Where L_1 and L_2 are self-inductance of inductors and $M_{12}=M_{21}=M$ which is mutual inductance of the coupled coils,

$$M = k\sqrt{L_1 L_2} \quad (2.2)$$

k is the coupling coefficient that in ideal cases is close to one, but as the distance is increased from the primary it misses more and more of the secondary magnetic field therefor mutual inductance decreases dramatically.

2.3.3 Circuit Model Analysis

A typical equivalent AC circuit model for inductive power transfer is shown in Figure 2.1 which used for AC analysis, parasitic resistance (R_t , R_r) of coils are included in this circuit model.

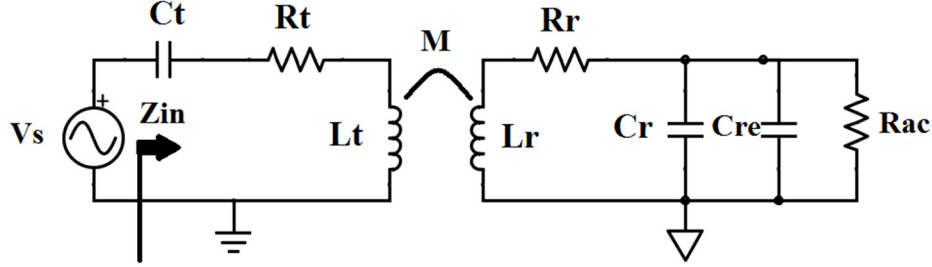


Figure 2.1 : AC model of typical series resonant circuit

In the AC model C_{re} represents the capacitance added by the rectifier and R_{ac} is an AC equivalent resistance calculated as follow [17],[26],

$$R_{ac} = \frac{V_r^2}{P_{load} + P_{rect}} \quad (2.3)$$

Where P_{rect} is the power loss of the rectifier and P_{load} is the power dissipation in the load resistance R_{load} of RIC system. The currents can be calculated by multiplying with the inverse of the Z matrix,

$$\begin{bmatrix} I_1 \\ I_2 \end{bmatrix} = \frac{1}{Z_1 Z_2 + \omega^2 M^2} \begin{bmatrix} Z_2 & -j\omega M \\ -j\omega M & Z_1 \end{bmatrix} \begin{bmatrix} V_s \\ V_2 \end{bmatrix} \quad (2.4)$$

The input impedance from the voltage source would be V_1/I_1 ,

$$Z_{in} = \frac{V_1}{I_1} = Z_1 + \frac{\omega^2 M^2}{Z_2} \quad (2.5)$$

if both coils are resonating at the same frequency then the impedance is real at this frequency. The input impedance using Q_1 as the quality factor of the primary resonator $Q_1 = \frac{\omega L}{R_1}$ and Q_2 as the quality factor of the secondary circuit including R_{ac} can be simplified to,

Transmitter and Receiver Design

$$Z_{in} = R_t(1 + kQ_1Q_2) \quad (2.6)$$

The input and output power could drive as follow:

$$P_{in} = Re \left(\frac{Z_2(\omega)V_s^2}{Z_1(\omega)Z_2(\omega) + \omega^2M^2} \right) \quad (2.7)$$

$$P_{out} = \left(\left| \frac{\omega MV_s^2}{Z_1(\omega)Z_2(\omega) + \omega^2M^2} \right| \right)^2 Re(Z_2(\omega) - R_r) \quad (2.8)$$

the transmission efficiency η also can also be defined as below,

$$\eta = \frac{P_{out}}{P_{in}} = \frac{\omega^2M^2}{R_t(R_r + R_{Leq}) + \omega^2M^2} \times \frac{R_{Leq}}{R_{Leq} + R_r} \quad (2.9)$$

where $Z_1=R_t$, $Z_2=R_r+R_{Leq}$ and R_{Leq} is the equivalent series resistance of R_{ac} and the capacitors C_r and C_{re} .

$$R_{Leq} = \frac{R_{ac}}{1 + (\omega R_{ac}(C_r + C_{re}))^2} \quad (2.10)$$

to simplify the expression transmission efficiency in (2.9) with use of coupling coefficient and quality factors of the coils it can be re-written like (2.11) which results in the same equation as in [27],

$$\eta = \frac{k^2Q_1Q_2}{1 + K^2Q_1Q_2} \times \frac{Q_2}{Q_1 + Q_2} \quad (2.11)$$

the first term in equation (2.11) represents the efficiency of transferring power from one coil to the another and the second term indicates the power division between transferred power to the load and the losses in the received power in the second coil. The last important design factor is the voltage at the receiver side. This voltage is given in [16] as:

$$V_2 = \frac{V_s}{k} \times \sqrt{\frac{L_2}{L_1}} \times \frac{k^2Q_1Q_2}{1 + k^2Q_1Q_2} \quad (2.12)$$

This equation reveals that the voltage at the receiver side is proportional to the square root of the inductance ratio, and depends on the coupling coefficient and the first term of the power efficiency. The maximum voltage for a constant quality factors occurs when $k^2 Q_1 Q_2 = 1$. Therefore, this is a good design choice to minimize the voltage variation when the coupling coefficient changes due to distance variation. Also, where $k^2 Q_1 Q_2 \gg 1$ the efficiency can be close to 100 %, but then the voltage will approximately have inverse relation to k . Therefore, it is impossible to achieve 100 % efficiency without changing the amplitude of the voltage source. In summary, to reach maximum voltage at the output the quality factor or coupling coefficient must be increased which lead to bigger coils or requires short distance between coils.

2.4 Conventional Coil Design

For transmitter and receiver nodes in wireless systems, coils or antennas play very critical role. These components establish the connection in various and unreachable environments such as harsh and hazardous ones. For far-field power and signal transmissions, antennas are preferred structures since they have long distance transmission capability. In near-field signal transmission applications, radiation is not required and the operation frequency is lower than far-field systems. Therefore, coils are more desired as they have less radiation loss and compact sizes compared to radiating antennas at that frequency. Coil structure can be divided to two main categories, coils with ferromagnetic core and coils with air core [29],[30]. Coil with ferromagnetic core can have smaller size and low radiation field. In the cored inductance structure, with closed magnetic paths inductors radiation is much less serious. As the diameter increases towards wavelength ($\lambda = c/f$), loss due to electromagnetic radiation will become significant and air core coils are preferred [31]. Air coil is used as a proximity sensor, loop antenna, induction heater, Tesla coil, electromagnet or driving coil. Air core coil is unaffected by the current it carries and free of the 'iron losses' which affect ferromagnetic cores [31]. This advantage becomes progressively more important as frequency is increased. Higher Q-factor, greater efficiency, greater power handling, and less distortion can be achieved with air cored inductors. Operation frequency is another selection factor, where ferromagnetic core coils have significant loss of the core in frequencies higher than 100 MHz, therefore their operation frequency is limited, while air core coils can operate as high as 1 GHz [31]. Antenna coils are generally operating in resonance circuit and can be modeled as a

parallel LC circuit. The operation frequency for these structures can be defined according to the following equation [32],[33]:

$$f_0 = \frac{1}{2\pi\sqrt{L_{coil}C_{tune}}} \quad (2.13)$$

where L_{coil} and C_{tune} are inductance of resonant coil and resonance tuning capacitance respectively. The coil inductance at the carrier resonant frequency can be extracted from equation (2.14):

$$L_{coil} = \frac{1}{(2\pi f_0)^2 C_{tune}} \quad (2.14)$$

The inductance value for coil of different C_{tune} values at a given tuning frequency is presented in **Table 2.1**.

Table 2.1 : Inductor's values for operation frequency at 13.56 MHz for long-range and short-range distances

Product	C_{tune} (pF)	Tuning frequency (MHz)	Antenna Coil Inductance (μH)
LR (long-range)	21	13.56	6.56
	28.5	13.56	4.83
	23.5	13.56	5.86
	97	13.56	1.42
SR (Short-range)	64	13.56	2.15
	64	14.4	1.90

Coils in WPT systems can have different physical shapes. Circular, square, hexagonal and octagonal are more popular coil structures which are generally used. Circular structures have uniform wiring in comparison to square or hexagonal spiral structures since their sheet-resistance has variant value on the corner areas and creates non-uniformity of the surface current and electromagnetic field consequently. Additionally, it has been demonstrated that circular spiral coils have higher efficiency than orthogonal structure with the same size in WPT applications [34]. Spiral design are made with the center winding contacted to the outside using a connection to

another layer which is electrically isolated with a thin dielectric layer the axis of the RF coil is oriented perpendicular to the external static field.

2.4.2 Circular Spiral Coil Design

Inductance of a single turn planar coil with a radius of r can be calculated using the following equation [35]:

$$L_{coil} = \mu_0 \times N^{1.9} \times r \times \ln\left(\frac{r}{r_0}\right) \tag{2.15}$$

Where r is the mean coil radius in millimeters, r_0 is the wire diameter in millimeters, N is the number of turns, $\mu_0 = 4\pi \times 10^{-7}$ H/m, and L is measured inductance in Henry. A spiral coil can be considered as the combination of several number of single turn inductances. **Figure 2.2** shows the structure of a spiral coil with a mean diameter of d . Equation (2.16) is governing the size and inductance relation in this type of planar coils [35].

$$L_{coil} = 31.33 \times \mu_0 \times N^2 \times \frac{d}{8d + 11c} \tag{2.16}$$

where d is the mean coil diameter in millimeters, c is the thickness of the winding in microns, N is the number of turns, $\mu_0 = 4\pi \times 10^{-7}$ H/m and L is inductance in Henry.

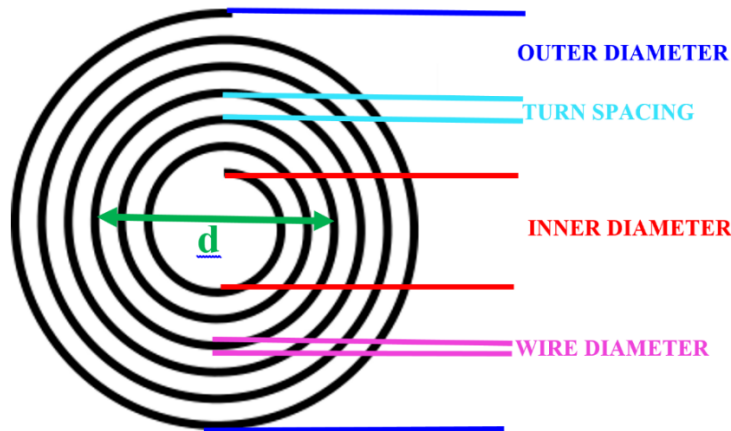


Figure 2.2 : Spiral shape inductance for WPT systems.

For the square coils the inductance can be achieved using the following equation:

$$L_{coil} = K_1 \times \mu_0 \times N^2 \times \frac{d}{1 + K_2P} \tag{2.17}$$

where d is the mean coil diameter $d = (d_{out}+d_{in})/2$ in millimeters, d_{out} = outer diameter, d_{in} = inner diameter, $p = (d_{out} - d_{in})/(d_{out} + d_{in})$ in millimeters, and K_1 and K_2 depend on the layout and shape of the coil according to **Table 2.2** [35].

Table 2.2 : Values for K_1 and K_2

Layout	K_1	K_2
Square	2.34	2.75
Hexagonal	2.33	3.82
Octagonal	2.25	3.55

In this work several circular-spiral coils are implemented with different sizes and their operation efficiency have been investigated for WPT system. **Table 2.3** summarizes the implemented coils geometries and inductances which are used in this work.

Table 2.3 : Implemented coils geometries

	Inductance (μH)	Inner Diameter (mm)	Outer Diameter (mm)	Trace Width (mm)	Trace spacing (mm)	Wire Length (mm)	Number of Turns
Transmitter	23.55	140	170	1.4	1	4.5	9
	3.064	44	99	2	0.7	1.13	6
Receiver	5.97	62	95	0.7	1.8	1.74	7
	6.25	40	84	1	1.4	1.74	9
	5.95	8	86	1	2	1.91	13

2.5 Design Procedure and Electromagnetic Simulation of the Conventional Coils

Concentric rings structure is the coil-type for the transmitter and receiver coils in the WPT system used in this research. The transmitter coil is selected to be larger than the receiver coils to save the area on receiver side and to increase the transmitted power distance from the transmitter regarding to (Table 2.1).

For initial coil design either in transmitter or receiver, no mutual coupling effect is considered. The input impedance of the resonant coils is matched to 50Ω power source impedance to have standard impedance for the designed system (this is a design assumption and can vary for different WPT systems). **Figure 2.3** shows the implemented transmitter coil in HFSS software with air environment including the impedance matching network. The coil has 8 turns with inner diameter of 56 mm and trace width of 1 mm. The spacing distance between the traces is 2 mm. An impedance matching network is established between the input port and coil to achieve the impedance matched condition with respect to source impedance of 50Ω . Magnetic field distributions over the cutting plane perpendicular to the surface of the coil is presented in **Figure 2.3**. A coil can create a magnetic field $B(r)$, where r is the distance from the center of the coil to the field point, with respect to an AC current associated with that field. The strength of the field $B(r)$ is proportional to the current I in the coil. The strength and direction of the field also depend on radius r . For large distances from the coil $r \gg a$, where a , is the radius of the coil, the shape of the magnetic field of the coil is identical to the electric field produced by a point electric dipole. For large distances both fields are reduced as distance increases ($1/r^3$).

In WPT systems, coils are used to transmit or receive the electric power with no wire in a distance of 5-20 cm; therefore, the magnetic field distribution around the coil surface is important at that range to ensure the availability of the magnetic field at that distance. **Figure 2.4a** demonstrates the magnitude of the magnetic field on the plotting plane, 50 mm above the surface of the Tx-coil, showing the high concentration of fields in the center for highly constructive behavior of the magnetic field.

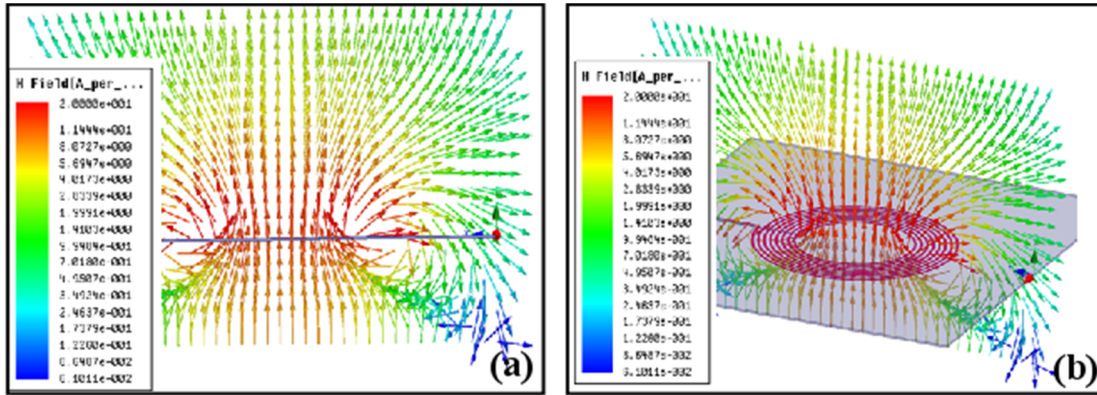


Figure 2.3 : Electromagnetic field distribution around the transmitter coil

Figure 2.4b shows the magnitude of the magnetic field distribution over two orthogonal plotting planes, magnetic vector also represents the fact that maximum magnetic field is concentrated in the center of the structure as there is a constructive adding of all magnetic fields in the center of each turn of the coil. These simulation results are presented at operation frequency of 13.56 MHz, which is the resonant frequency of the resonant coils and have minimum reflected to transmitted power ratio (S_{11}) at that frequency.

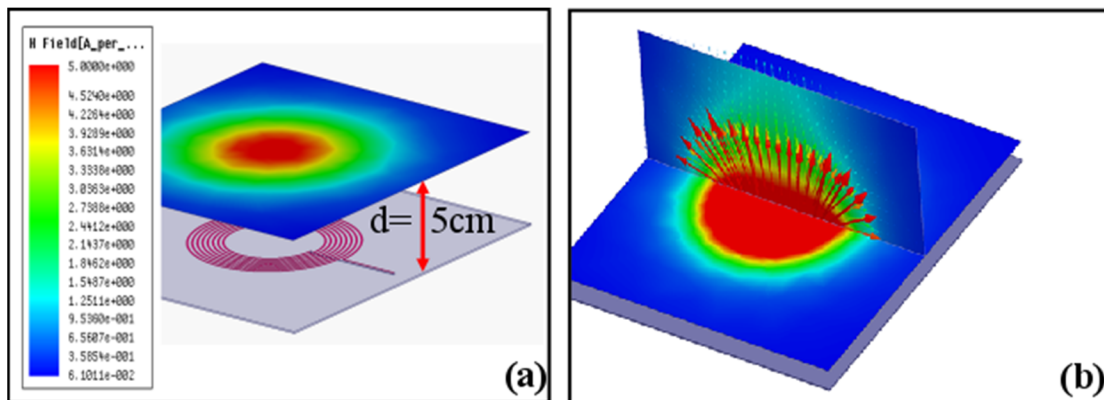


Figure 2.4 : (a) Magnetic field distribution on a distance of (50 mm) from the coil surface and (b) perpendicular to coil surface.

2.6 Coupling effect of conventional transmitter and receiver coils on power transmission efficiency

In WPT systems, mutual coupling between the transmitter coil and receiver structure plays an important role. Coupling the power from one coil to the other using magnetic signals is the key feature of the WPT system which eliminates the wiring and contact condition and enables the noncontact remote power delivering operation. Having a secondary coil in the vicinity of the transmitter one creates a coupling inductance and coupling factor consequently, while degrading the self-standing resonant profile for either transmitter or receiver.

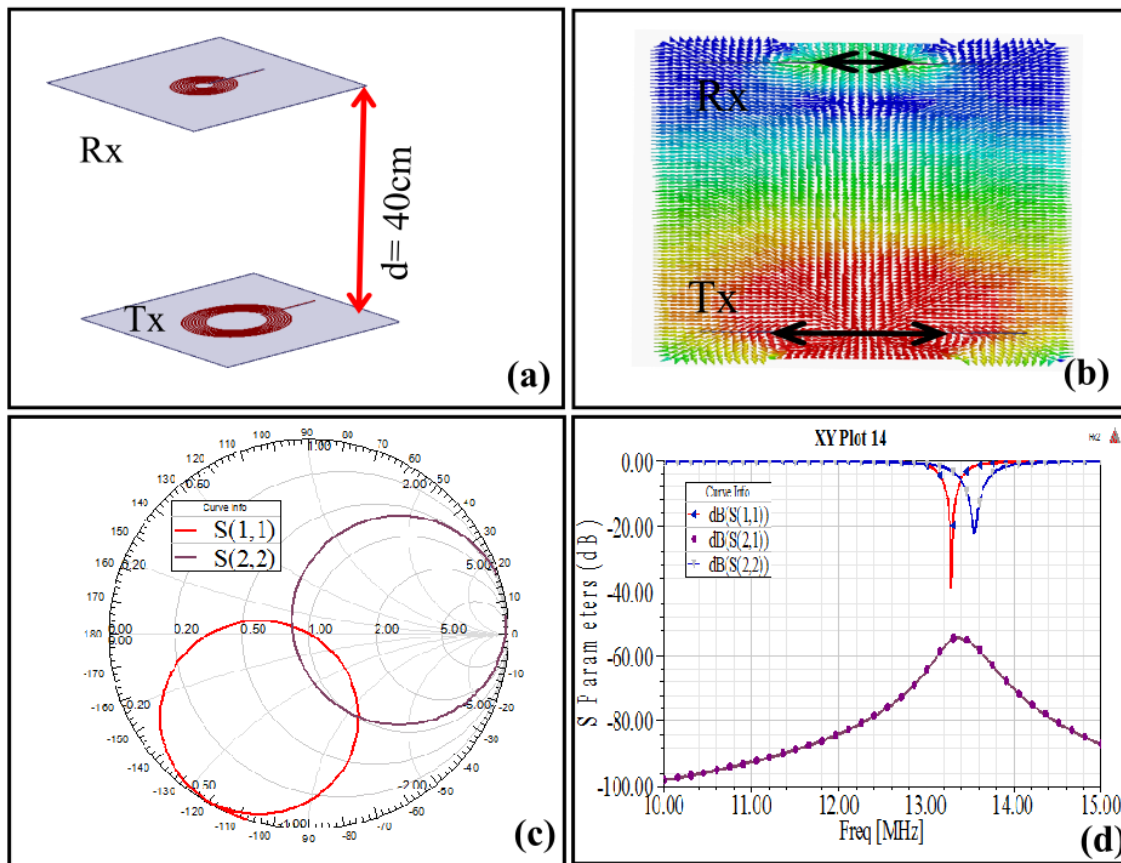


Figure 2.5 : (a) Configuration of the Tx and Rx coils in WPT system at $d=40$ cm, (b) magnetic field in vector for over the plotting plane perpendicular to the surface of the structure, (c) smith chart of the transmitter and receiver impedance, (d) S-Parameter of the Tx and Rx coils, demonstrates the transmitted power.

Transmitter and Receiver Design

While coupling is inevitable in WPT systems, it causes frequency splitting, where the operation frequency is divided to two frequencies, one goes up and the other goes down from the operation frequency and consequently reduces the efficiency of the transmitted power. The coupling effect can be studied by having two coils in HFSS model, which are matched at 13.56 MHz to 50 Ω impedance and considering zero coupling as the initial condition. Having a long distance between the receiver and transmitter coils creates a small mutual inductance in between the coils and low amount of transmitted power as a result. This effect is simulated considering a distance of 40 cm between the coils which is presented in **Figure 2.5**.

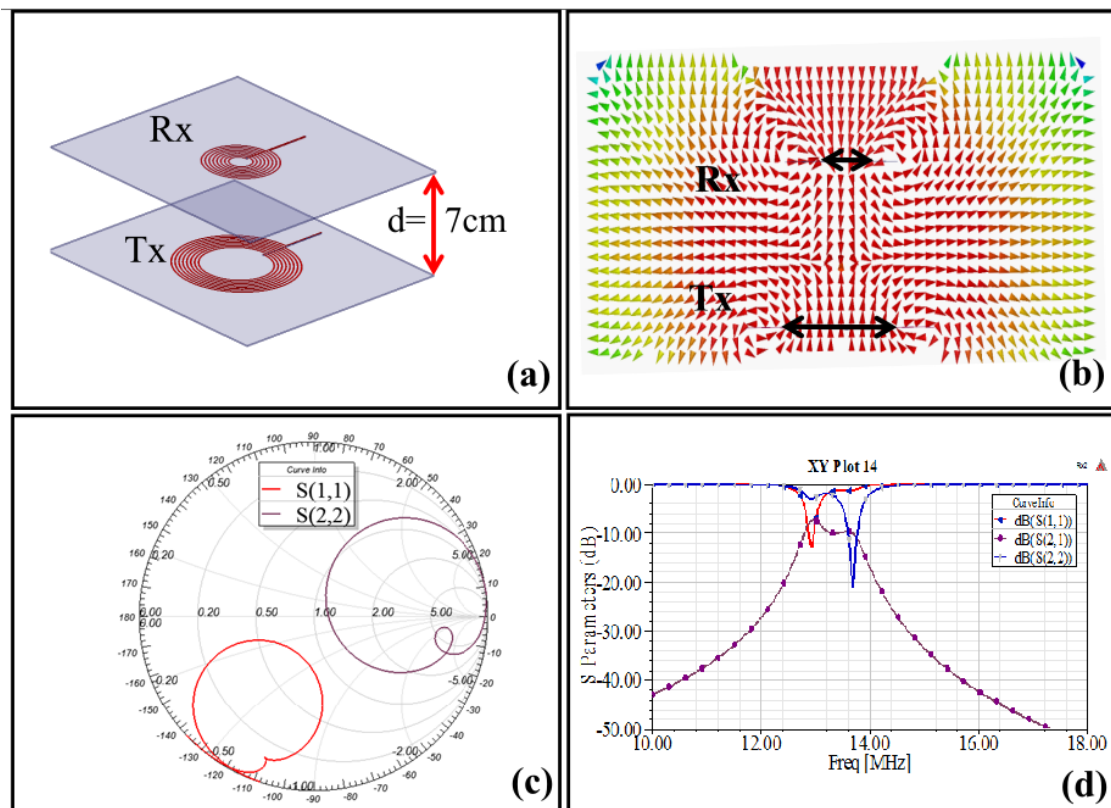


Figure 2.6 : (a) Configuration of the WPT system with coil distances of $d=7\text{ cm}$, (b) magnetic field in vector over the plotting plane perpendicular to the surface of the structure, (c) smith chart of the transmitter and receiver impedance, (d) S-Parameter of the system considering Tx and Rx coils demonstrates the transmitted power.

Reducing the distance between the transmitter and receiver coil, increases the coupling factor and the field in between the coils and increases the level of the transmitted power from the Tx to Rx coil. This is shown in **Figure 2.6**, where the Tx to Rx coil distance is reduced to 7 cm.

Transmitter and Receiver Design

Simulation results for various distances between the Tx and Rx coils obviously demonstrate the fact that, decreasing the distance between the coils increases the magnetic field in between the coils and effectively enhances the mutual inductance between them. However, beyond a certain distance, the coupling is still increased and affects the matching network both for transmitter and receiver and decreases the available power over the Tx coil and delivered power to the Rx load. This condition is called frequency splitting and achieved considering no post-impedance matching between the load and the Rx coils and Tx coil to the power source.

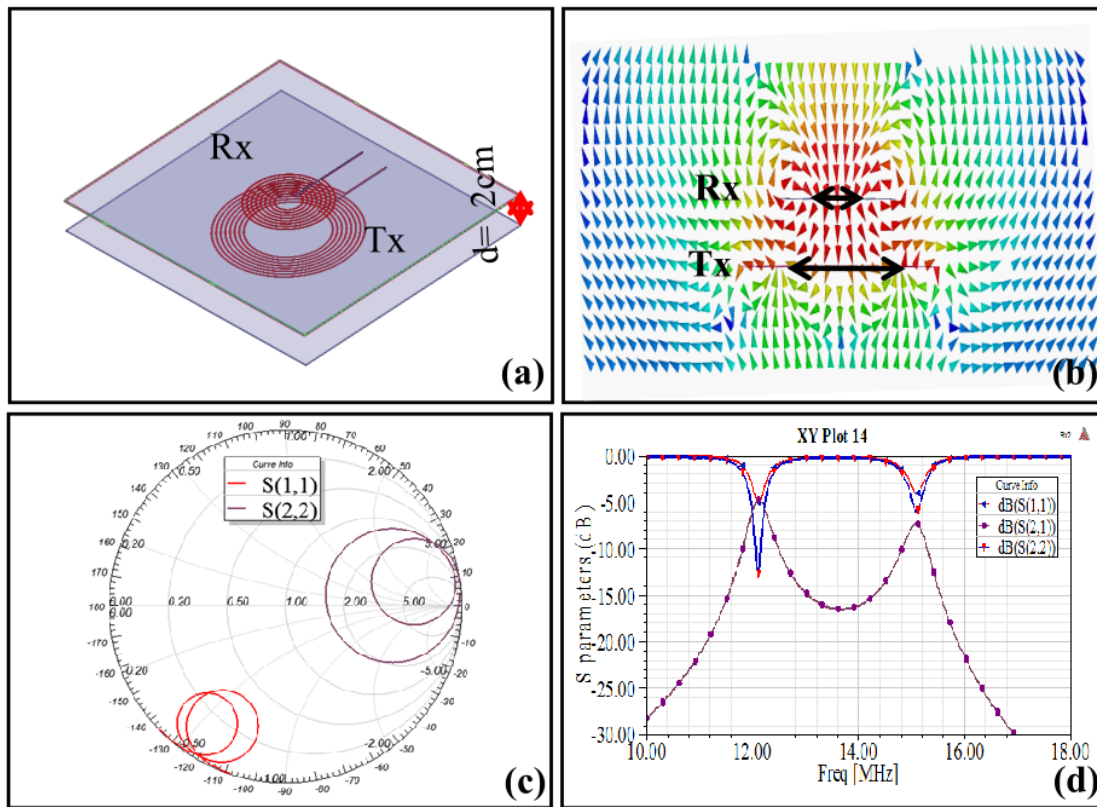


Figure 2.7 : (a) Configuration of the WPT system with coil distances of $d=2$ cm, (b) magnetic field in vector over the plotting plane perpendicular to the surface of the structure, (c) smith chart of the transmitter and receiver impedance, (d) S-parameter of the system considering Tx and Rx coils demonstrates the transmitted power.

A conclusive simulation result shows S_{21} parameter, which is a representative for the transmitted power versus different distances of the coils, has an optimum value in a distance range of 0 to 400 mm between coils. Further studies of circuit model and FEM model illustrates that, this optimum value can be a load, distance or coupling coefficient. The optimum value for all the

mentioned parameters can be extracted in a WPT system for a well-defined environment, but since WPT systems are designed to operate in industrial environments and have potential of operating in a chaotic environment, an intelligent system is required to readjust the matching network and satisfy the maximum power efficiency at the operating frequency for any unknown conditions.

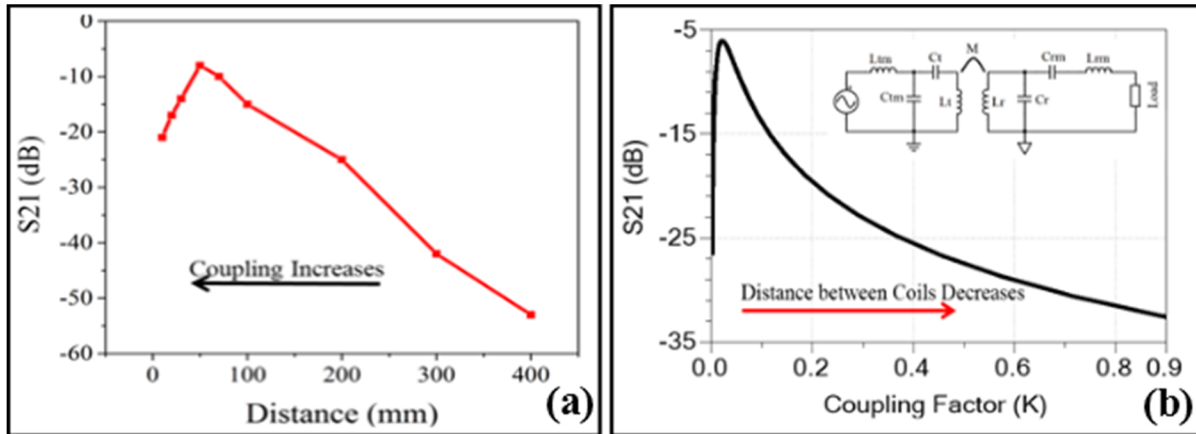


Figure 2.8 : (a) EM simulation results for S_{21} parameter for a Tx/RX WPT system in air for different distances at operation frequency of 13.56 MHz. (b) circuit model and S_{21} simulation analysis for different coupling factor, the results of this model are confirmed by HFSS analysis.

For the electromagnetic simulations a circuit model is used to represent the coupling between two coils for different coupling coefficients. This model and results, which are validated by the EM-HFSS analysis, will further be used in Chapter 4 to model the WPT system with real-time dynamic matching network (**Figure 2.8b**).

2.7 Measurement Results for the fabricated Coil Structures

Final conventional coil structures are fabricated on high quality substrates from Rogers Corporation (5880). The substrate has very low loss factor and electrical permittivity of 0.009 and 2.2, respectively. Different coils with different structures are fabricated with an AC to DC converter (rectifier) circuit and the output DC voltage is measured. For each receiver coil, DC output signal is recorded in distinct distance from the transmitter coil. Measurement results are presented for different coil structures in **Figure 2.9**. A signal generator from RIGOL DG4102 drives the transmitter coil and different types of receiver coils are placed at different distance from the transmitter. Output voltage drops exponentially when the distance between receiver and transmitter

Transmitter and Receiver Design

is increased. Spiral circular coils have demonstrated higher DC voltage in comparison to the same size of square coils. In the presented measurements, no matching network is considered for either transmitter or receiver coil, which affects the output signal amplitude and effectively reduces the power transmission efficiency of the system.

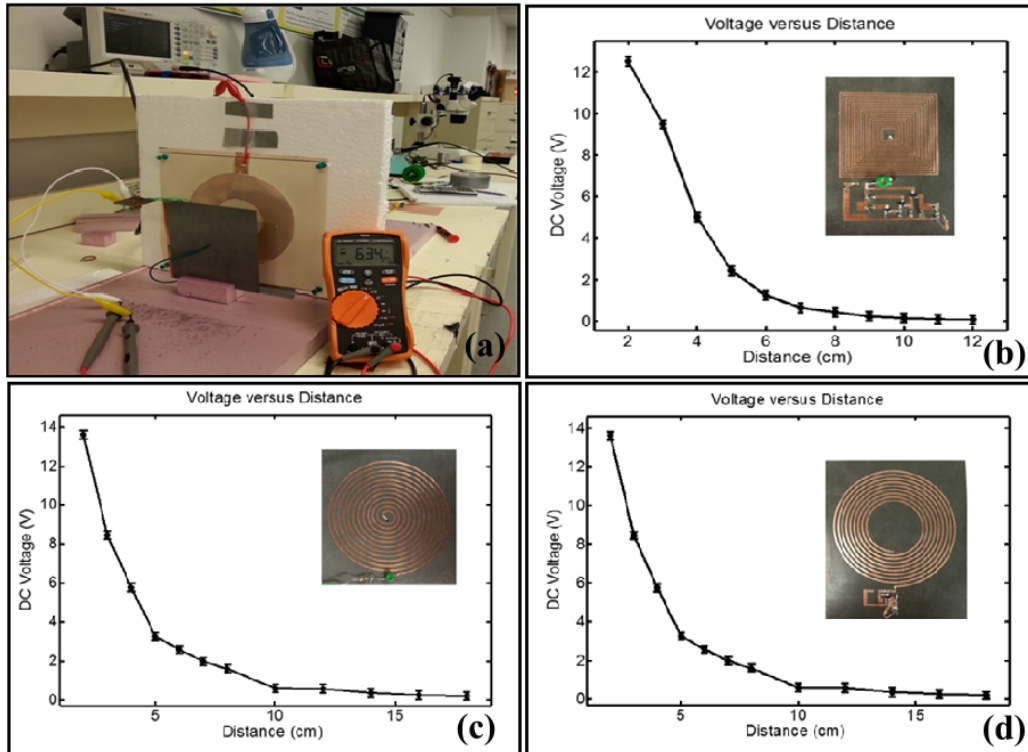


Figure 2.9 : (a) WPT system for unmatched transmitter/receiver coils, (b) output DC voltage versus Tx to Rx distance for, square shape planar coil, (c) Spiral, (d) Concentric rings coil.

Simulation results in the previous section illustrated the effect of distance variation on the resonant frequency of the Tx/Rx coils. This also has been observed running S-parameter measurements using a Vector Network Analyzer (VNA). Change in the distance not only affects the resonant frequency but also disturbs the amplitude level of the transmitted power to the receiver load. The frequency variation versus coils distance measurements demonstrate, square and circular spiral coils are less susceptible to frequency shift than the concentric ring coil. The resonant frequency for concentric ring coil is changed from 14 MHz to 13.45 MHz, which is 4% of the operation frequency (**Figure 2.10**).

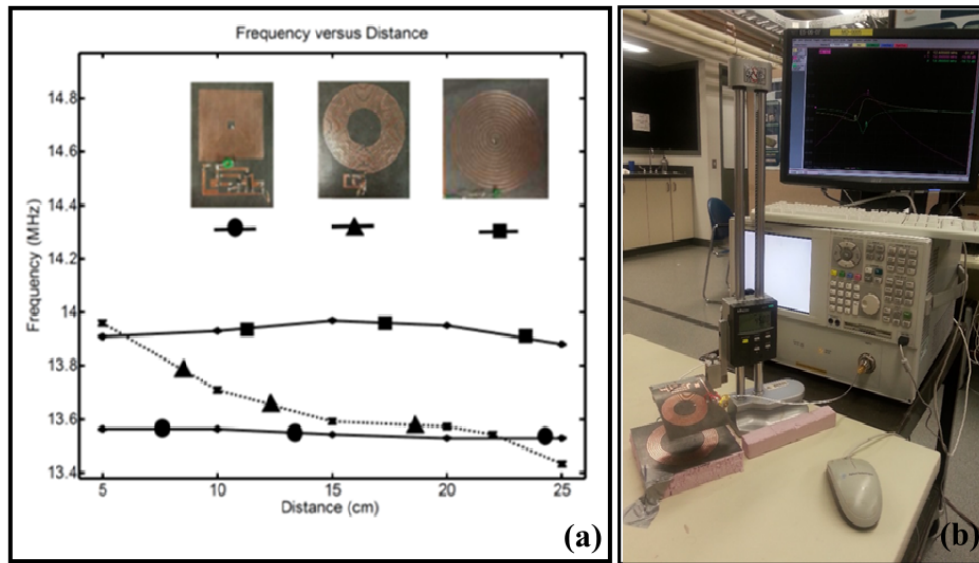


Figure 2.10 : (a) Resonant frequency versus transmitter coil to receiver coil distances, (b) measurement setup.

A practical experiment is performed to demonstrate the WPT application while delivering power from one transmitter to several receivers (**Figure 2.11**). The delivered power is used to light up a LED on each receiver which has different distances from the transmitter coil. The minimum required DC voltage and current to turn on the LEDs are 1.8 V and 20 mA respectively. The light intensity of the LEDs demonstrates that the power level which is delivered to the load is higher than 36 mW for each receiver unit.

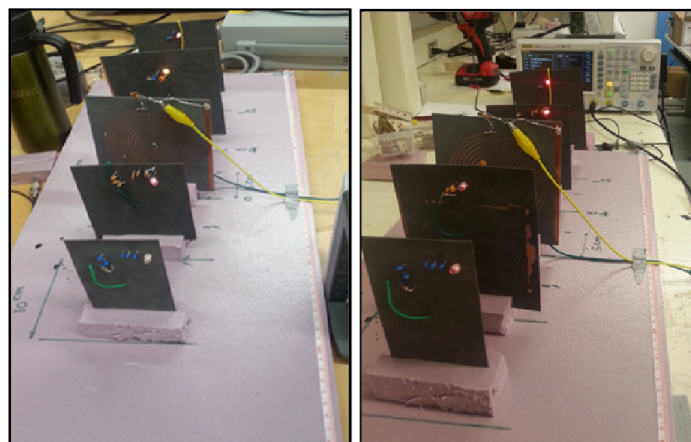


Figure 2.11 : Experimental setup, using a single Tx coil to drive multiple Rx units.

2.8 Open-ended Coil structure for WPT systems

In the previous section, conventional resonant based coupling inductors are studied for WPT purpose. These structures are well known for biomedical and industrial applications and have demonstrated a reliable and high yield structures. Recently researches demonstrate the potential of using a metallic infrastructures to transfer the electric power to receiver devices in the vicinity of the structure for large scale power delivering purposes [36]. In other reported research [37], benefits of end-fire helix antenna, which is a $\lambda/2$ open-ended conductor, is used to generate near field alternative magnetic field for power delivering to the micro-balls in endoscopy system at operating frequency of 24.05 MHz. This technique has advantages of reducing the power transmission loss in the air and, delivering the power to a large number of clients, locally. This approach can significantly reduce the cost of system implementation and increase the efficiency of power delivering system. A challenging part for this idea is, it still needs a device which locally radiates the electrical power in its close-medium. To achieve such a device, electrical coils and resonators are best options; meanwhile they need two wires to establish a potential difference across input ports for normal operation.

The second wire which is a common signal or (ground) is not available in such power transmission systems. Therefore, for each of the local transmitters additional ground wiring is required for matching purposes, which consequently can increase the cost and complexity of the system. **Figure 2.12** shows a metallic structure driving three power transmitter coils. The structure is connected to a single electric source. As shown in this figure each transmitter needs a grounded wire to establish a closed-loop circuit to allow the electrical current to flow.

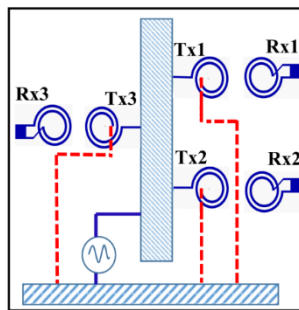


Figure 2.12 : A metallic structure used for delivering electrical power to several power transmitter nodes

Transmitter and Receiver Design

Different antenna structures were proposed previously by Hertz, Marconi and Tesla for low-frequency wireless systems. First structure is the Hertz antenna, a vertical $\lambda/2$ dipole antenna, center fed, positioned half a wavelength above the ground. Hertz antenna has challenges in practical implementation of the configuration at low frequencies. This structure for antennas, also known as the $\lambda/2$ dipole antenna, is reflected the physical embodiment of an electric dipole in free space. Second structure is the Marconi antenna, which is a modified half-wavelength dipole Hertz antenna. This structure has less practical challenges than Hertz antenna for implementation and satisfies conditions for low frequency transmitter's (**Figure 2.13**). Tesla antenna has a quarter-wavelength helical resonator with capacitive top loading. The top capacitor is an elevated terminal with large surface area [38].

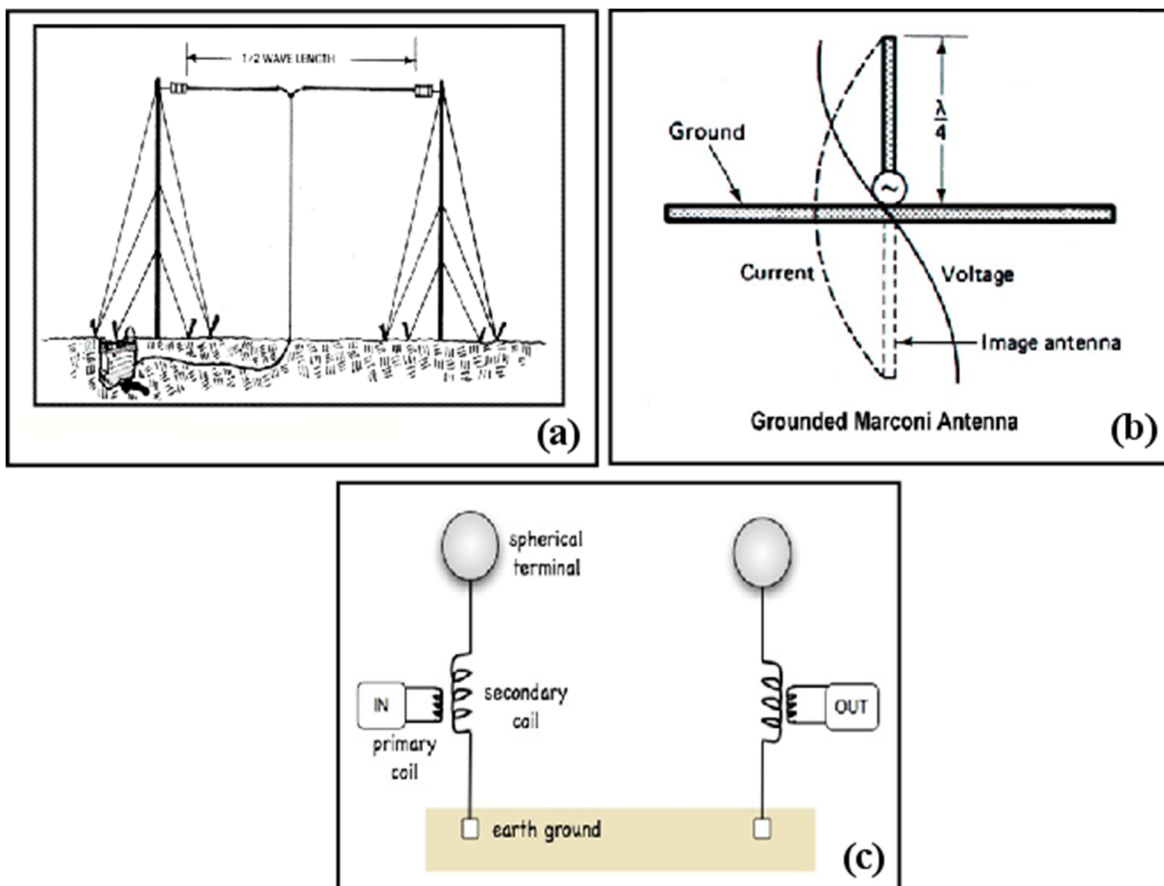


Figure 2.13 : Three different antenna structures, (a) Hertz, (b) Marconi, (c) Tesla.

To eliminate the secondary wire in the power transmitter coils of **Figure 2.12**, and based on the different antenna structures, Marconi antenna is investigated since it has an open-ended coil

Transmitter and Receiver Design

structure. A planar spiral coil is implemented in HFSS software and the ground is initially considered to be 1 m away from the coil surface. This assumption is very close to real-world application since the transmitter coil can be mounted 1 m above a ground floor as its normal operation. **Figure 2.14** presents the HFSS simulation for Ground Eliminated (GE) open-ended resonant coil structure. This coil has a distance of 1 m from the ground plane and is matched to the power source at 13.56 MHz. A deep S_{11} parameter at resonant frequency of 13.56 MHz with below -20 dB is shown, which depicts an acceptable matching condition has been achieved in this distance.

Open-ended Coil

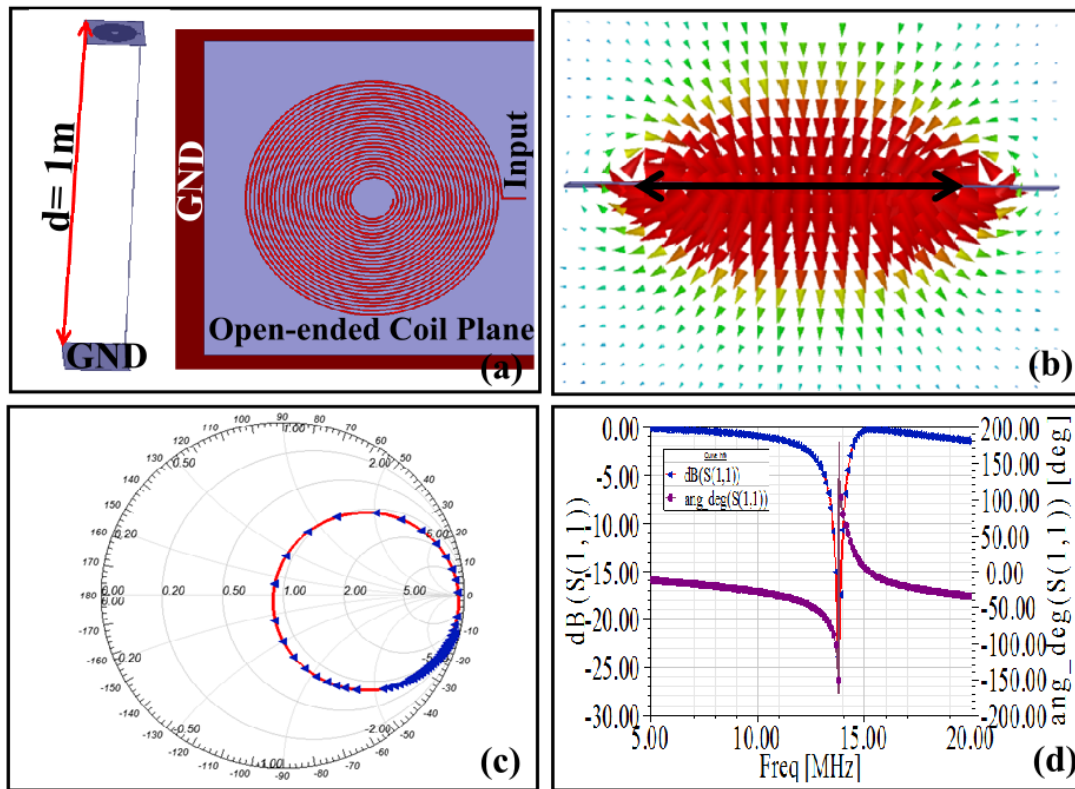


Figure 2.14 : (a) The structure of the coil and simulated system in HFSS, (b) magnetic field in vector for over the plotting plane perpendicular to the surface of the structure at matched frequency, (c) smith chart of the structure and (d) S-parameter phase and magnitude which demonstrate the resonance at 13.56 MHz.

Effect of the distance variation in between the ground plane and the open-ended coil is demonstrated in the next two figures for two distances of 20 cm and 2 m to investigate the effect

of the ground plane on the amplitude of the field and matching condition of the single-ended structure. **Figure 2.15** shows the simulated structure and results for an open-ended coil in a distance of 20 cm from the ground plane. The impedance matching between coil and input power source is degraded and the amplitude of the magnetic field around the coil is reduced at 13.56 MHz.

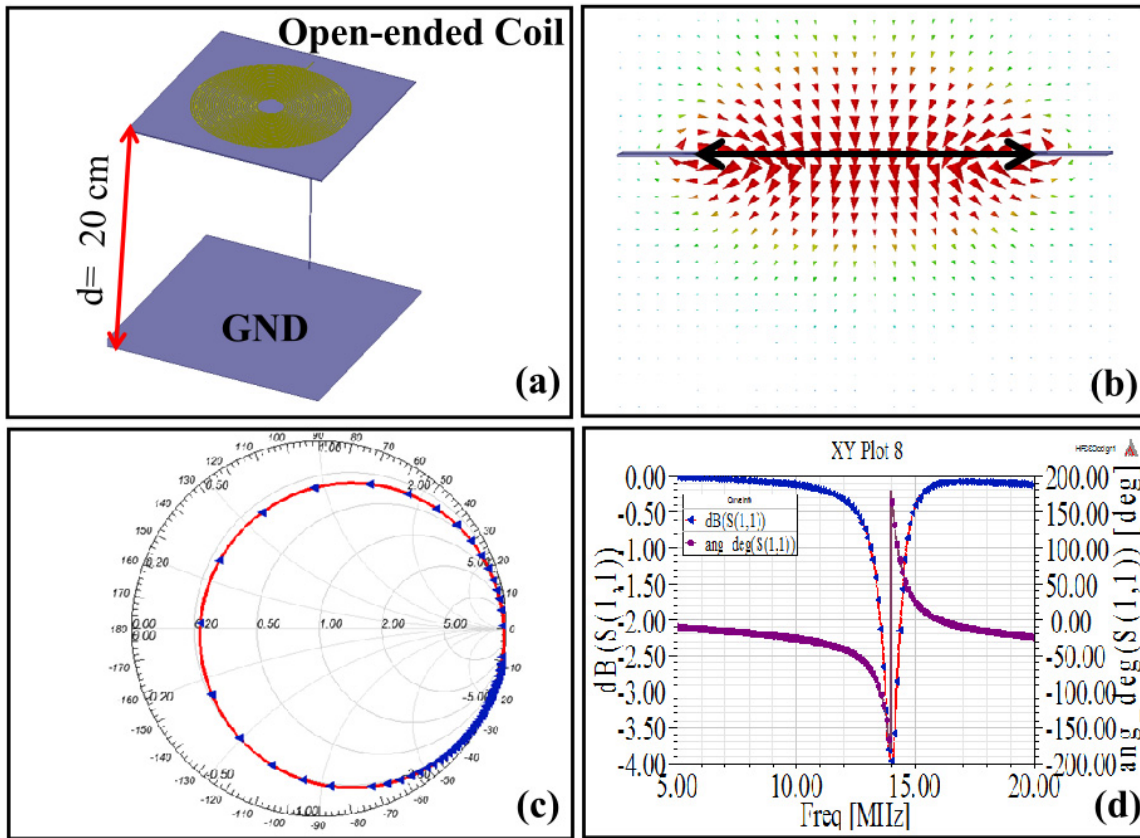


Figure 2.15 : (a) The structure of the coil and simulated system in HFSS, (b) magnetic field in vector for over the plotting plane perpendicular to the surface of the structure at matched frequency, (c) smith chart of the structure and (d) S-parameter phase and magnitude which demonstrate the resonance at 13.56 MHz.

The effect of ground plane to the open-ended coil with distance of 2 m is studied in simulation and presented in **Figure 2.16**. The input impedance of the coil is initially matched to the power source impedance at a distance of 1 m to ground and operation frequency of 13.56 MHz. The presented results demonstrate that increasing the distance of the coil from the ground also affects the matching, reflected power from the port to the source device. Comparing the magnetic field

and depth of S_{11} at operating frequency (13.56 MHz) with the results of **Figure 2.16** indicates, increasing the distance of coil and ground has less effect on the field than reducing it.

Open-ended Coil

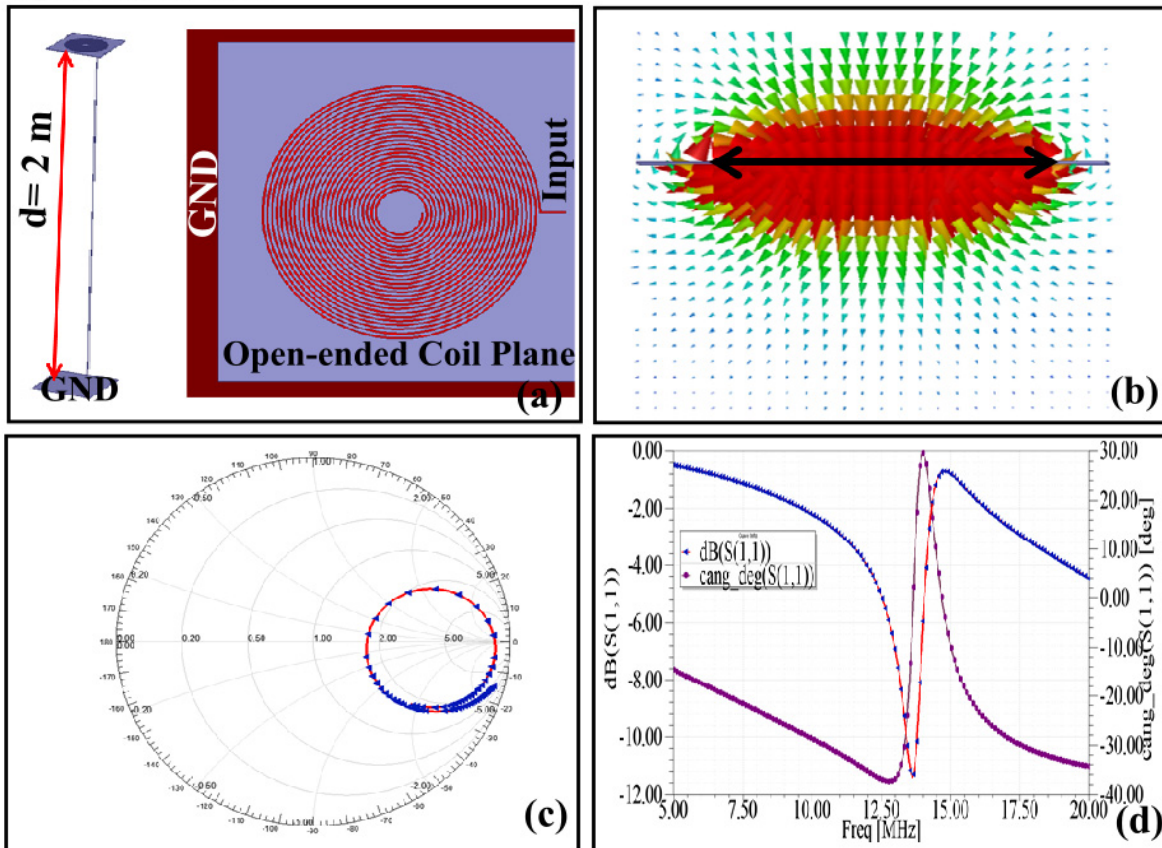


Figure 2.16 : (a) The structure of the coil and simulated system in HFSS, (b) magnetic field in vector for over the plotting plane perpendicular to the surface of the structure at matched frequency, (c) smith chart of the structure and (d) S-parameter phase and magnitude which demonstrate the resonance at 13.56 MHz.

According to the simulation results presented above, the distance of the open-ended coil to the ground is playing an important role on the matching network from the power source to the coil and consequently the amplitude of the electromagnetic field around the coil. A conclusive simulation is performed for different distances between the coil and ground plane and results are presented in **Figure 2.17**. The results depict the coil physical location regarding to ground plane can affect the efficiency of the radiated power. The simulations also illustrate, if the coil is initially matched for 1 m distance from the ground at operating frequency of 13.56 MHz, -25 % and +75% variation in

the distance is still in the acceptable region regarding to the S_{11} amplitude. These results emphasize the importance of having dynamic, real-time, in-situ, and intelligent matching structure to retrieve the maximum efficiency in power radiation for the GE open-ended coil structure in unknown conditions.

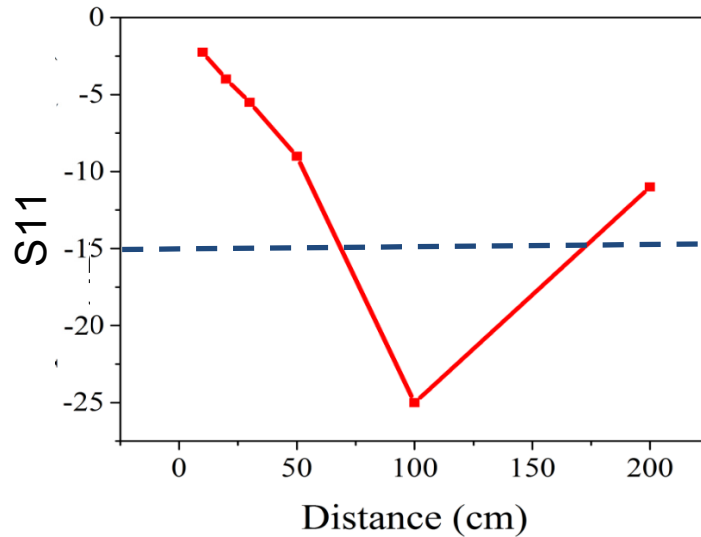


Figure 2.17 : Amplitude of S_{11} parameter at 13.56 MHz for different distances between ground and the coil

Having an open-ended inductor for wireless power transmissions can significantly reduce the cost and complexity of the transmitter coil. Also, it has been shown the coil to ground distance is an important design parameter to achieve high efficiency in power radiation in the coil. For WPT system, the transmitter to receiver coil coupling and mutual inductance is also important to demonstrate the operation of power transmission. This can be demonstrated using an open-ended coil with a receiver node in HFSS software, extracting the S_{21} parameter in between the coils. **Figure 2.18** shows the Rx coil in a distance of 4 cm from the Tx open-ended coil. The ground of the Tx coil is considered 1 m beneath the coil plane. **Figure 2.18c** presents the S_{21} parameter which in the operation frequency of the system has amplitude of better than -7 dB. Magnetic field in between and the center area of the coils has maximum and uniform value.

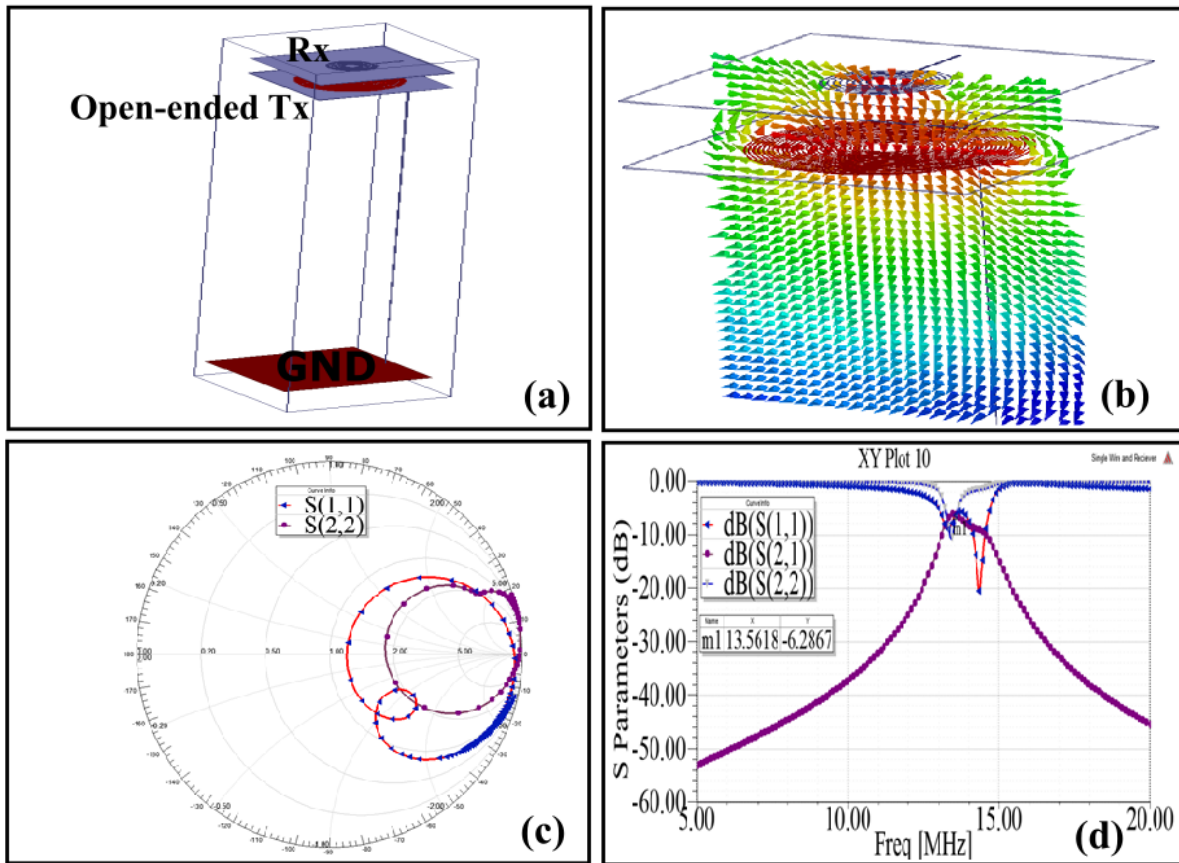


Figure 2.18 : (a) The simulated WPT structure in HFSS, (b) magnetic field in vector form in between the coils at the operation frequency, (c) smith chart of the coupling coils, (d) S-parameter of the coupled coils, where S_{21} shows an acceptable level of transmitted power from Tx to Rx coil.

2.9 Studying the ground plane size on S_{11} parameter

In the above simulations, the effect of variant distance between the ground plane and open-ended spiral coil was studied considering an equal area size of the ground plane and the coil plane. To study the effect of ground plane size on the matching and the transmitted power from the source to the coil, different ratios between the ground plane to the coil plane are considered as, 0.5, 1.5, 2, 2.5 and 5. In each configuration the distance between the ground and coil is also changed to demonstrate the distance effect. According to the presented results in **Figure 2.19**, different ground plane sizes affect the transmitted power from the source to coil and the power efficiency consequently.

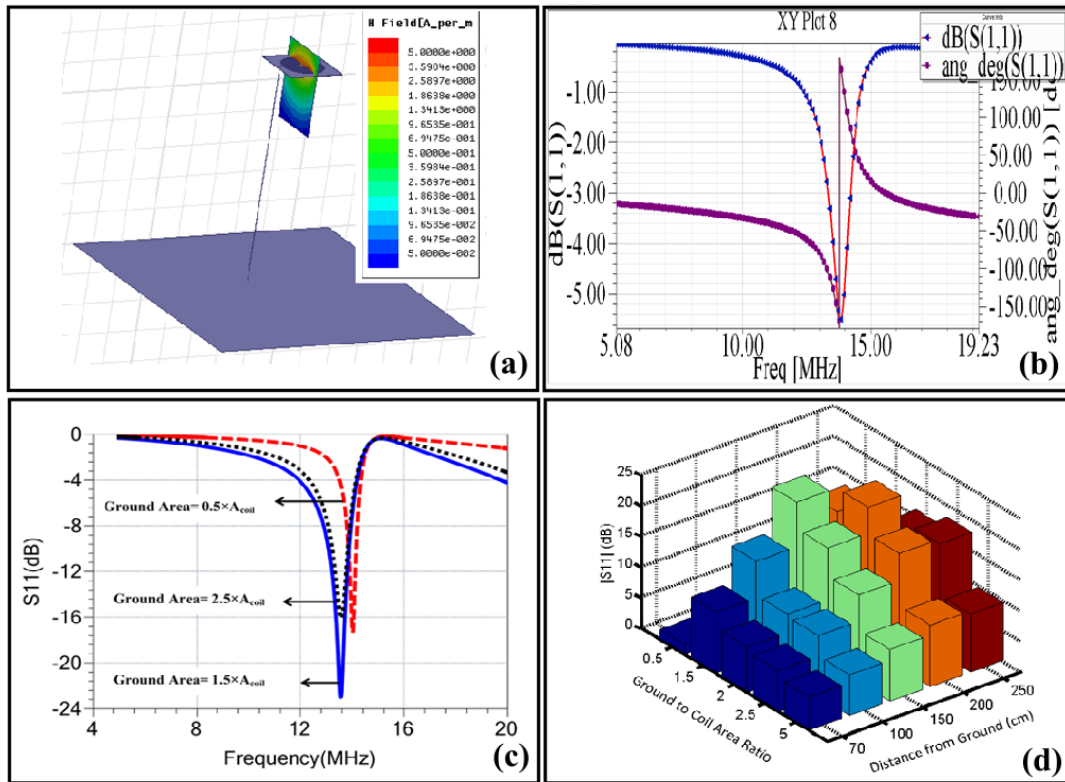


Figure 2.19 : (a) Simulated GE open-ended coil with a distance of 70 cm from the ground and $A_{Ground}/A_{Coil} = 5$, (b) phase and amplitude profile of the S_{11} parameter for the configuration presented in (a), (c) comparison of S_{11} profile for different area size of the ground plane at distance of 150 cm above ground plane, (d) S_{11} for different distances between the ground plane and coil and different ratios of area between the ground plane to the coil plane.

2.10 Measurement results for Ground Eliminated Open-ended Coil

A high quality substrate from Rogers Corporation (5880) is used for implementation of planar coils. The substrate has very low loss factor and electrical permittivity of 0.009 and 2.2, respectively. Coils with different sizes and form-factors are fabricated and connected to an AC to DC converter (rectifier) circuit. For each receiver coil, DC output voltage is recorded in distinct distances from the transmitter coil.

The Ground Eliminated (GE) open-ended resonator coil with planar spiral structure has 26 turns, the inner diameter of the coil is 21.7 mm, trace width of 0.7 mm and the spacing in between the traces is 1.5 mm. Based on these parameters the length of the coil is 6.44 m which is equal to

$\lambda/4$ at the 13.56 MHz. **Figure 2.20a** presents the implemented open-ended coil for transmitter side. As presented in coil simulation section, distance between the ground and coil plane has significant effect on the matching parameters of the open-ended coil. The distance from ground to coil is studied in measurement in **Figure 2.20b,c**. The distance variation affects the coil input impedance and effectively degrades the matching between the power source and the load.

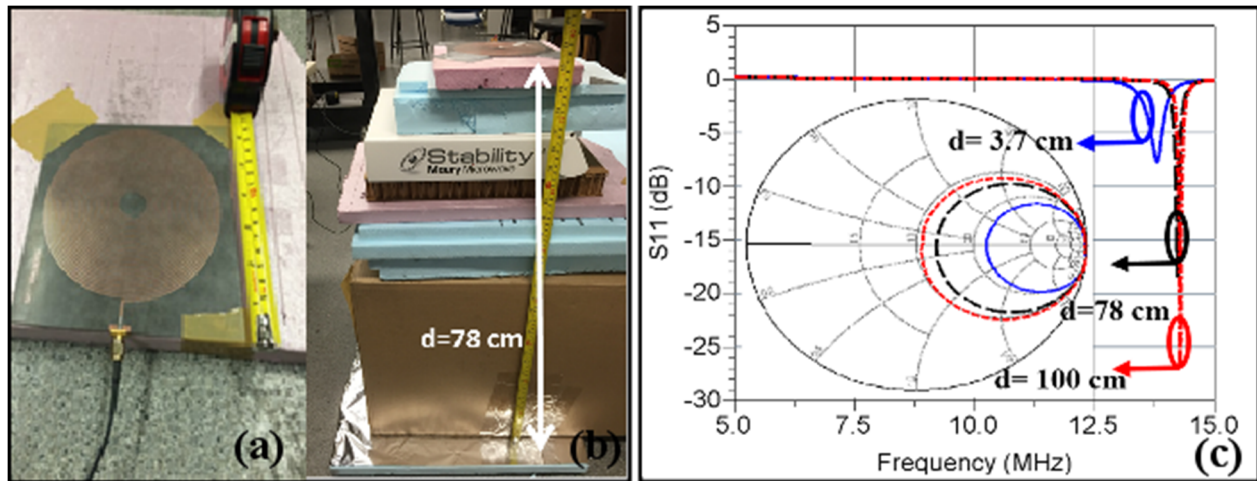


Figure 2.20 : (a) Implemented $\lambda/4$ coil resonator at 13.56 MHz, (b) different distance between open-ended coil and ground, (c) S_{11} parameter of open-ended coil for different distances.

Transmitter open-ended coil is fabricated on microwave substrate, 5880, from Rogers Corporation. The thickness of the substrate is 0.79 mm and has a dielectric property of 2.2 with loss factor of 0.009. The open-ended coil has planar spiral structure with 48 turns with an inner diameter of 3 cm, trace width of 0.5 mm and the spacing in between the traces is 0.5 mm. Based on these parameters the length of the coil is 11.2 m with is equal to $\lambda/2$ at the 13.56 MHz. This length stimulates the second harmonic of the resonant frequency. **Figure 2.21a** presents the implemented open-ended coil for transmitter side. The matched transmitter parameters for the Tx coil are presented in **Figure 2.21c, d**.

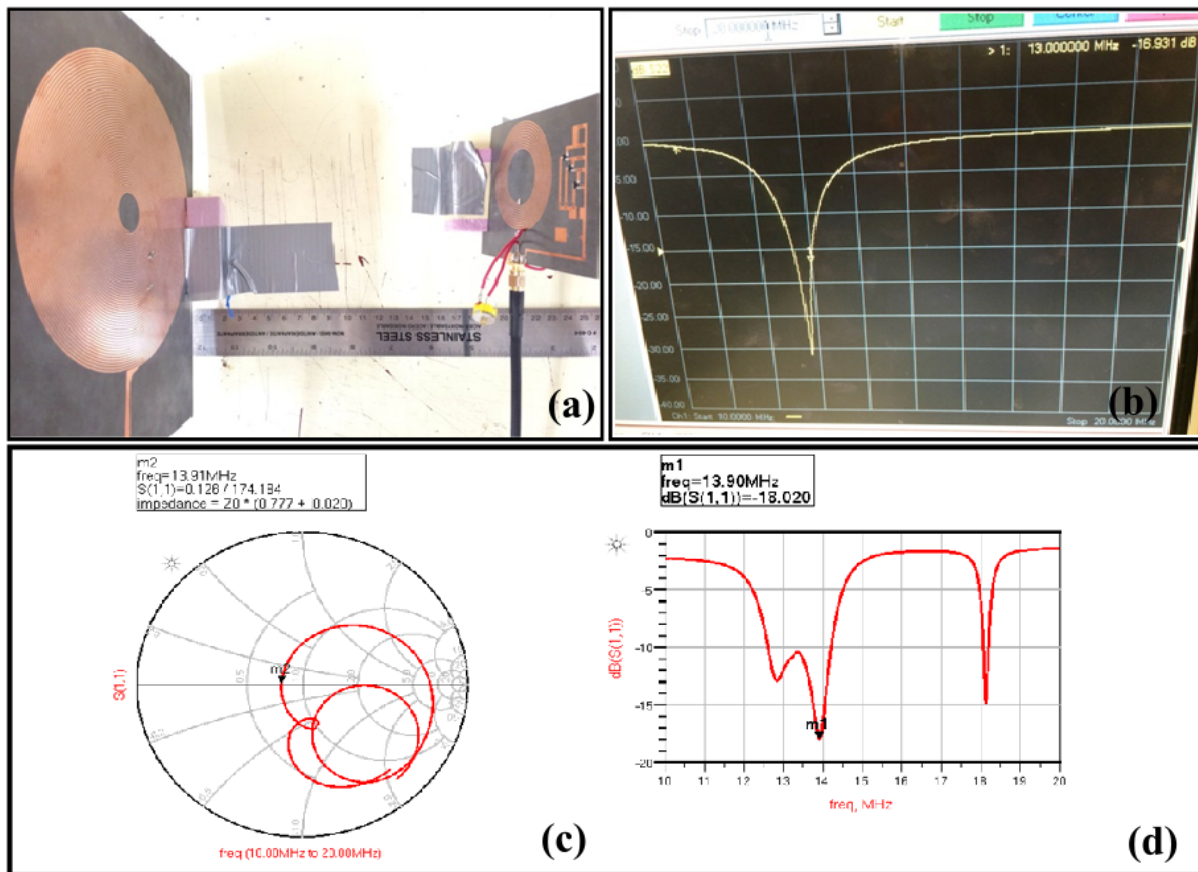


Figure 2.21 : Experimental results for open-ended transmitter coil after implementation of the matching circuit.

The next experiment is performed using a ladder as an arbitrary structure. The experimental structure is shown in **Figure 2.22** where a signal generator from RIGOL at 13.56 MHz is used with sinusoidal amplitude of 20 V_{p-p}. In this experiment an open-ended coil is connected to the arbitrary structure using a single wire. Two receiver coils with rectifier and LED is used as the load in different distances of 2.5 and 12.5 cm from the Tx coil. The Tx-coil, which is used in this experiment, is fabricated on flexible substrate from Rogers, ULTRALAM 3000, with dielectric constant of 2.9 and loss factor of 0.01. The coil has 30 turns with inner diameter of 65 mm and trace width and spacing of 0.5 mm. The signal line of the voltage source is connected to the structure while the ground wire is floating and has no connection.

Transmitter and Receiver Design

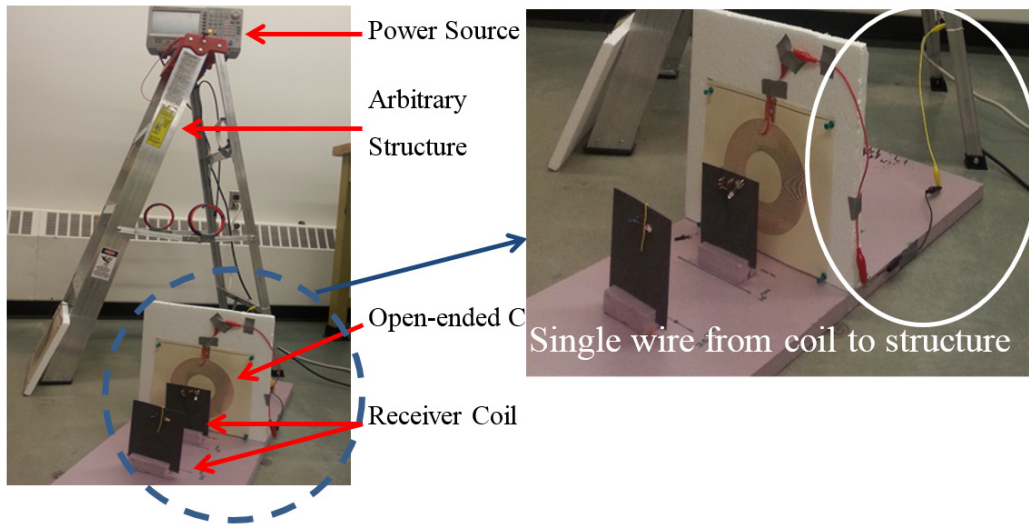


Figure 2.22 : Power delivering to two independent loads with different distances from an open-ended spiral coil, the metallic arbitrary structure is the main signal carrier in the environment.

Based on the observed and recorded voltage and current signals, more improvement can be achieved on the efficiency of the WPT system described above, by establishing an impedance matching condition between the power source and the metallic structure. This matching network enables the power flow from the source to the structure and from the structure to the Tx coil.

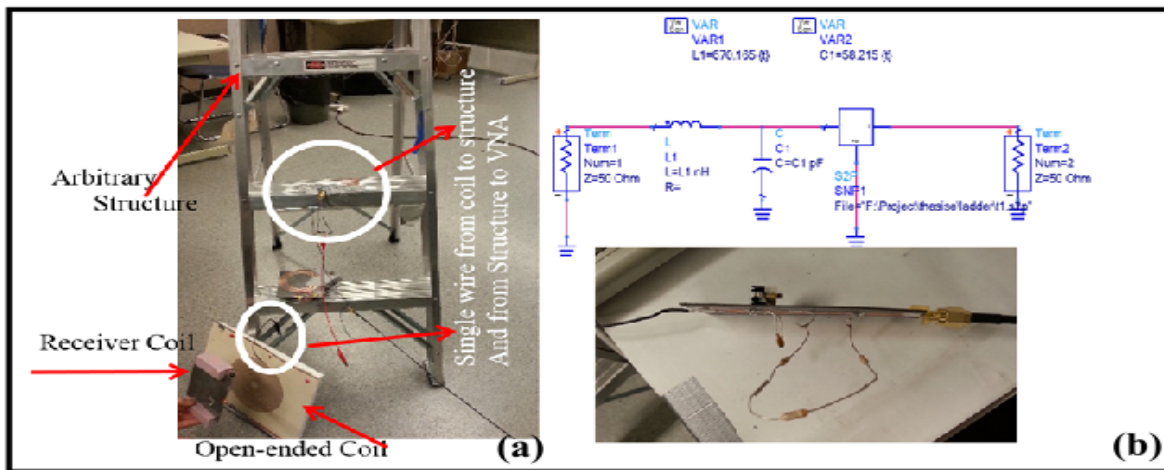


Figure 2.23 : (a) Matching network design for an arbitrary structure connected to Tx coil with a power load, (b) schematic of the matching network and its practical implementation

Figure 2.23 shows the metallic structure with connected open-ended coil. A secondary coil is placed in front of the Tx coil acting as a load and VNA signal line is connected to the structure

Transmitter and Receiver Design

while the ground is floating. The S-parameters of the unmatched structure is recorded and the data is extracted to ADS simulator. A matching network is designed in ADS and the simulation results using the extracted data are presented in **Figure 2.23a,b**. In these figures unmatched and matched S-parameters are presented and compared with experimental results in **Figure 2.23c,d**.

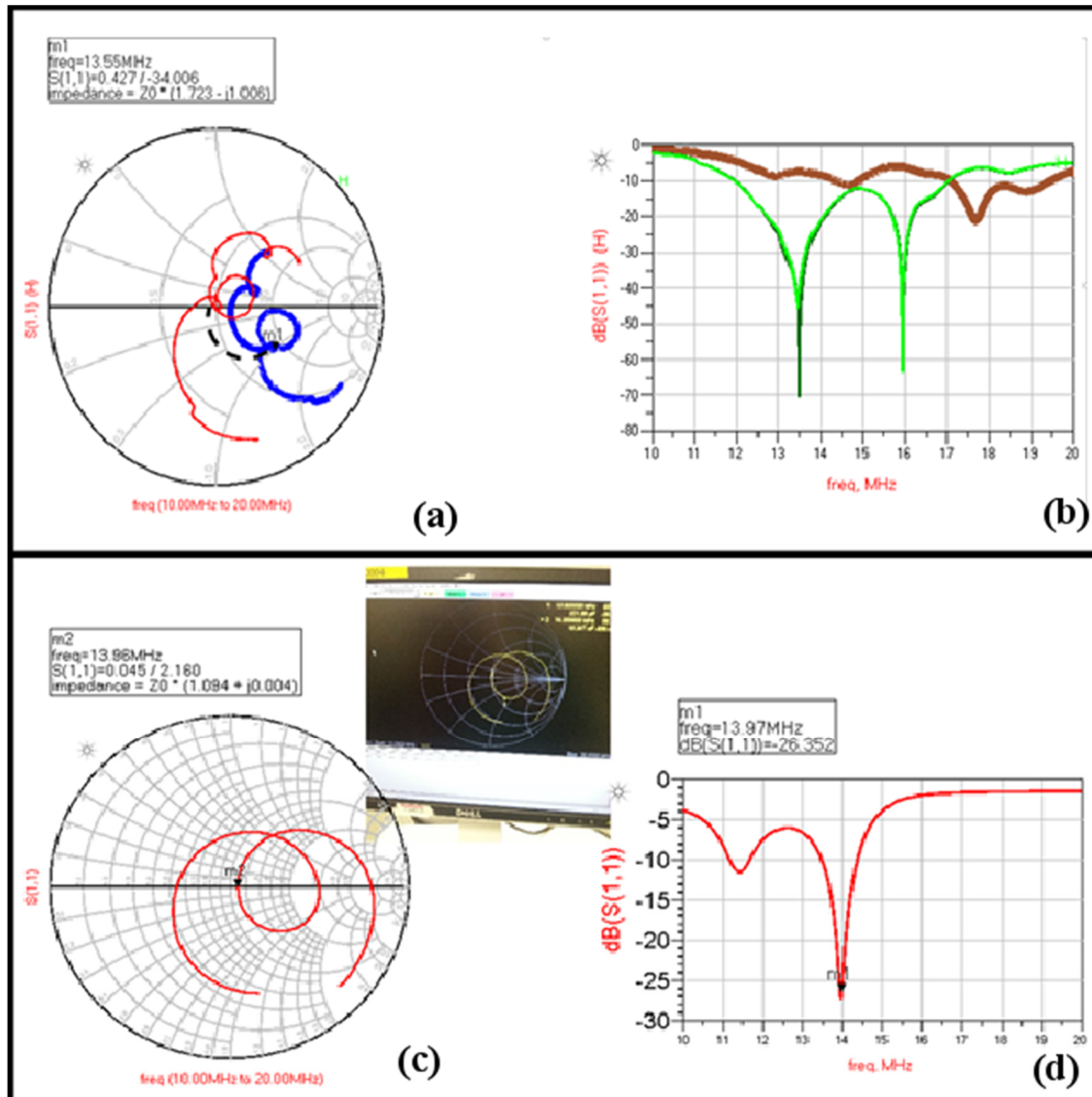


Figure 2.24 : (a) Comparison of matched and unmatched S-parameters in ADS software, Smith chart, (b) magnitude of the transmitted to reflected power, S_{21} , (c) smith chart of the measured S_{11} parameter for matched condition considering the load, transmitter and arbitrary structure impedance, (d) measured magnitude of the S_{11} for matched condition from power source port.

2.11 Tunability and Matching of a Ground Eliminated Open-ended Resonator Coil structure

Impedance matching is a commonly used technique in wireless power transfer and communication systems to improve the efficiency and maximize the available power or signal from a transmitter to receiver. The transferred power to the load can be maximized when Z_{source} is the conjugate of Z_{load} ($Z_{source} = Z_{load}^*$). Except for the conventional matching networks, which have ground signals, the matching network design is more challenging when the ground signal is inaccessible. To eliminate the ground signal issue, virtual ground technique in standing waves systems is introduced. As shown in **Figure 2.25a**, the main resonant frequency occurs at f with wavelength of λ where it has a relation to the length of wire trace according to equation (2.18):

$$f = \frac{c}{\lambda} \tag{2.18}$$

where f is the main resonant frequency, c is the speed of the light and λ is $4 \times L$. L is presenting the length of the implemented wire. Considering the main resonant frequency as the operation frequency, n_2 node on the trace can be used as virtual ground.

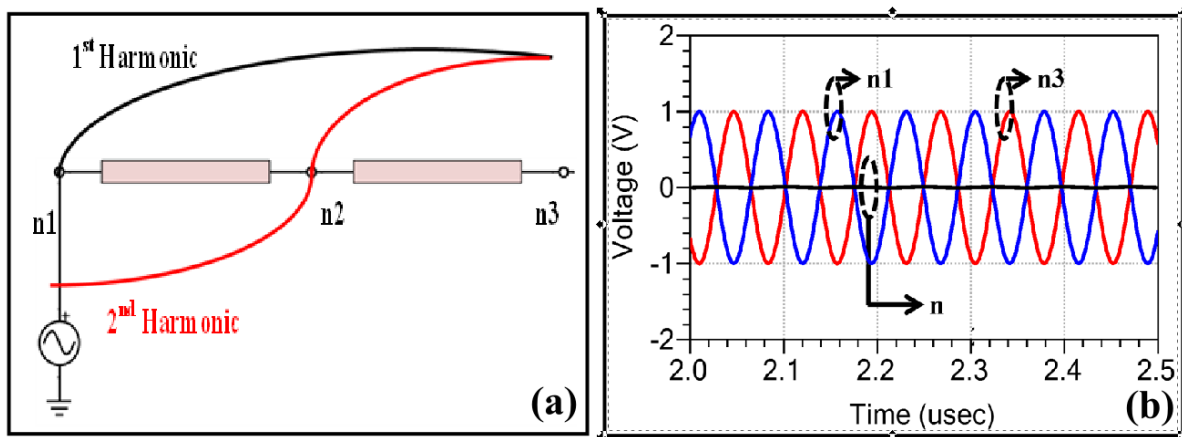


Figure 2.25 : (a) Schematics of a coil with associated voltage propagation profile along the wire for first and second harmonics, (b) transient response of the voltage signal at selected nodes on the coil wire.

The virtual ground nodes appear from 2nd harmonics and since the physical size of the coil is critical with respect to cost and coil size, that can be used as the most preferred operation frequency

in open-ended coils. The WPT system in this work is considered to operate at 13.56 MHz. This frequency is the second harmonic of the 6.78 MHz, considering these numbers the physical length of the coil is $L=11.06$ m. According to coil wire length, the physical location of the virtual ground is expected on 5.53m from the open-ended side.

Transient responses in **Figure 2.25b** are clearly demonstrated that node n_2 can be used as virtual ground (V_G) and conventional matching networks can be applied using this node. This configuration is shown in **Figure 2.26a** where LC matching components are used and node V_G in the middle of the coil wire is performed as virtual ground which is required for the matching network. A comparison between S_{11} parameters in matched and unmatched condition is presented in **Figure 2.26b**. Smith chart for matched and unmatched conditions are also shown as inset.

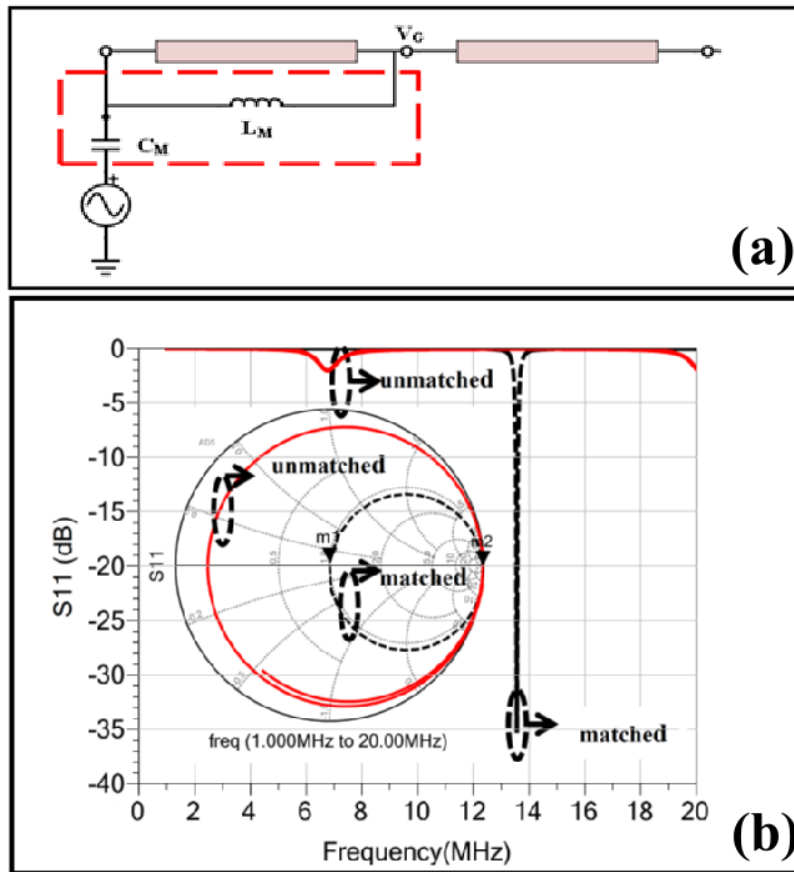


Figure 2.26 : (a) Matching network using virtual ground for open-ended coil, (b) S_{11} parameters for matched and unmatched open-ended coil.

The fabricated open-ended coil has 35 turns, an inner diameter of 30 mm, a trace width of 0.7 mm and spacing between the traces of 1.4 mm. Based on these parameters the length of the coil is 11.38 m which is equal to $\lambda/4$ at 6.78 MHz. To demonstrate the effectiveness of the proposed technique, the measured S-parameters of an open-ended unmatched-coil with Rx receiver at 13.56 MHz is recorded (**Figure 2.27a**). Having a Rx coil in distance of 6 cm from the Tx coil affects its impedance matching and transmitted power from the source to Tx coil. Employing the described impedance matching technique, and using the standing wave virtual ground, a T-type impedance matching network is implemented to establish the impedance matching at the operating frequency of 13.56 MHz. Measured results demonstrate a strong correlation between the theoretical analysis and simulations (**Figure 2.27b**).

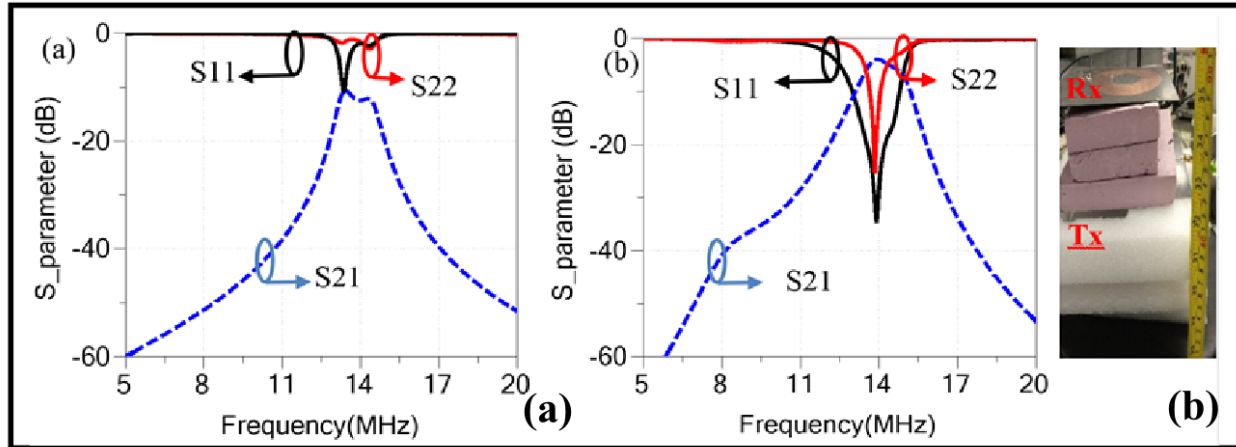


Figure 2.27 : (a) Measured S-parameters for open ended Tx and conventional Rx resonant coils in unmatched condition, (b) S-parameter of the system in matched condition (coils have distance of 6 cm and open-ended coil has 79 cm distance from the ground plane).

2.12 Conclusion

In this chapter design and analysis of conventional coil structure followed by a GE open-ended resonant coils with quarter wavelength size, were discussed. HFSS simulations comprehensively demonstrated the dependency of wireless transmitted power efficiency to the distance in between the Tx and Rx coils. Over coupling and critical coupling conditions were studied in simulation and measurements and frequency splitting phenomena, which occurred in over coupling condition, was

demonstrated. An optimum distance between the designed Tx and Rx coil was shown to achieve the maximum efficiency in transmitted power.

The second focus of this chapter was on GE open-ended resonant coil structure design, study and analysis. It also was proven that an impedance matching network was inevitable to achieve the highest power efficiency in open-ended resonant coils. Additionally, in FEM simulation and measurement results the dependency of transmitted power efficiency on ground-plane size and distance from the coil plane was demonstrated. For different ground-plane sizes, optimum distance and for different distances optimum size of ground plane was investigated to achieve the highest power transmission efficiency.

As a novel approach, a non-grounded metallic environment was employed to deliver the wireless power to the distributed receiver nodes in the vicinity of this medium. The main challenge in this system was inaccessibility of the ground signal for each transmitter, which was fed by the metallic structure. Without ground signal, matching network design using conventional well-known techniques was very challenging and problematic. To solve this issue, virtual grounds and common nodes which were created in a standing wave system was proposed and used. The operation efficiency of the proposed techniques, methods and systems were investigated and demonstrated in simulations and measurements.

Chapter 3

AC to DC Power Converters in WPT

3.1 Introduction

The process of converting AC signals to DC is called rectification, and devices that employ this process are known as rectifiers. Rectifiers and voltage multipliers are extensively used in the power supplies of consumer electronics like radios, televisions and other computer equipment that requires a steady, constant DC voltage supply. In these applications the output of the rectifier is smoothed by an electronic filter (such as a capacitor) to produce a steady DC voltage [39].

In many applications such as WPT systems where the input signal usually has limited strength, it is required to produce output DC voltages that are higher than the amplitude of input AC signal. Among other techniques, voltage multipliers can be used to produce output voltages higher than its input voltage. Generally, the peak value of the sinusoidal input voltage limits the output DC voltage level, but by using combinations of rectifier diodes and capacitors together this peak input voltage can be effectively multiplied to obtain a DC output voltage which is equal to some odd or even multiple of the peak AC input voltage. The basic unit of a voltage multiplier is a voltage doubler where its DC output voltage is twice as large as its DC input voltage or the maximum

amplitude of its AC input signal. A cascade of “N” voltage doublers can produce any desired $(N) \times (V_p)$ output voltage, assuming no losses, without the use of a transformer [40].

The diodes and capacitors which are used in voltage multiplier circuits have a minimum reverse breakdown voltage rating of at least twice the peak voltage across them in order for multi-stage voltage multiplication circuits to operate efficiently [39]. Voltage multipliers also usually supply low currents to high-resistance loads as the output voltage quickly drops away with increased load current. One of the main challenges in the multiplier rectifier circuit design is to deliver the maximum power to the load from the received power from the coil. **Table 3.1** presents the previous works on voltage rectifier-multiplier while comparing their matching efficiency and number of stages at different operation frequency.

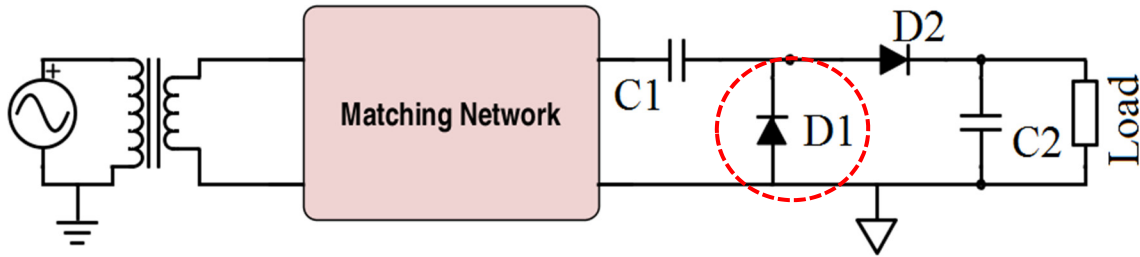
Table 3.1 : Summarizes prior reported designs on the rectifier-multiplier structure

Ref.	Frequency (MHz)	Efficiency	V_{output} (V)	P_{in}	V_{input} (V) AC	P_{output} (mW)	Load Resistance (M Ω)	Number of stages	Type of Multiplier
Heljo et. al. [41]	13.56	-	8.4 11.8	-	10	0.071 0.014	1 10	2	Charge pump
Heljo et. al.[41]	0.125	-	18.4 23.3	-	10	0.340 0.054	1 10	2	Charge pump
H.Takhdem et. al.[42]	2450	-	0.85 3	-5dBm -15dBm	-	-	100	6	Cockcroft-Walton
H.Takhdem et. al.[43]	2450	69%	1.1	20 μ W/c m ²	-	-	0.0025	-	-
Nintanavongsa et. al.[44]	915	70%	2.07	-10dBm			0.1	7	Dual stage composed
Park et. al.[45]	13.56	-	20	-	20	300	1	-	Tripler rectifier with 3 diodes

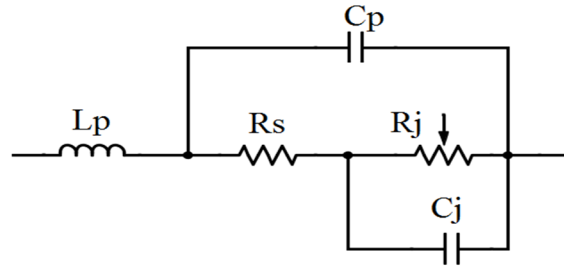
3.2 Voltage Doubler Operation

A single-stage voltage doubler, also known as half-wave voltage doubler is shown in **Figure 3.1a**. During the negative half cycle of the sinusoidal input waveform, diode D_1 is forward biased and charges the pump capacitor, C_1 to the peak value of the input voltage, (V_p) . Since there is no

path for capacitor C_1 to discharge into, it remains fully charged and acts as a storage device in series with the voltage supply.



(a)



(b)

Figure 3.1 : (a) The rectifier system with matching network and load, (b) diode small signal combined with packaging model.

During the positive half cycle, diode D_1 blocks the discharging of C_1 since it is reverse biased, while diode D_2 is forward biased and charging capacitor C_2 . But as the voltage across capacitor C_1 is equal to the peak input voltage, the capacitor C_2 charges to twice the peak input voltage. In other words, in the negative half-cycle, D_1 charges C_1 to V_p , and in the positive half-cycle, the peak of the input AC signal plus the stored voltage V_p in C_1 is transferred to C_2 through D_2 . The voltage across C_2 can be discharged through the load creating voltage ripple at the output voltage [39]. The voltage across capacitor C_2 can be calculated as: $V_{out} = 2V_p$, (assuming negligible voltage drops across the diodes used). The output voltage gradually increases with each input cycle, eventually settling to $2V_p$. As the capacitor C_2 only charges during one half cycle of the input waveform, the voltage across C_2 discharges into the load which results in ripples with frequency equal to the AC input signal frequency. C_2 has a DC voltage rating at least twice the value of the peak input voltage.

By reversing the direction of the diodes and capacitors in the circuit we can also reverse the direction of the output voltage creating a negative voltage output. By cascading multiple doubler stages the DC output voltage can also be increased in integer steps [46].

3.3 Rectifier Design

In a WPT system, a rectifier circuit is required to convert received RF signals to DC signals with constant, stable levels. To design reliable, efficient and miniaturized rectifiers, we must consider parameters such as the input impedance, the number of nonlinear device (diode) stages, the operating frequency, the minimum available power at the rectifier input and the load which is driven by the rectifier circuit. These parameters are defined by the standards and requirements of the WPT system. In this work an operational frequency of 13.56 MHz is used for designing rectifier as the coils are operating at this frequency. The minimum available power to the input of the rectifier is 0 dBm, and the standard load is considered to be 4.7 k Ω . The other parameters, such as the number of stages and the matching network, should be determined based on these initial parameters.

A single stage doubler structure for RF to DC conversion utilizing two diodes is presented in **Figure 3.1a**. In this structure, the output DC voltage across the load is two times the maximum signal amplitude at the rectifier input. The doubler circuit consists of nonlinear rectifying devices, typically diodes, and voltage storage devices such as capacitors. The selection of diodes for the rectifier design and the value of the capacitor are very important since they determine the remaining design parameters such as matching and efficiency. Additionally, the capacitor's value affects the ripple in the DC voltage supplied to the load which should be kept as small as possible. In this design, which requires converting an incoming weak RF input power to a DC voltage, low threshold voltage diodes with very fast switching response are preferable. Since Schottky diodes use a metal-semiconductor junction instead of semiconductor-semiconductor junction, they can operate much faster than conventional p-n junction diodes at lower forward bias voltage such as 150mV. In this work, Schottky diodes from Avago-technologies Company (HSMS 2820) are used which have the forward bias voltage of 150 mV. This diode is a low bias Schottky detector diode with an operational frequency of less than 4 GHz, designed for WPT applications where the

primary DC power is not available. This model is designed for input power levels greater than -20 dBm (**Figure 3.1b**).

A Schottky barrier diode chip consists of a metal-semiconductor barrier produced by the deposition of a metal layer on a semiconductor layer. **Figure 3.1b** presents the small signal model for the selected diode and its parameters. R_s is here defined as the parasitic series resistance of the diode, which contains the effects of the bond-wire and lead-frame resistance, as well as the resistance of the silicon bulk layer. RF energy coupled into R_s is dissipated as heat and doesn't contribute to the rectified output of the diode. C_j is the parasitic junction capacitance of the diode, controlled by the thickness of the epitaxial layer and the diameter of the Schottky contact. R_j is the junction resistance of the diode, which varies as a function of the total current flowing through the diode. L_p and C_p are fabrication-dependant inductance and capacitance parameters related to the packaging technology. Values of these parameters are available from Avago-Technologies Company[47].

There are important parameters that must be considered to determine the size of capacitor in the multipliers, such as frequency of the input signal, and voltage rating of the capacitor. In practice, capacitor ranges which are used in off-line, 60 Hz applications are usually 1.0 to 200 μF , while in high frequency applications, the range of 0.02 to 0.06 μF is acceptable [48]. The other important parameter is the voltage rating of capacitors, which shows the capability of the capacitor to withstand to maximum voltage across its terminals. This factor is determined by the type of the multiplier circuit. As an example in voltage doubler circuit of **Figure 3.1**, C_1 must be capable of withstanding a maximum voltage of $1 V_p$, while C_2 must withstand a voltage of $2 V_p$. To have a reasonable selection of capacitors to operate efficiently in multipliers, the voltage rating must be approximately twice of the actual peak of the applied voltage [40].

Therefore, according to the operation frequency and system requirement, the value of voltage storage capacitance is selected as 470 pF to minimize voltage ripple and provide a short settling time for the output DC voltage signal. The power transferred to the input of the rectifier is affected by the mismatch between the output impedance of the receiver antenna or coil and the input impedance of the rectifier circuit. To increase the efficiency of the power conversion and transfer the maximum available power to the rectifier an impedance matching network is required. The matching network provides impedance matching between the receiver coil and rectifier,

maximizing the power transfer from the coil to the rectifier and hence increasing the power conversion efficiency of the overall system. **Figure 3.2** presents a comparison between matched and unmatched rectifiers with respect to power transfer efficiency. According to the results, the matching network between the receiver coil and the rectifier circuit is necessary in order to achieve high power efficiency.

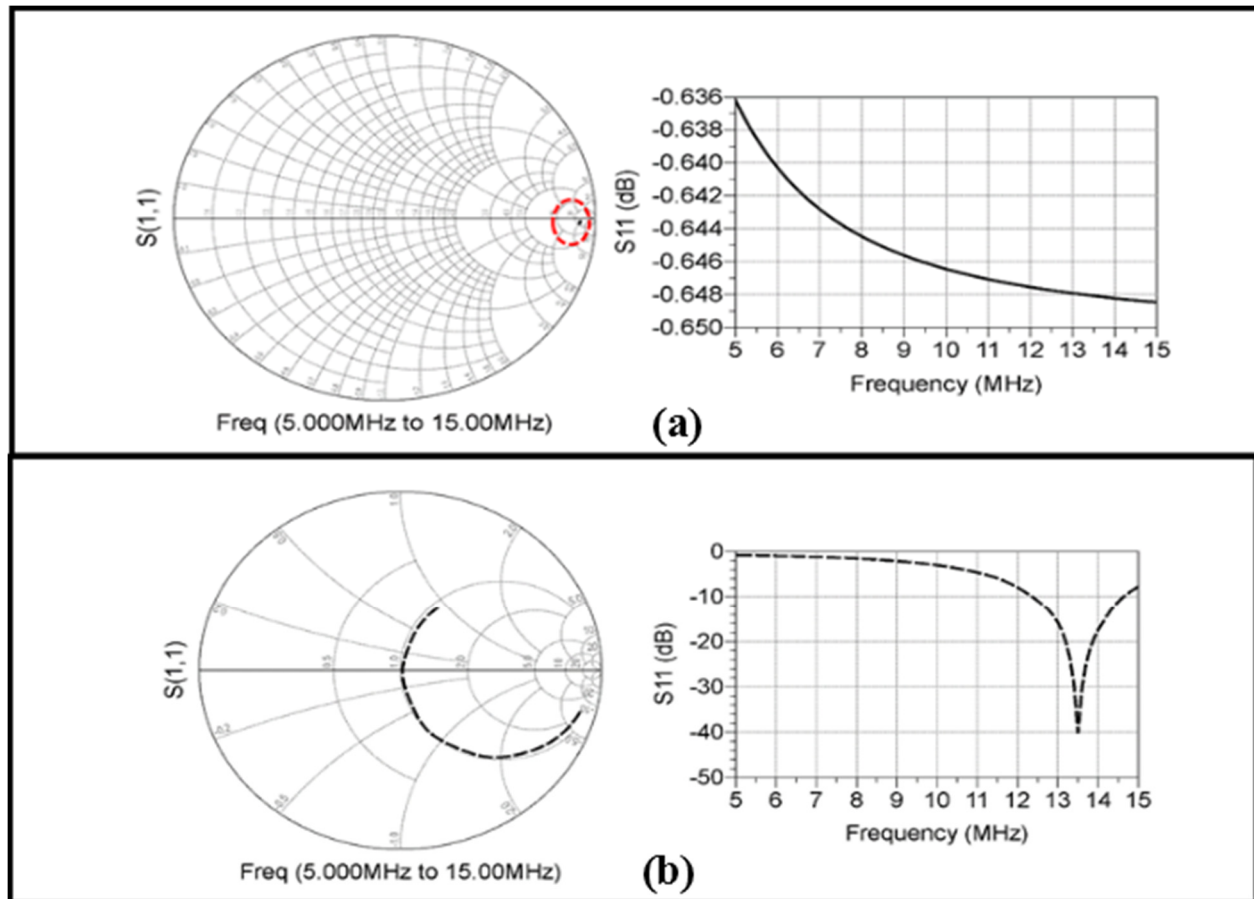


Figure 3.2 : Comparison between (a) unmatched and (b) matched conditions for doubler rectifier

The diodes in voltage doubler circuits perform in a nonlinear regime. Therefore, Large Signal S-parameter (LSSP) simulation in ADS software was performed. LSSP simulation in Agilent ADS is a tool to compute the S-parameter for nonlinear circuits that includes nonlinear effects such as gain compressions at different levels of input power. Therefore, the large-signal S-parameters are called power-dependent S-parameters. It is based on harmonic balance simulation and uses harmonic balance techniques [49].

The effects of load resistance variation are studied in **Figure 3.3**. Changing the load from 2.7 kΩ to 8.7 kΩ affects the S_{11} parameter as shown in **Figure 3.3a,b**. An extensive study of load variation effects on Matching Efficiency (ME) is presented in **Figure 3.3c** where the maximum power efficiency is achieved when the rectifier is matched to the source with a load of $R_L=4.7$ kΩ. This also indicates that if a dynamic matching system is utilized, the matching can change with the load and retrieve the maximum matching efficiency for the new load. The results for **Figure 3.3c** are obtained at 13.56 MHz and the matching efficiency calculation [50] was achieved using the following equation:

$$ME = 1 - |S_{11}|^2 \quad (3.1)$$

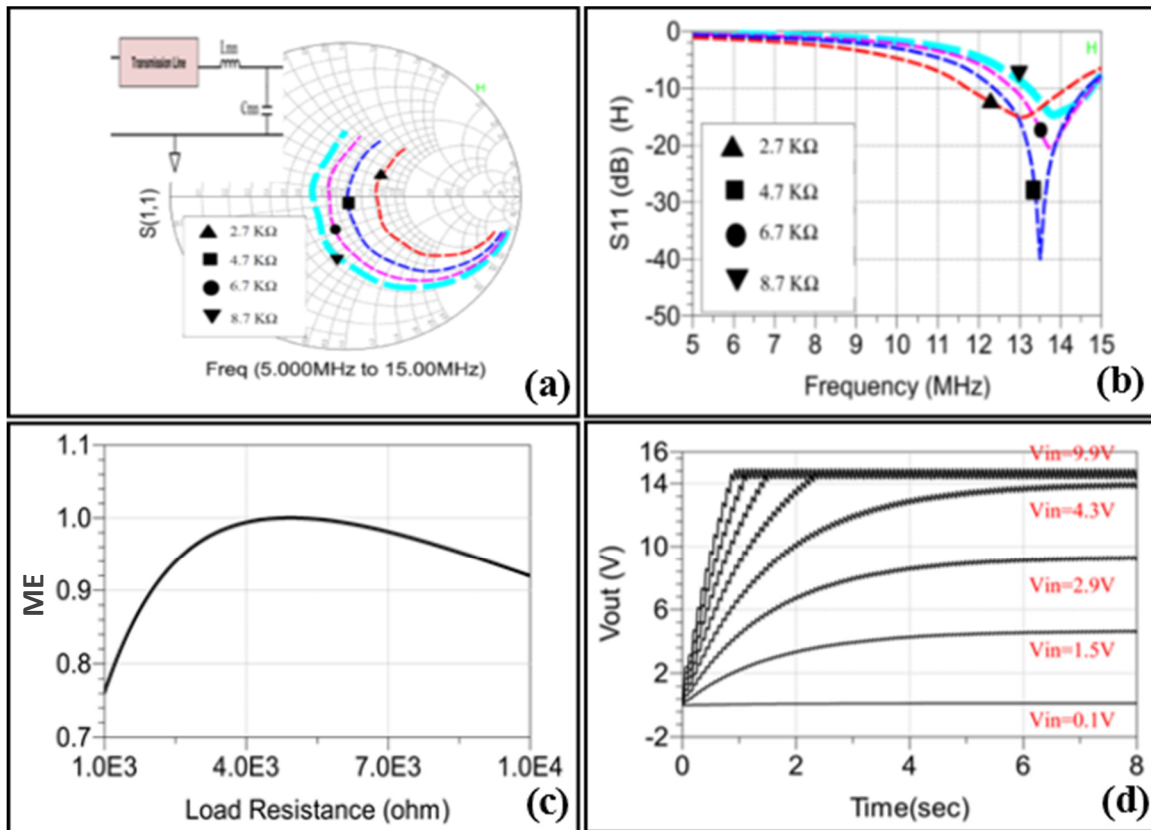


Figure 3.3 : S_{11} simulation for various load resistances, (a) smith chart, (b) log chart, (c) matching efficiency analysis versus load change at 13.56 MHz in the doubler structure, (d) transient simulation results for different input voltages.

3.3.1 Dickson Doubler Analysis

The basic building for multi-stage Dickson rectifier is a diode doubler which is shown in **Figure 3.1a** derived from a charge conservation analysis while considering the charge loss per AC cycle due to I_{Load} . The AC to DC voltage conversion is given by :

$$V_{DC} = \left(V_{in} \left(\frac{C_1}{C_1 + C_2} \right) - V_D \right) \times N - \frac{I_{Load} \times N}{(C_1 + C_2) \times f} \quad (3.2)$$

where V_{DC} indicates the DC output voltage at steady-state, V_{in} is peak value of AC voltage at rectifier input, V_D is threshold voltage of Schottky diode C_1 is the input coupling capacitor, C_2 is the stray capacitance, f is the switching frequency, I_{Load} is the load current, and N is the total number of diodes (2 for a doubler). As it was mentioned previously, capacitors play a critical role in rectifiers and multipliers. For instance, C_2 must be capable of driving the load current without getting influenced by the parasitic capacitance in Schottky diodes, while maintaining a constant output DC voltage with small ripples.

In multistage Dickson rectifiers, diodes are placed in parallel therefore incident sinusoidal RF input is directly applied to every diode. The total voltage drop across each diode calculated as:

$$V_d = -\frac{V_{out}}{2N} + V_{inRF} \cos(2\pi f_0 t + n\pi) \quad (3.3)$$

Subsequently, diodes current could be found from:

$$I_d = I_s \left[\exp\left(\frac{V_d}{V_T}\right) - 1 \right] \quad (3.4)$$

where I_s is the reverse-saturation current and V_T is the thermal voltage.

3.3.2 Multistage Dickson Rectifier

To study the effect of the number of doubler stages on the output voltage and efficiency of the rectifier circuit, two and three stage doublers are simulated with their input impedances matched to the 50Ω impedance of the power source. **Figure 3.4a** shows the 2-stage rectifier circuit with impedance matching network and the load connected to its output. **Figure 3.4b** presents the effects

of load variation in the range of 1 to 10 k Ω at 13.56 MHz on the matching efficiency of the rectifier. The maximum efficiency is achieved with a load equal to 4.7 k Ω , where the matching condition is satisfied.

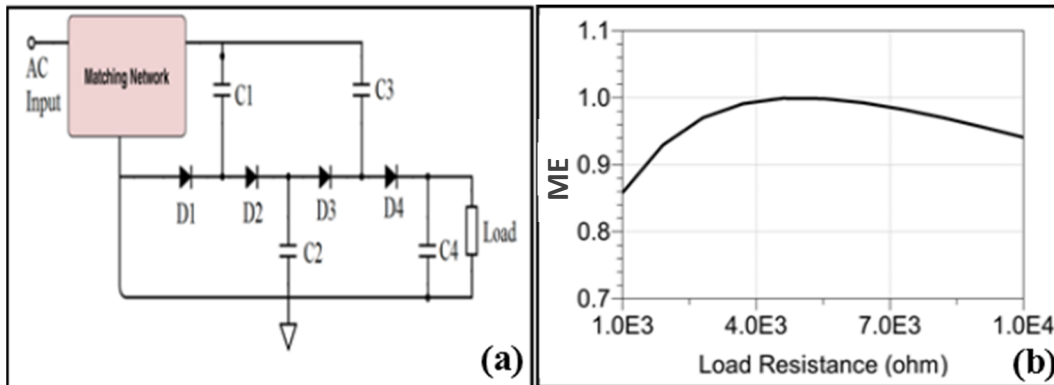


Figure 3.4 : (a) Circuit schematic of the two stages Dickson rectifier, (b) matching efficiency analysis for load range of 1 to 10 k Ω .

The transient response of the output voltage of the rectifier should also be considered, as it contains information about the settling time and ripple signal of the output voltage. To perform the transient simulation, a voltage source with output impedance of 50 Ω was used. The settling time and output DC voltage are studied for sinusoidal signals of various amplitudes (**Figure 3.5**).

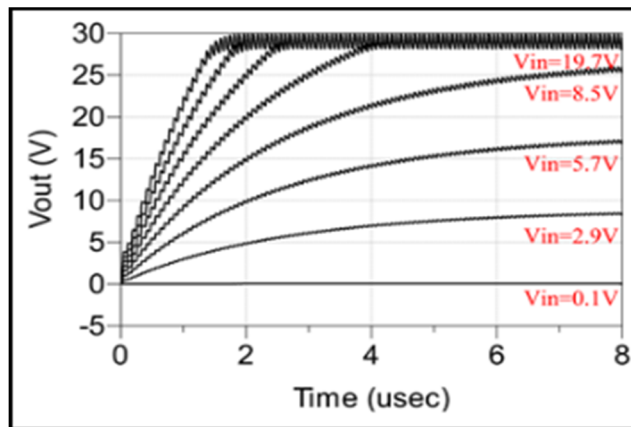


Figure 3.5 : Transient response of the output voltage in a 2-stage Dickson rectifier for different input signal amplitudes.

According to the simulation results, increasing the input signal amplitude reduces the settling time of the output voltage. Increasing the input signal amplitude beyond a certain point, however, has

no effect on the output signal amplitude since it is clamped by the reverse breakdown voltages of the diodes used in the rectifier structure.

Having an extra voltage doubler stage on the output of the 2-stage Dickson rectifier results in a 3-stage rectifier, as is shown in **Figure 3.6**. As presented in the circuit schematic, C_1 to C_6 are voltage storage capacitors with values of 470 pF. A matching network is used to ensure impedance matching between the receiver coil and the rectifier input. The implemented diodes in this structure are low bias Schottky diodes with reverse breakdown voltages of 15 V.

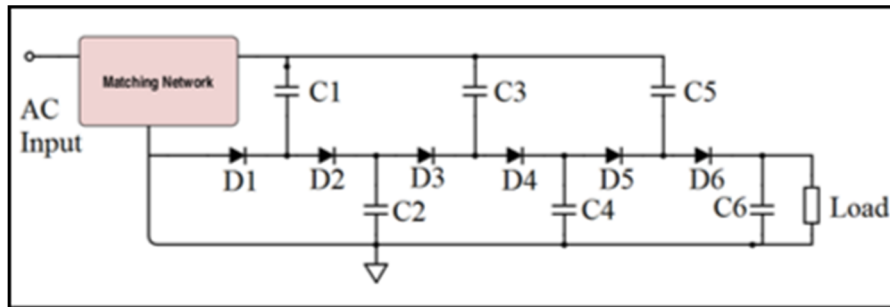


Figure 3.6 : Simulated circuit Schematic for a 3-stage Dickson rectifier with matching network

A complete set of S-parameter and transient response simulations of the 3-stage rectifier are presented in **Figure 3.7**. The Smith chart for the S_{11} simulation shows strong impedance matching at 13.56 MHz with respect to an input power of 0 dBm. The S_{11} magnitude result depicts acceptable power transmission from source to rectifier system for ± 2 MHz deviation from the matching frequency. Matching efficiency analysis is performed over a load variation from 1 to 10 k Ω . It has been demonstrated that the maximum efficiency is available at the load associated with the matching network, but the variation range is still within 90% of the converted power efficiency and is acceptable for WPT systems. A transient analysis is also provided to demonstrate the appropriate operation of the rectifier circuit for input sinusoidal signals with different amplitudes.

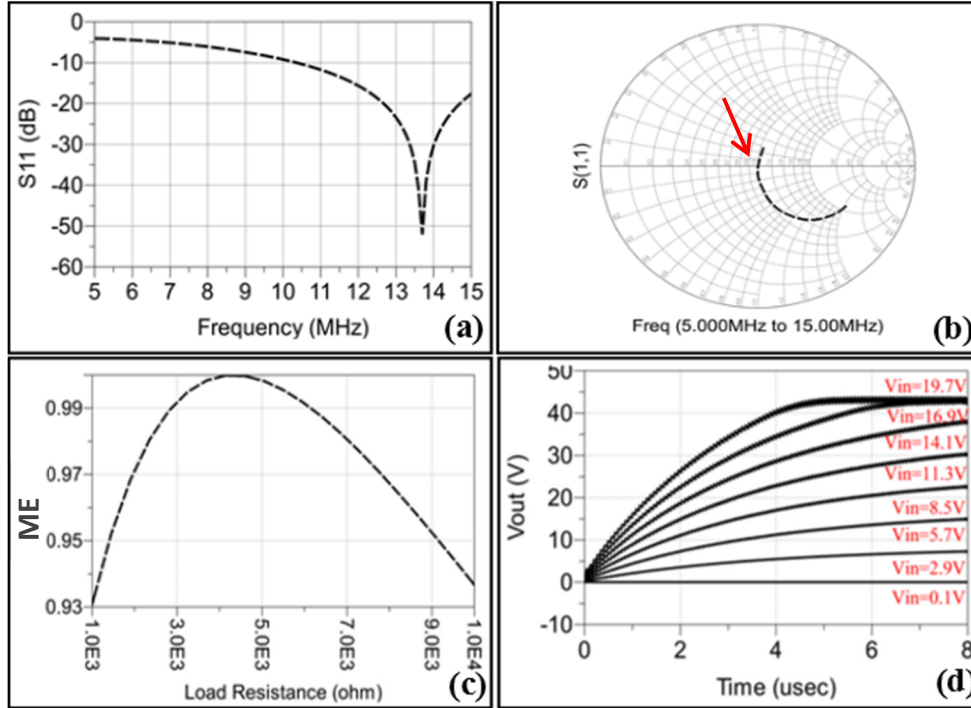


Figure 3.7 : (a) Smith chart of S₁₁ parameter, (b) magnitude of the S₁₁ at matching state, (c) matching efficiency analysis versus different resistance load, (d) transient analysis of the rectifier circuit for variable inputs

3.3.3 Multi-stage Rectifiers

Increasing the number of cascaded rectifiers affects the output voltage directly. In the ideal case the output voltage can be calculated using the following equation:

$$V_{out} = n \times \alpha \times 2V_{in} \quad (3.5)$$

where n is the number of stages and α is the compensation factor, which is determined by the matching network and component effects. In theory, any incremental output voltage can be achieved by increasing the value of n . In practice, voltage regulation and efficiency become increasingly poor as n increases. **Figure 3.8** presents the output voltage change versus response to variation of the input voltage amplitude at 13.56 MHz in the impedance matching condition.

As is shown, increasing the number of stages increases the dynamic range of the rectifier as a higher signal level is achievable in 2 or 3 stage rectifiers than what can be achieved with a single stage. The input signal amplifier should thus be designed with regard to the specific application.

For small input signal amplitudes (in this design < 5 V) using more than a single stage rectifier only increases the complexity of the circuit at the cost of implementation. However, consideration of the matching efficiency graphs in **Figure 3.8** supports the idea of using a higher order cascaded rectifier.

According to these results, increasing the number of rectifier stages reduces the effects of load variation on the matching efficiency significantly for loads in the range of 1 to 10 k Ω . Increasing beyond 3 stages would have less impact on matching efficiency, but potentially affects the power consumption, cost, complexity and required area of the implemented system.

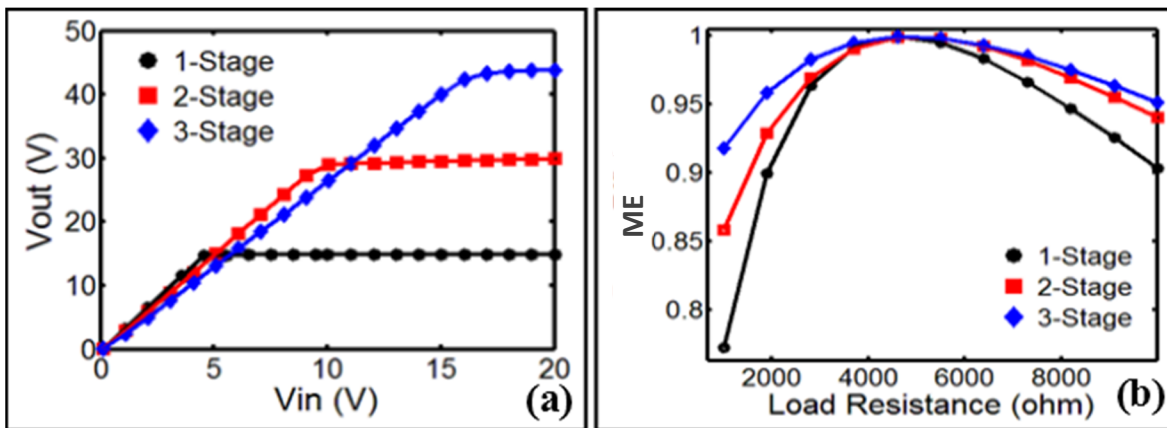


Figure 3.8 : (a) Output voltage versus input signal amplitude at 13.56 MHz for different numbers of rectifiers, (b) matching efficiency analysis and comparison of 1, 2 and 3-stage rectifiers versus output load

3.4 Implementation and Measurement Results

Simulation results for different numbers of stages suggest that the 3-stage Dickson rectifier is an appropriate, cost effective structure to implement, considering the initial requirements of the rectifier. Therefore a 3-stage rectifier was designed using ADS moment for the electromagnetic simulation and layout generation and fabricated by conventional circuit implementation on PCB, by performing heating lamination and chemical etching to realize the rectifier circuit (**Figure 3.9a**). **Figure 3.9b** shows the implemented 3-stage rectifier circuit with matching network and **Figure 3.9c** presents the Smith chart for the measured S_{11} parameter of the rectifier in unmatched, matched and open-load state.

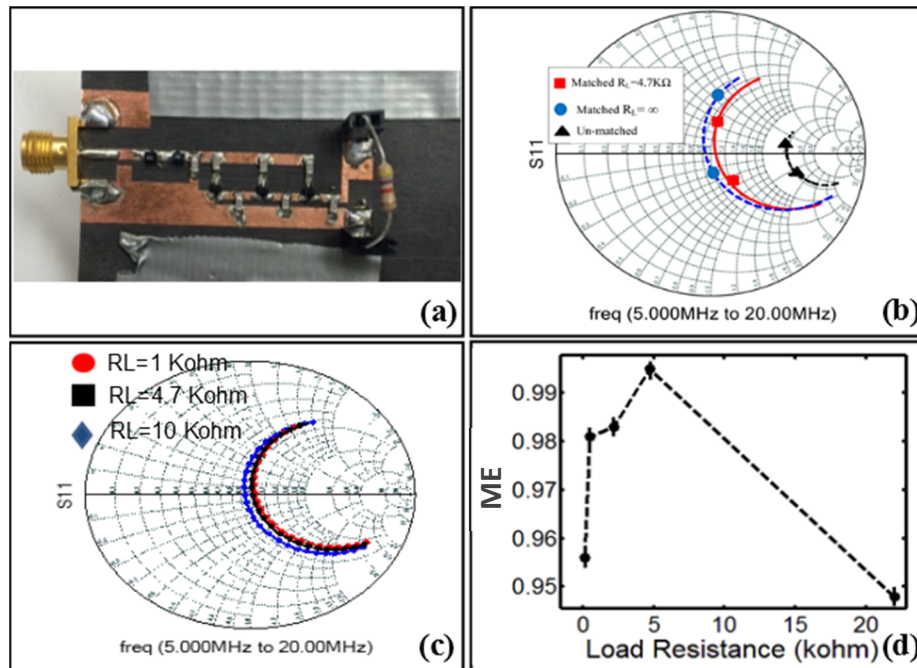


Figure 3.9 : (a) Circuit implementation for 3-stage rectifier circuit, (b) comparison for the matched and unmatched condition of rectifier circuit for 4.7 k Ω and open-load, (c) smith chart of S_{11} parameter for different loads, (d) effect of output load variation of the rectifier on matching efficiency

As mentioned, increasing the number of stages in the rectifier from 1 to 3 reduces the load dependency of the input impedance, and retains a matching efficiency better than 90 percent over a load variation of 100 Ω to 22 k Ω (**Figure 3.9d**). **Figure 3.9c** presents the measurement results of S_{11} for different load values of 1 k Ω to 10 k Ω . Smith chart analysis confirms that the resistance load variation has a very small effect on the impedance matching parameters.

According to the simulations, input applied power to the rectifier system can affect the input impedance and, consequently, the power efficiency since it changes the voltage across the nonlinear devices (diodes). This effect is studied in **Figure 3.10** for three different input powers of -20, -10 and 0 dBm. The initial matching circuitry is designed for 0 dBm input power, which shows a deep notch at 12.5 MHz. Changing the power from 0 to -10 and -20 dBm affects the diode operation and changes the diode current. Many diode parameters such as C_j and R_j are highly dependent on the bias voltage and the diode current, therefore change their values, affecting the entire rectifier system. These variations are demonstrated in the S_{11} parameter variation either in notch frequency or the notch depth. Dynamic matching circuitry can readjust the matching parameters in response to the variable input power and improve the rectifier operation significantly.

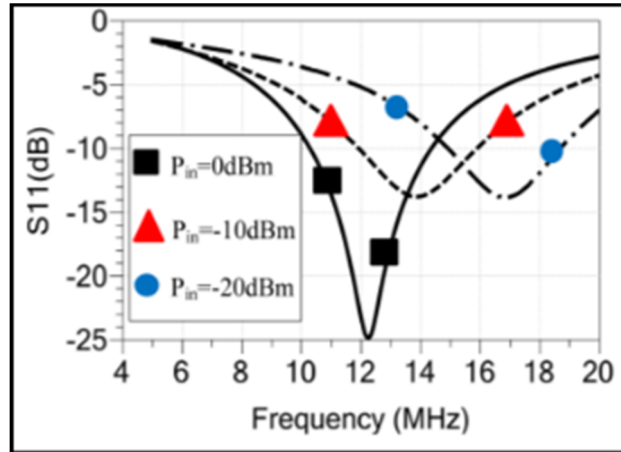


Figure 3.10 : Measured S_{11} parameters for different available power at the rectifier input.

3.5 Conclusion

Multistage voltage multipliers use diodes to rectify incoming RF signals and then charge capacitors during alternating duty cycles to provide higher multiples of the input voltage at the output of the circuit. The output voltage of voltage multipliers degrades quickly if the rectifier is highly loaded. Increasing the input signal amplitude is shown to decrease the settling time required for the voltage multiplier to reach its target voltage, but has limited effect on the output voltage. The output voltage clamps at a certain point, and ceases to increase with the input. Adding multiple rectifier stages is shown to increase this range of the output voltage, but multiplies power losses within the non-linear devices and does nothing to solve the voltage regulation problem.

The implementation of multistage voltage multipliers may not solve the voltage regulation problem, but provides superior performance in terms of the matching efficiency degradation observed with load variation. A three stage multiplier is shown to allow the rectifier to maintain a matching efficiency of better than 90% over a load resistance variation from 1 k Ω to 10 k Ω . The multistage device is thus able to provide a wider range of DC voltages to a wider range of load impedances for applications that do not have high loading requirements.

In order to maximize the power transferred to the rectifier from the antenna or coil that feeds it, a matching network is implemented. Such a matching circuit enables the multiplier to maintain high power efficiency, but its efficacy is dependent on the load resistance of the rectifier drives.

A given matching network is optimized for a given load resistance, however it performs poorly when the loading is varied. A dynamic matching network, which optimizes the impedance matching parameters to suit the varying load impedance, is suggested as a potential solution.

Chapter 4

Dynamic Real Time Matching and Tuning System

4.1 Motivation

One of the main objectives in wireless power transfer is to obtain high efficiency in the system. Several parameters can affect the efficiency, such as coil structure, distance between coils, load on the receiver side, number of simultaneous loads connected to one transmitter, and electric properties of WPT environment. Some of these parameters can be determined initially and properly treated; other parameters such as load, distance between coils and environment change are more chaotic and require real-time and in situ treatment. This chapter presents a novel-matching approach and dynamic impedance matching using capacitor matrix for real-time impedance matching. The effect on having dynamic matching network is studied in simulation for different coupling inductances for the transmitter and receiver side. Results demonstrate an improvement in power transmission efficiency in one to multi-node transmission systems, while the matching is mounted on the receiver node. The proposed WPT system is implemented and verified to provide 256 searching steps using eight capacitors and CMOS switches for large range of distance variation in between the transmitter and receiver coils.

4.2 Introduction

Different approaches have been reported to enhance the efficiency of wireless power system. The primary approaches are to increase the transmitter circuit efficiency [52]-[54]. This can be achieved either by increasing the efficiency of the signal-converter or using optimization technique in circuit selection. Additionally, several methods are described in different coil structures for enhancement of the WPT efficiency such as strongly coupled coils, repeater coils between transmitter and receiver coils and resonant coupling structures [55]-[57]. Optimization techniques are also studied and reported for power efficiency enhancement, altering the matching network circuit performing adaptive matching [58],[59].

Beh *et al.* have recently presented an automated impedance matching technique for WPT systems. They have mainly matched the resonance frequency of the resonator pair to the frequency of the power source in the transmitter side, using a capacitor bank and controllable switches. This has reduced the effect of varied air-gap on the efficiency of the WPT system and enhanced the power transmission efficiency. The search algorithm in this automated approach is the best step steepest descent search, which is feasible and simple in implementing the structure [58].

An adaptive matching network has been demonstrated by Lim *et al.* for power efficiency enhancement in WPT systems. It has been illustrated that the impedance mismatch occurs when the distance between the Tx and Rx coil changes. They have proposed a serial/parallel capacitor matrix in the transmitter, where the impedance can be automatically reconfigured to track the optimum impedance-matching point in different distances. Presented experimental results with 1W power transfer show that the transfer efficiency increases up to 88% when the distance changes from 0 to 1.2 m [59].

Evolutionary techniques using intelligent algorithms have recently demonstrated an attractive performance in WPT systems. Han *et al.* has demonstrated the genetic algorithm (GA) performance in optimum matching structure for transmitter node. Proposed structure has used GA to calculate the matching network components (capacitors) to reduce the frequency splitting effect and achieve the optimum efficiency in the system. The genetic algorithm utilizes a predefined circuit model as the fitness function and the extracted parameters are further used to obtain maximum efficiency [60].

Sondos Mehri *et al.* [61] used GA for geometry optimization of inductively coupled printed spiral coils for the powering of biomedical implantable systems. They realized an iterative design procedure using a genetic based algorithm to optimize the coil geometries for a maximum power efficiency. Reported results show that the inductive power efficiency was enhanced up to 17.5%.

European Space Agency [62] reported an evolutionary strategy and a method of moment antenna analysis to enhance the power transfer between multiple coils. In this work the shape of the coils and distance in between the transmitter and receivers are optimized performing optimization method based on GA. Coils with different shapes are the individuals for each generation chosen for the fitness function, which considers power transfer and wideband capability, to create a new generation of individuals. The process is then reiterated until an individual fulfilling some minimum fitness criteria is found. This method achieved an efficiency of 82% for single frequency power transfer over a distance of 0.65m.

In the previously reported researches on GA and WPT, the parameters of the WPT system were extracted at the first step. Then an evolutionary strategy was applied by using software, afterward a new system is built based on the optimized values. This methodology is not really efficient or applicable in most industrial cases since it has a delay between the optimization operation and applied improvement, which can be considered as a semi-offline method.

4.3 Study of Matching Effect on Power efficiency

This work studies resonance-based near-field power transmission using two air-coupled spiral coils which are associated with two resonance capacitors on the Tx and Rx sides. No coupling effect was considered in the initial design, and the capacitor and inductor values were calculated. The coupling effect is considered in the later designs, and compensation parameters are applied. The capacitor and inductor values in resonant-mode power transmission systems can be calculated using the following frequency equation, which is mostly used to present the resonant frequency in parallel RLC structures:

$$f = \frac{1}{2\pi\sqrt{LC}} \quad (4.1)$$

Here, f is defined by WPT standards (13.56 MHz), L is inductance value and a design parameter while C is the capacitor size depending on L at operation frequency. For the transmission side, the L and C parameters were calculated to be $L_t = 6.8 \mu\text{H}$ and $C_t = 13.25 \text{ pF}$. In practice, a variable capacitor with a maximum of 30 pF is used. On the receiver side, inductance and capacitance values of $L_r = 2.2 \mu\text{H}$ and $C_r = 53 \text{ pF}$ (variable capacitor with maximum value of 80 pF) are utilized. In addition to the LC resonant structure, matching networks are used on both the Tx and Rx sides to match the source impedance (standard 50Ω) to the LC network. The circuit model configuration of the transmitter/receiver structure is presented below in **Figure 4.1**.

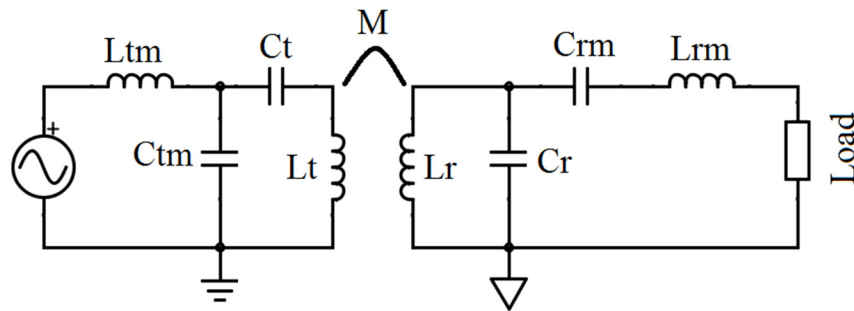


Figure 4.1 : The schematic of the wireless power transmission system

The simulation results for the S_{11} and S_{22} parameters are presented in **Figure 4.2**. As shown in this figure, narrowband matching can be achieved once the matching network has been established. This narrow band response can be very sensitive to the value of the components (L and C) and a very small variation or mismatch in the operation frequency or components can prevent power transmission and reduce the efficiency of the WPT system. In this design, two series resistances with value of 6Ω are used in both the transmitter and receiver to reduce the quality factor of the LC system and increase the band width of the LC circuits on the Tx and Rx sides.

Effect of coupling factor on the matching network and the reflected power can be considered as the load variation on the coil of the Tx node. A matched load can have constructive effect while unmatched load introduces destructive effects on the S_{11} parameter of Tx node.

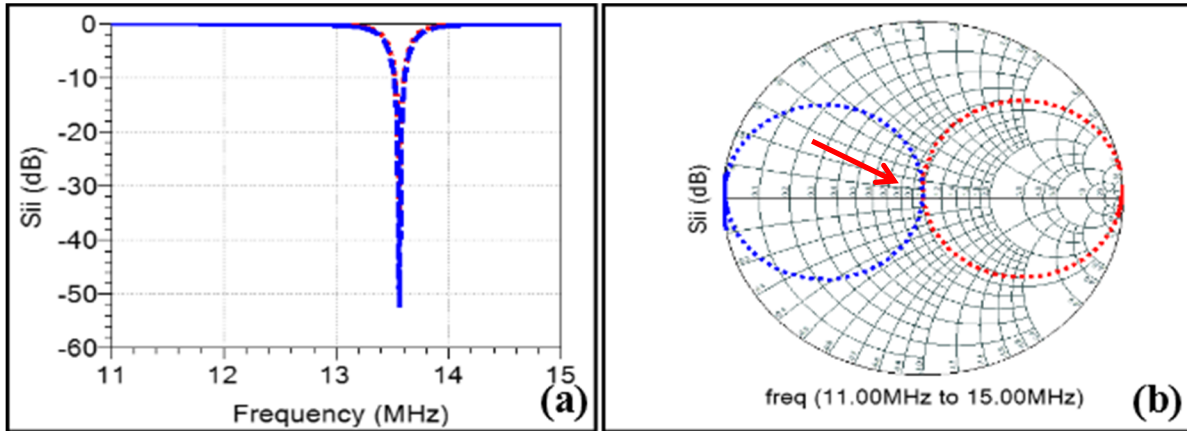


Figure 4.2 : (a) S₁₁ and S₂₂ simulation for Tx and Rx, log magnitude, (b) smith chart

The coupling effects of three different coupling factor parameters of $K=0.001$, $K=0.01$ and $K=0.1$ in Tx/Rx power transmission systems are studied in **Figure 4.3**. Increasing the coupling factor changes the initial matching S-parameters and frequency but enhances the power transmitted to the receiver side. A more extensive study of the K factor is performed at the system operating frequency (13.56 MHz) and the simulation results are presented in **Figure 4.4**.

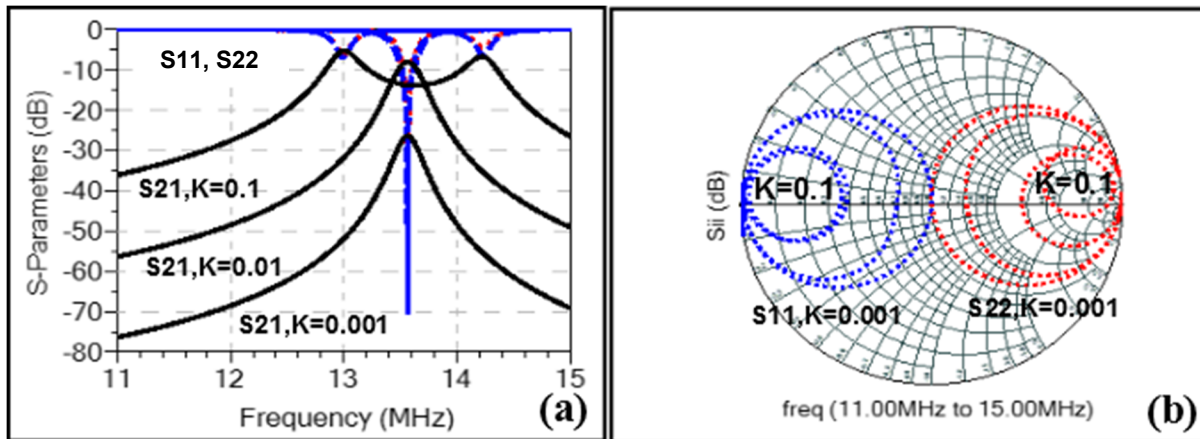


Figure 4.3 : S-parameters analysis for different coupling factors (K)

Increasing the coupling factor provides limited improvement in the transmitted power, but beyond a certain point begins to degrade power transmission exponentially as demonstrated in **Figure 4.4**. The presented graph has been extracted based on a single time matching method, where the matching was performed for only the initial coupling factor and kept constant for all other K values.

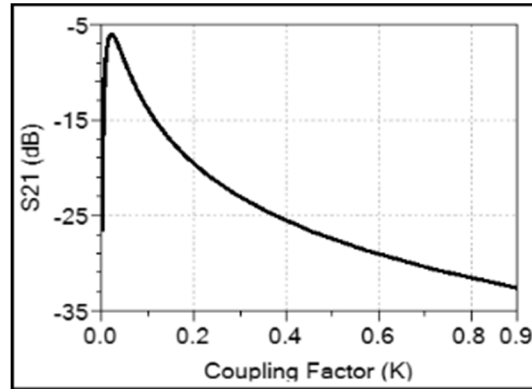


Figure 4.4 : Effect of coupling factor variation on the S_{21} parameter of a two coil WPT system with constant matching parameters.

The coupling factor is defined by the following equation:

$$K = \frac{M}{\sqrt{L_{Tx}L_{Rx}}} \quad (4.2)$$

Where K is the coupling factor, and M is the mutual inductance between the inductors L_{Rx} and L_{Tx} . The coupling factor is mainly affected by the mutual inductance between the coils. This mutual inductance can be affected by the physical shape of the coils, the distance between them, and the operational environment, and leads to change in coupling factor.

Change on the coupling factor between the transmitter and receiver coils affects not only the transmitted power level but also changes the resonant frequency of the coupled Tx/Rx coils. This variation consequently reduces the efficiency of the WPT system which operates at a standard constant frequency (13.56 MHz in this design). **Figure 4.5a** shows the effect of change in the coupling parameter from 0.001 to 0.5. The coupling factor affects the S_{21} parameter of the WPT system and the resonance profile of the WPT system, shifting the resonant frequency from 13.56 to 11.32 MHz and the S_{21} amplitude at 13.56 MHz from -3.5 to -27.4. Matching of S_{11} and S_{22} on both the Tx and Rx sides are degraded significantly (**Figure 4.5b**).

In conventional WPT systems the transmitter side is designed to transmit power at a standard frequency, which generally feeds more than one power receiver device. Therefore, changing the matching network parameters on the transmitter node, during the operation is not recommended. To achieve maximum delivered power efficiency, dynamic matching structure should be placed on the receiver node. This has been shown in **Figure 4.5c** where the changes in the matching network

(C_r and C_{rm}) values shifts the resonant frequency of the system back to 13.56 MHz. An enhancement of 24.5dB is observed after matching is performed at 13.56 MHz. This is an improvement of a factor of nearly 200 in the transmitted signal over reflected signal from the Tx to Rx receiver. It should be emphasized that the post-matching operation is performed on the receiver port (S_{22}) to avoid any change in the transmitter hardware and to deliver the maximum power to the load at the receiver side. The matching impedance is considered to be equal to 50Ω . As discussed in the previous chapter, the input impedance of the rectifier stage is matched to 50Ω and is almost completely independent of the load connected to the circuitry.

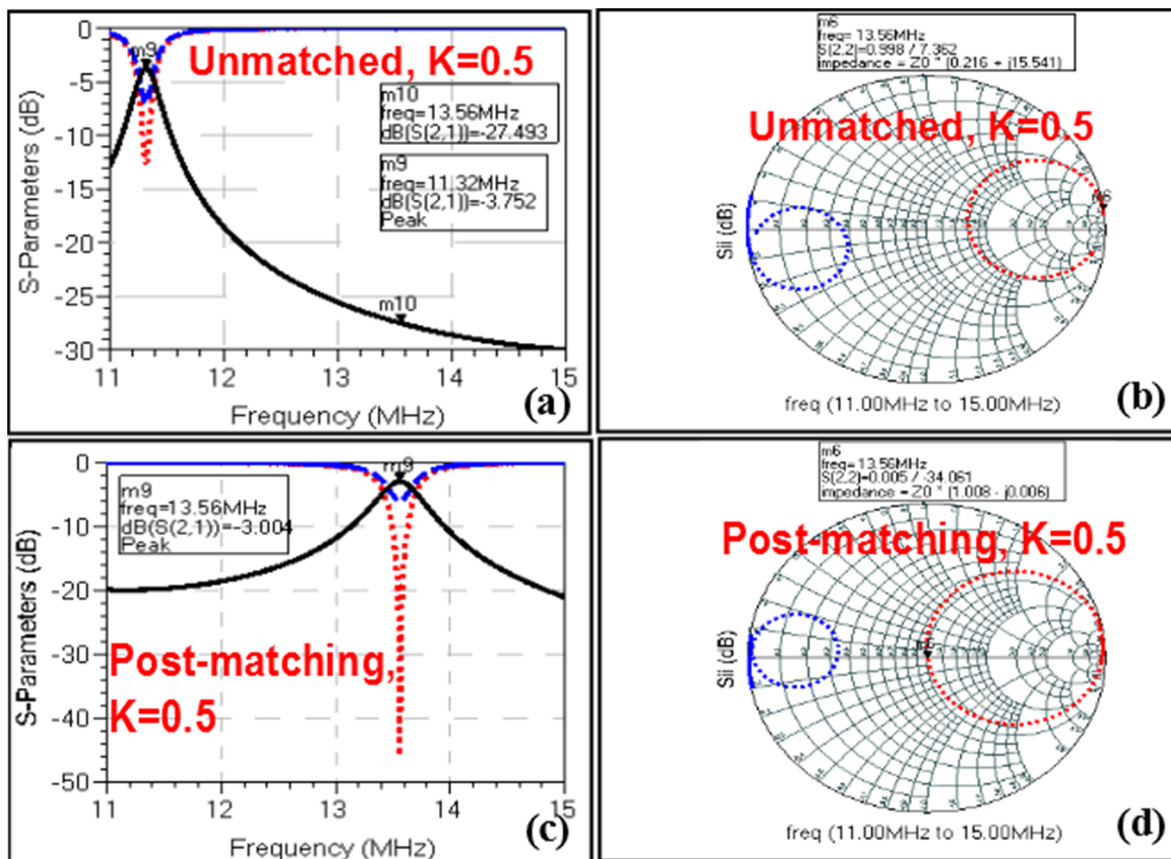


Figure 4.5 : (a, b) S_{21} Analysis of the WPT system for $K=0.5$ in unmatched state, and (c,d) after post-matching operation at an operational frequency of 13.56 MHz.

The simulation results presented in **Figure 4.5** demonstrate the main objective of this thesis, which is, the use of a dynamic matching network in the receiver node to optimize the power efficiency of the system for different coupling factors or variation in the system components. This technique is more advanced if it is used to transmit power from a single source to multiple receivers.

The post-matching operation can potentially improve the power efficiency of the WPT system in real time.

In most of the wireless power delivery scenarios, a transmitter coil feeds several independent receivers. This is considered in the circuit schematic of **Figure 4.6**. To simplify the simulation, no mutual inductance is considered between Rx₁ and Rx₂. In practice, this inductance can exist but will not affect the fundamental study presented in this section. The transmitter and two receivers are initially matched to 13.56 MHz without considering any coupling effect.

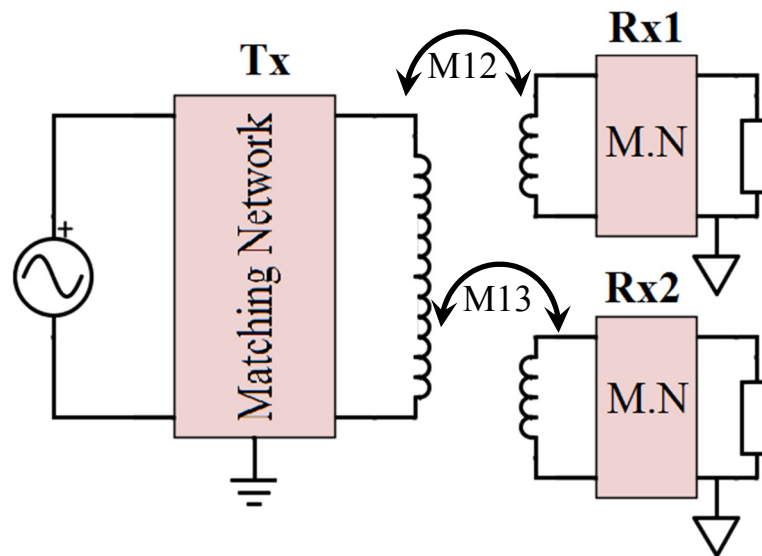


Figure 4.6 : Circuit schematic for a WPT system using a single transmitter to feed power to two independent loads.

The electromagnetic coupling is then applied between the Tx, Rx₁, and Rx₂ ports to yield the unmatched condition simulation as presented in **Figure 4.7**. For a more general model, the coupling factor between Tx to Rx₁ is considered to be $K=0.1$ and between Tx to Rx₂ to be $K=0.5$. Considering these coupling factors, the resonant frequency of S_{31} and S_{21} are shifted to 11.2 MHz and the amplitude of the S_{21} and S_{31} parameters at 13.56 MHz has dropped below -25 dB. This loading effect also has a negative impact on impedance matching as shown in **Figure 4.7b**. According to the presented simulation results in **Figure 4.7b**, without post-matching operation in the receiver node, the power efficiency will be highly affected when pairing other receiver devices to a single transmitter system.

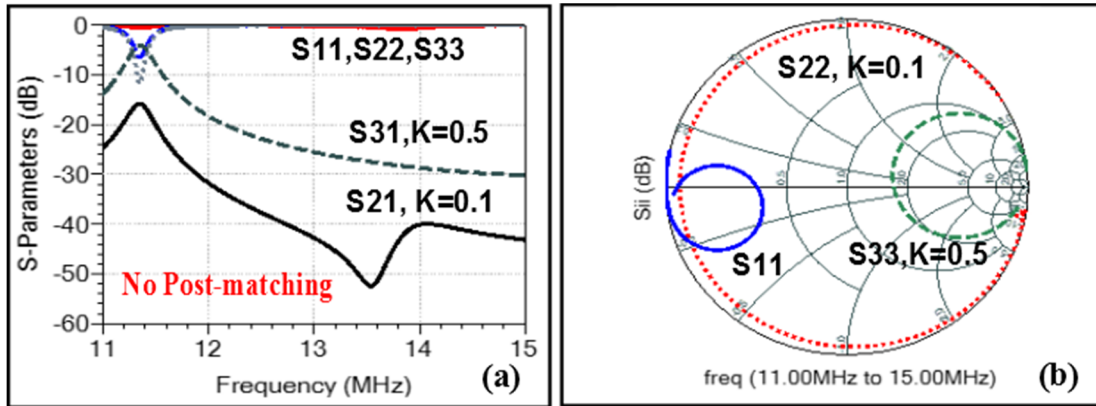


Figure 4.7 : (a) S-parameter simulation with no post-matching for the single transmitter WPT system with two independent receiver loads with different coupling factors of $K=0.1$ and $K=0.5$: Power transmission analysis, (b) matching analysis.

In the presented system, having a mutual coupling between the Tx and Rx coils degrades the initial matching of the nodes to the standard impedance (50Ω), and reduces the power efficiency consequently as discussed above.

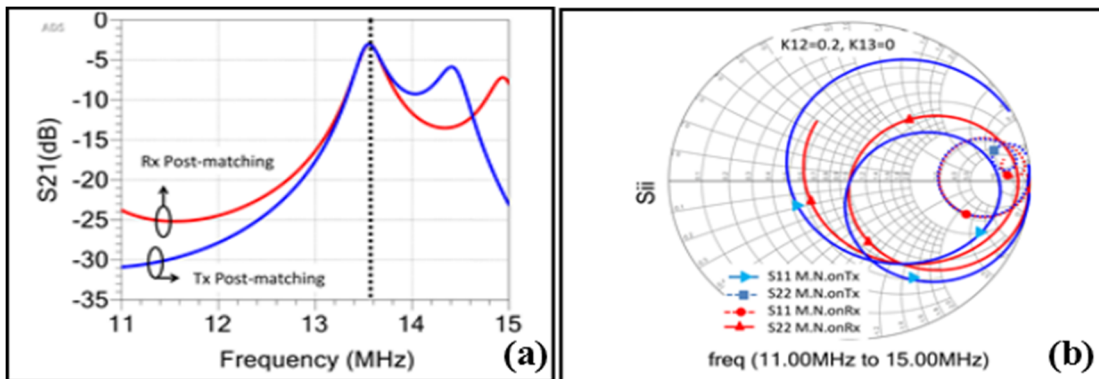


Figure 4.8 : (a) S_{21} for Tx to Rx for matching on Tx or Rx (b) matching performance results for Tx or Rx side.

A dynamic matching network can retrieve the efficiency by changing the matching network component's value and reestablish the matched condition. This dynamic system can be used either in Tx or Rx side, which generally is reported in the Tx side [59],[60]. The effect of matching network for both Tx and Rx sides is studied in simulation and presented in **Figure 4.8**. According to the presented simulation results in **0a**, in case of having loose coupling between the Tx and Rx₁ ($M_{13}=0$), the matching system can be used either in Tx or Rx₁ side and identical results on the power efficiency can be achieved.

To increase the power level delivered to the loads at port 2 and port 3 at a given operating frequency of 13.56 MHz, post-matching is applied. Implementing post-matching on receiver coil 2 should be expected to affect the power delivery efficiency on port 3 as well. This can be described by considering the following model. The voltage and current of the coils in Tx to Rx₁ and Tx to Rx₂ can be presented using the following equations:

$$V_1 = L_1 \frac{di_1}{dt} + M_{12} \frac{di_2}{dt} + M_{13} \frac{di_3}{dt} \quad (4.3)$$

$$V_2 = L_2 \frac{di_2}{dt} + M_{12} \frac{di_1}{dt} + M_{23} \frac{di_3}{dt} \quad (4.4)$$

$$V_3 = L_3 \frac{di_3}{dt} + M_{13} \frac{di_1}{dt} + M_{23} \frac{di_2}{dt} \quad (4.5)$$

Here, M_{12} and M_{13} are the mutual inductance between the transmitter coil and receiver coil 1 and 2, respectively, while M_{23} is assumed to be zero. Changing the coupling condition in Rx₁ can affect the response of Rx₂ therefore few iterations are required to achieve a semi-matched condition (to achieve complete matching more iterations are required).

Considering the coupling coefficients between Tx to Rx₁ is 0.2 ($K=0.2$), and Tx to Rx₂ is 0.5 ($K=0.5$), with a matching circuit at the transmitter side, the maximum power is delivered to the coil with higher coupling coefficient and the other coil with lower coupling coefficient, receives very low amount of the transmitted power at the operation frequency (13.56 MHz) permanently. Meanwhile, if no matching is performed on the Tx node and each Rx nodes have individual dynamic matching system, the delivered power to the receiver coils would be divided equally and both nodes can receive sufficient amount of power. This has been demonstrated in **Figure 4.9**. Therefore, for an ideal WPT system, dynamic matching networks should be placed in both Tx and Rx sides to prevent the unbalance power effect on the receiver nodes. This can increase the cost and complexity of the WPT system.

The simulations presented above show the significance of post-matching operations on the receiver sides. These operations can be used to enhance the power efficiency in case of any changes in the environment of the WPT system, the distance between the coils, or the system components, without interruption to the WPT regular operation. This post matching process can be performed using a portion of the received power by the receiver load.

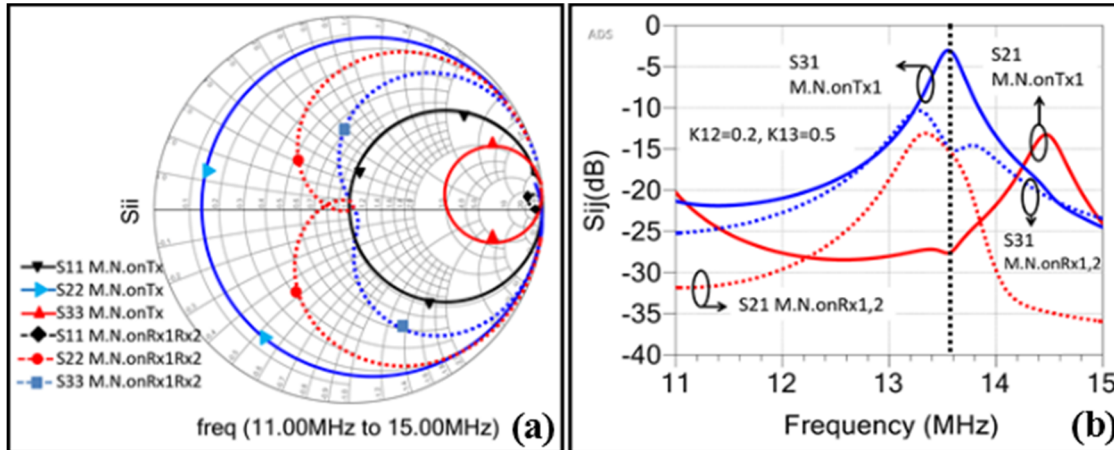


Figure 4.9 : S-parameter simulation with post-matching for a single transmitter WPT system with two independent receiver loads with different coupling factors of $K=0.1$ and $K=0.5$. Post-matching study on Tx coil or Rx₁ and Rx₂ coils, (a) matching analysis, (b) S_{21} and S_{31} analysis for post-matching on Tx coil or post-matching on Rx₁ and Rx₂ coils.

The main task for such a system is to sample the delivered power to the load, then adjust the matching and tuning capacitors C_m and C_r (**Figure 4.1**) through a switching capacitor bank to maintain maximum power output. Selecting the value of these capacitors can be frustrating, time consuming, and costly since all capacitors in a certain range must be implemented on the PCB board along with large numbers of switches to change the capacitor configuration so as to achieve the appropriate value.

The approach that has been proposed and implemented in this thesis uses a GA which is implemented by a microcontroller in a feedback loop to control the capacitor switches to achieve a large span of capacitor values. This technique is not a blind random selection technique. It uses the output DC signal from the rectifier and adjusts the capacitor values to maximize the DC voltage delivered to the load. Using DC voltage also has additional advantages. It avoids the use of high speed analog to digital converters or switches, it reduces the cost and implementation complexity and increases the system reliability for industrial and biomedical applications.

A system level architecture for the power receiver as discussed in the previous section is presented in **Figure 4.10**. This structure utilizes a capacitor bank to provide a wide range of tuning and matching capacity, an AC to DC converter, an analog to digital converter for sampling the DC signal from the rectifier output, and a microprocessor unit which implements a GA to adjust the matching and tuning capacitors. This structure has the advantages of real-time, low-power

operation while consuming minimum system power. This system has an idle mode where, if a sufficient amount of power is received on Rx side, the processing unit can reduce the power of the digital circuits and enhance its power conservation by operating in idle mode. In the next sections, more details for each block for the proposed system will be discussed.

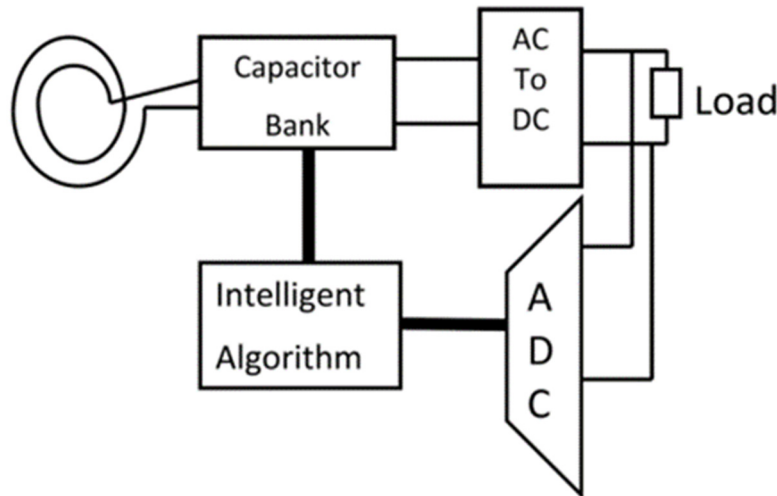


Figure 4.10 : System level description for the receiver unit of a WPT system with dynamic matching and tuning capabilities.

4.4 Motivation for Implementing an Intelligent Algorithm

Among the set of search and optimization techniques, the development of Evolutionary Algorithms (EA) has become very important in the last decades. EAs are used successfully in many applications with great complexity. Its success in solving difficult problems in the field of Evolutionary Computation (EC) is significant.

Most of the present implementations of EA come from one of three basic types: Genetic Algorithms (GA), Evolutionary Programming (EP) and Evolutionary Strategies (ES). Two groups have become particularly important: Genetic Programming (GP) pertains to many real problems and the lesser-used Classifier Systems (CS) are implemented for machine learning and for discovering rules in Rules Based Systems (RBS) (**Figure 4.11**) [63].

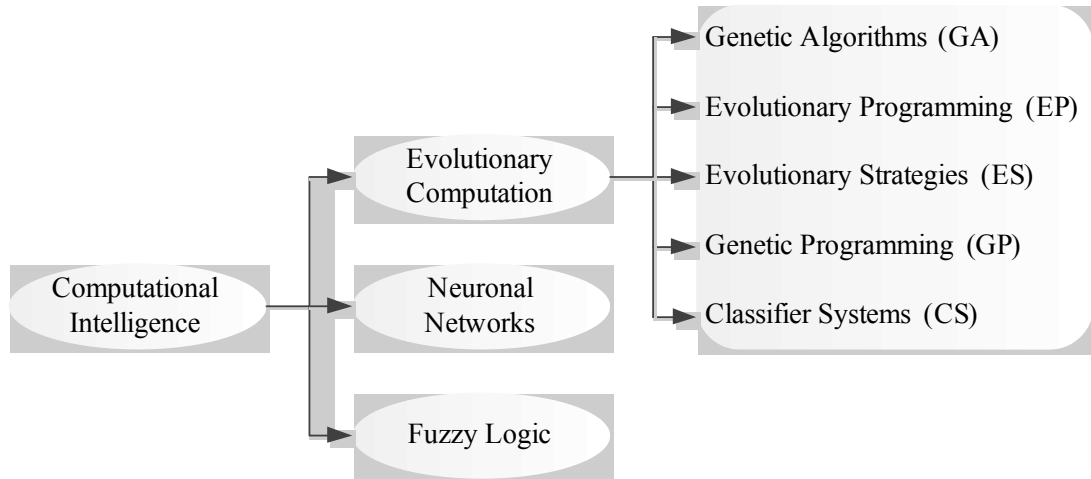


Figure 4.11 : Location of the different families of evolutionary algorithms

GAs function by maintaining a population of tentative solutions that are manipulated competitively through the application of variational operators to find a global optimum. GAs have proven to be the most popular of the three EAs. They are attempting to solve complex search problems in a simple frame work. Genetic algorithms effectively use two main EA operators: the cross-over as a main operator, and mutation as a background operation. Each run introduces new individuals by random number generators, which are defined as hybrid GA methods. This characteristic leads to escape from local optima, and requires high computational resources (large memory and search times). GAs have more advanced algorithms such as, Sequential GA, Parallel GA (PGA) and Hybrid genetic algorithm.

GA is applied to a population of strings (chromosomes), where candidate solutions are tested and assigned a fitness value in order to optimize and encode for an optimum solution. Traditionally, solutions are represented in binary strings of 0s and 1s, but other encodings are also possible.

The development starts from a population of randomly generated individuals as a generation. In each generation, multiple individuals are selected from the current population based on their fitness. Afterward, they are modified by using different operators such as recombination (cross-over) and possibly randomly mutation of a previous generation to form a new population. The new population is then used in the next iteration of the algorithm. Usually, the algorithm terminates when either a maximum number of generations has been obtained, or has reached some defined

sufficient condition. If the algorithm is terminated by a maximum number of generations, a satisfactory solution may or may not be achieved [63].

GA work is headed toward the possibility of using GA for real-time applications, above all adaptive controllers. In this work, GA is used as an evolutionary algorithm to perform dynamic matching and tuning of the impedance matching network in WPT to enhance power efficiency in real-time fashion.

4.4.2 Genetic Algorithm Operation

In GA the next generation of individuals is created by two popular EA operators: the Crossover and Mutation operators. Crossover is the main operator in GA, whereas mutation is a background operator. Operation description of each mentioned operators is briefly presented in the next subsections.

4.4.2.1 Crossover

The cross-over method is used to replace a gene of an individual with that of another individual. Individual pairs are selected randomly. In this section, two types of crossover operations are demonstrated. Some literatures e.g., Sywerda [64] and De Jong and Spears [65] focus on the genetic operators comparing the various crossover operators, particularly the numbers of crossover points. A relevant result of these works demonstrates an improvement on the final output, if the number of crossover points are increased.

One-point cross-over

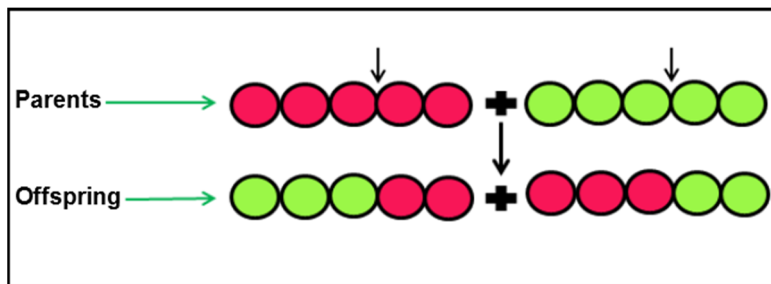


Figure 4.12 : One-point cross-over schematic

Two-point cross-over

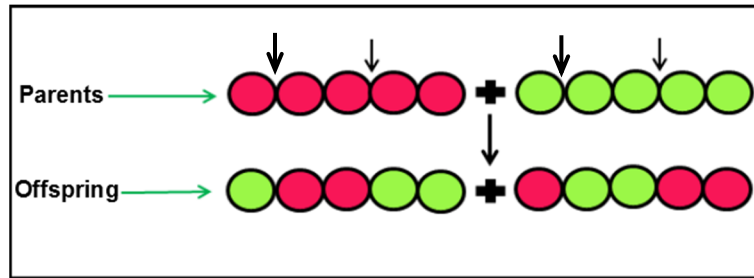


Figure 4.13 : Two-point cross-over schematic

4.4.2.2 Mutation

The mutation operator replaces the content of one bit of a chromosome with a randomly generated value.



Figure 4.14 : Mutation schematic

4.5 GA Algorithm Analysis and Implementation for Dynamic Matching Network

Different techniques have been recently investigated to perform the tuning or matching of the resonant frequencies in WPT systems. These techniques can be divided into two main categories of Online (or real-time) and Offline techniques. In real-time techniques, a feedback loop is implemented in conventional hardware to monitor the output of the WPT system. A microcontroller or processor has been used mainly to manage and analyze the feedback signal in order to control the matching network and achieve the highest possible output DC signal level. Changing the capacitor bank through the use of analog switches is the most common technique which is applied by an unguided search algorithm. In Offline techniques, if the output voltage drops substantially, analog switches associated with capacitor values are changed by a user to refine the output voltage.

In this technique, only limited number of states for the analog switches can be tested and though some improvement is usually achieved, it does not always result in the highest efficiency for the WPT system.

In the method proposed in this thesis, a real-time evolutionary hardware based technique is proposed to monitor the output voltage of the WPT system. An 8-bit analog to digital converter, which is internally mounted in the processing unit, is used to convert the sampled signal to the digital domain. Variation in the sampled signal, falling outside of the defined minimum or maximum level, triggers the processing unit and wakes it from the idle mode.

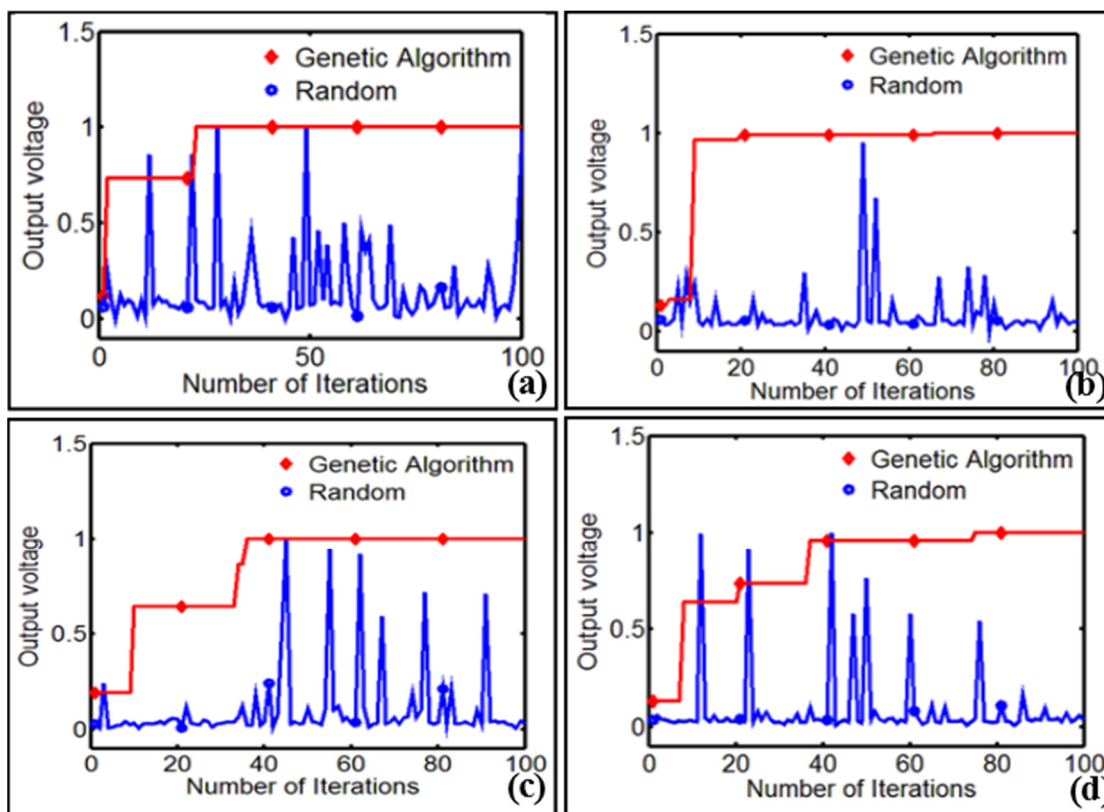


Figure 4.15 : Comparison on genetic algorithm convergence to randomly selected value of tuning capacitor in 2nd order transfer function

The processing unit runs the implemented GA and result of the first iteration is applied to the capacitor bank. Variation in the capacitor bank affects the output DC voltage of the rectifier. The DC voltage of the rectifier is used as the cost-function for the GA algorithm. The main task of the processing unit is to achieve the maximum possible DC voltage by changing the capacitor bank state. To evaluate the proposed evolutionary algorithm, a MATLAB program is developed

following the same procedure described above. The results of four different runs to a maximum iteration of 100 is presented in **Figure 4.15**. Since the program is implemented in MATLAB software with no access to the real-world hardware, a second order mathematical model (RLC-transfer function) is considered as the cost function. **Figure 4.15** compares the blind and GA search function regarding to converging rate (number of iterations) in order to achieve the maximum of the transfer function, which is considered to be equal to 1. The results presented in **Figure 4.15** clearly demonstrate the trend of GA to reach the optimal value. In GA the next generation is always improved, and unwanted genes are eliminated for the new iteration. To demonstrate the significance of GA, binary search algorithm is also implemented in MATLAB and the results are presented for variant resonant parameters. As shown in **Figure 4.16**, in binary search the number of iteration in two different runs has strong dependency on the parameter's value in the sorted format.

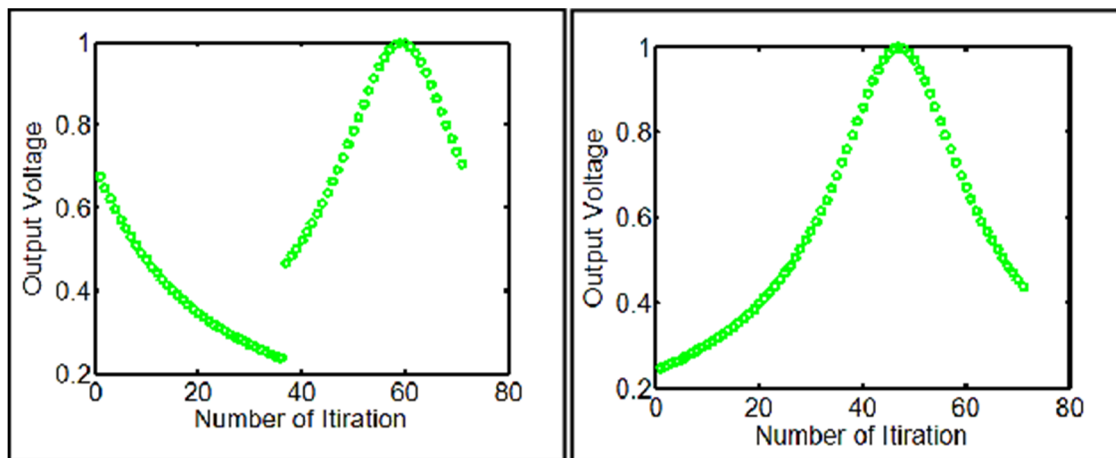


Figure 4.16 : Cost-function versus number of iteration in Binary search algorithm for two different runs

Genetic algorithm demonstrates a fast convergence rate, and directional convergence, where in each iteration GA has improved the result of the previous ones. A statistical analysis on the number of iterations for the GA in comparison to randomly generated tuning values is presented in **Figure 4.17**. In this study, both a GA and a fully random algorithm complete 200 runs, reaching a maximum of 100 iterations each run. As can be observed in the results, in 80 % of runs the GA converges to the maximum value in less than 40 iterations. For randomly generated numbers the distribution on the number of iterations versus the number of runs is almost uniform. 0.05% of the random search runs never satisfy the stop condition, whereas only 0.01% of the implemented

algorithm searches fail to reach stop. According the iteration distribution results, the proposed genetic algorithm converges to the desired value in 10 to 25 iterations with probability of 70 to 75%. These results confidently illustrate the advantages of using a GA algorithm over a random selection process when considering the convergence rate and response time of the algorithm.

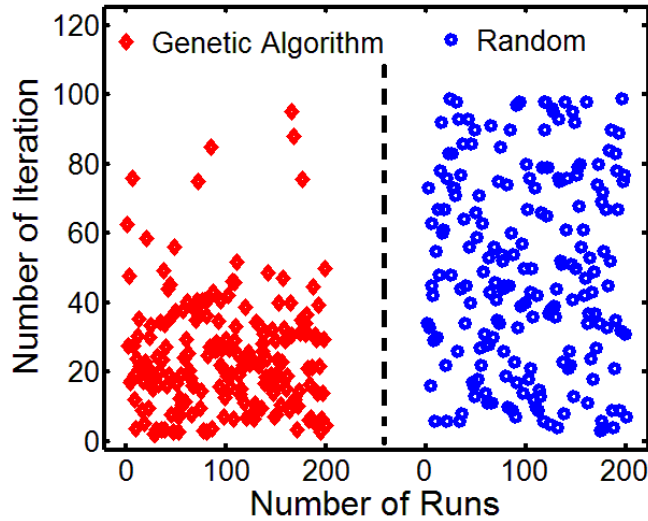


Figure 4.17 : Statistical analysis between genetic algorithm and random selection process for tuning of a second order transfer function.

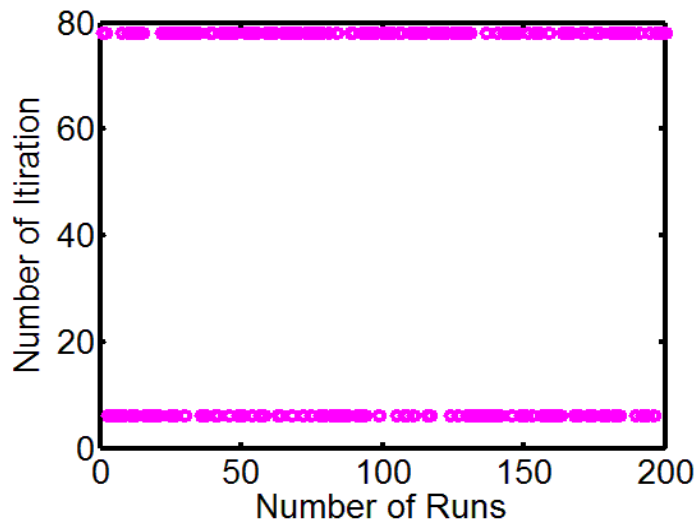


Figure 4.18 : Statistical analysis on Binary search algorithm over 200 runs.

The statistical analysis on number of required iteration for 200 runs is presented in **Figure 4.18**. According to these results, the number of iteration is always fixed and depends on the primary search direction on the sorted parameters.

Genetic algorithm has more complex and advanced methods such as parallel GAs, which have a higher conversion rate than the basic algorithm, which can decrease the response time of the hardware and increase the matching speed of the final system. However, these advanced algorithms have more complicated and difficult hardware realization. The complexity of the algorithms increases their convergence speed but require larger processors with more memory, logic gates, and input/output ports. Consequently, this increases the cost and power consumption of the receiver unit.

In WPT applications, it is common to use the received power as the power source for the control unit. It is imperative for the unit to utilize the minimum energy to avoid significant power consumption from the available power to the load. Power consumption, required hardware and area for algorithm implementation, and the response time are the three main parameters for both algorithm and the processor unit selection. **Figure 4.19** shows a flowchart of the algorithm implemented on a processor unit. Since this algorithm is implemented as proof of concept, it requires an external trigger to run the algorithm on the processor, but this can easily be replaced by a self-triggered operation system.

The algorithm starts by reading the output DC voltage, which is available at the output of ADC. The first generation with 8 digital control bytes are initiated. These control signals are applied to the switches and 8 analog DC voltages at the output of the rectifier are recorded associated with their digital control bytes. Then the recorded DC voltages are sorted and the control signal related to the maximum DC voltage is carried to the next generation. The next four bytes are generated as a nibble crossover between the four high ranked control signals while the fifth bit is a 1-bit mutation operation on the fifth ranked gen. The two minimum voltages with their associated control bits from initial generation are eliminated and new 2-bytes for the generation are generated randomly.

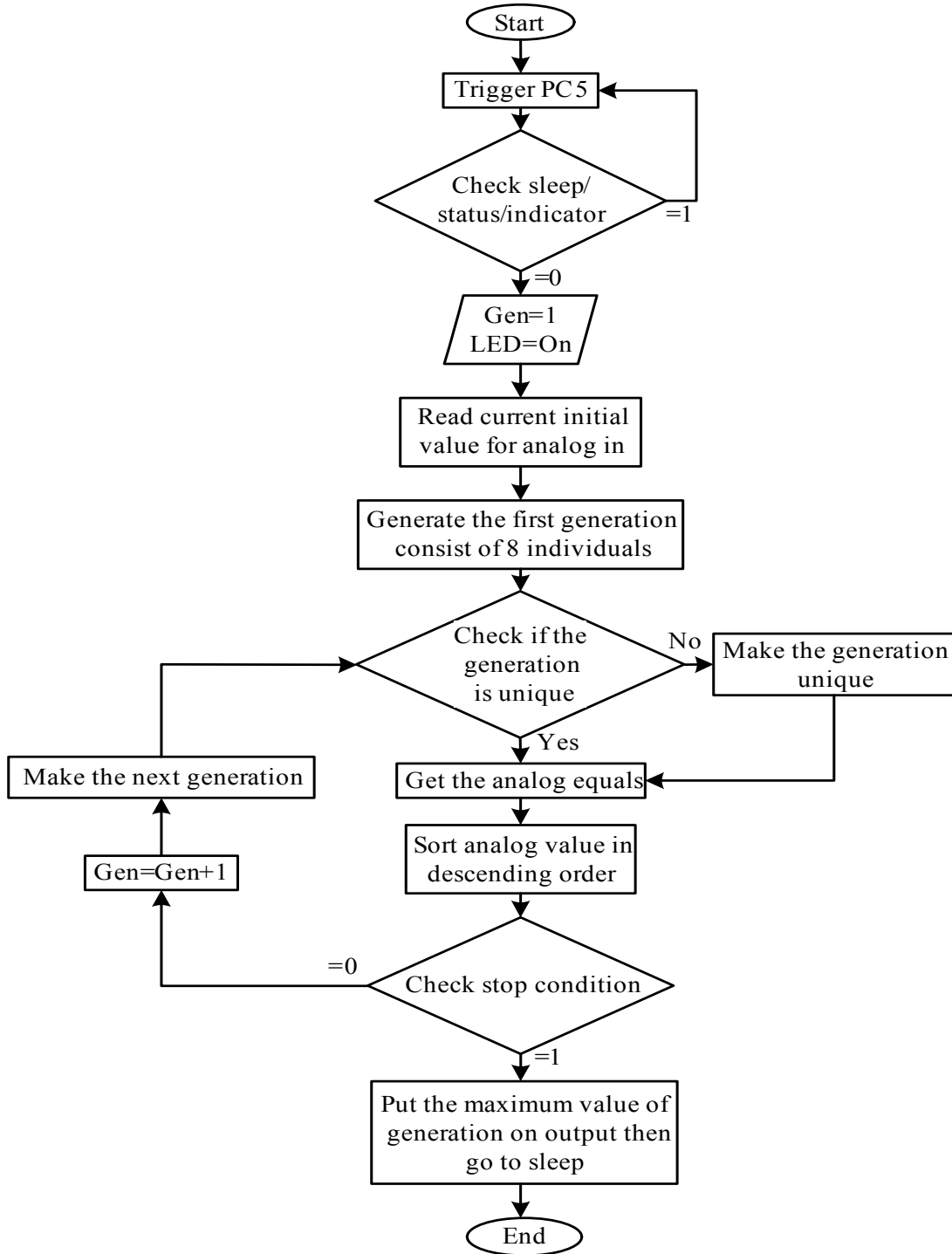


Figure 4.19 : Flow chart for the algorithm implemented in the processing unit for real time dynamic matching

The implemented algorithm is simulated in Proteus software and AVR studio. The results of the digital circuit simulation as well as the software environment are shown in **Figure 4.20**.

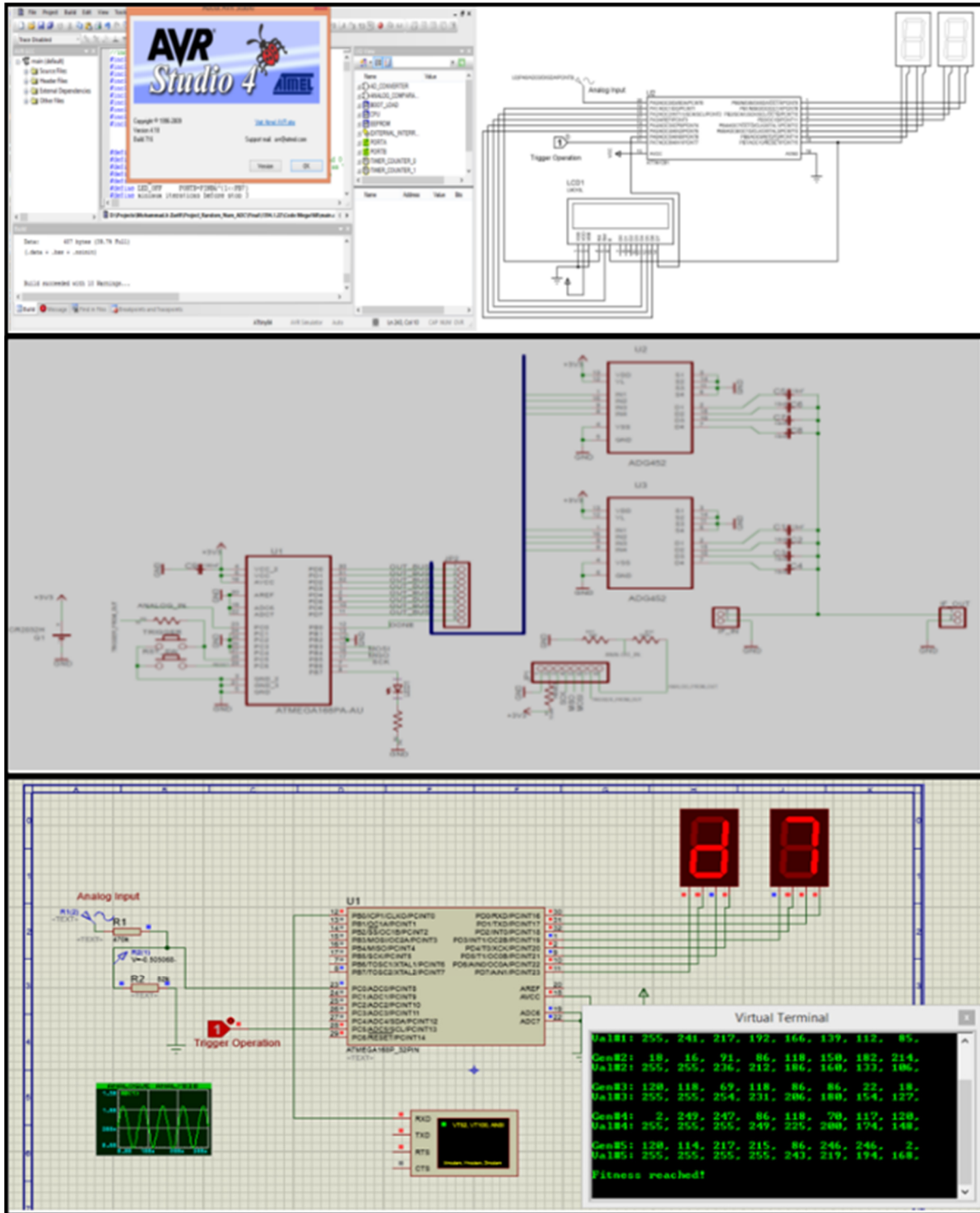


Figure 4.20 : Simulation environment for the digitally implemented algorithm, and the simulated hardware realization

4.5.1 Processing Unit and Intelligent Algorithm Implementation

The core of the processing unit in the proposed structure is an ATMEGA 168AP microcontroller from ATMEL Company. The selected microcontroller has a maximum full power consumption of 1 mW in its full operation cycle. This microcontroller has 8 internal analog to digital converters, though in this work only one of them is used to perform the sampling of the DC output voltage and convert it to the digital domain with 8 bit precision (for WPT applications 4 to 5 bits of precision is sufficient). The main considerations in selecting this microcontroller are the power consumption, the digital capacity to carry the algorithm, the physical size and the number of output pins available to directly control the switches associated with the capacitor network. Additionally, the operating supply voltage, power consumption in active mode and power-down mode, response time and operational frequency were also considered in selecting the microcontroller device. **Table 4.1** presents a comparison between different microcontrollers considering these main parameters.

Table 4.1 : Comparison of different microcontrollers with potential application for WPT systems

Specifications MCU	Pico Power?	Operating Voltage	Speed Grade	Power Consumption
Arduino-nano With core: AtMega(168P/321P)	Yes 28-pin PDIP, 32-lead TQFP, 28-pad QFN/MLF and 32-pad QFN/MLF	-1.8 - 5.5V	0 - 4MHz@1.8 - 5.5V, 0 - 10MHz@2.7 - 5.5V, 0 - 20MHz @ 4.5 - 5.5V	-Active Mode: 0.2mA -Power-down Mode: 0.1µA -Power-save Mode: 0.75µA (Including 32kHz RTC)
At-Tiny261/461/861	Yes 20-pin PDIP, 20-pin SOIC and 32-pad MLF	- 1.8 - 5.5V for ATtiny261V/461V/861V - 2.7 - 5.5V for ATtiny261/461/861	261V/461V/861V: 0 - 4 MHz @ 1.8 - 5.5V, 0 - 10 MHz @ 2.7 - 5.5V 261/461/861: 0 - 10 MHz @ 2.7 - 5.5V, 0 - 20 MHz @ 4.5 - 5.5V	- Active Mode (1 MHz System Clock): 300 µA @ 1.8V - Power-Down Mode: 0.1 µA at 1.8V
At-Tiny44A	yes 20-pin QFN/MLF/VQFN, 14-pin SOIC, 14-pin PDIP and 15-ball UFBGA	- 1.8 - 5.5V	- 0 - 4 MHz @ 1.8 - 5.5V - 0 - 10 MHz @ 2.7 - 5.5V - 0 - 20 MHz @ 4.5 - 5.5V	- Active Mode: • 210 µA at 1.8V and 1 MHz -Idle Mode: • 33 µA at 1.8V and 1 MHz - Power-down Mode: • 0.1 µA at 1.8V and 25°C
At-Tiny43U	Yes 20-pin SOIC and 20-pin QFN/MLF	- 0.7 - 1.8V (via On-chip Boost Converter) - 1.8 - 5.5V (Boost Converter Bypassed)	- Using On-chip Boost Converter • 0 - 4 MHz - External Power Supply • 0 - 4 MHz @ 1.8 - 5.5V • 0 - 8 MHz @ 2.7 - 5.5V	- Active Mode, 1 MHz System Clock • 400 µA @ 3V (Without Boost Converter) - Power-down Mode • 150 nA @ 3V (Without Boost Converter)
At-Mega8U	No - 28-lead PDIP, 32-lead TQFP, and 32-pad QFN/MLF	- 2.7V - 5.5V (ATmega8L) - 4.5V - 5.5V (ATmega8)	- 0 - 8MHz (ATmega8L) - 0 - 16MHz (ATmega8)	- Active: 3.6mA - Idle Mode: 1.0mA - Power-down Mode: 0.5µA

The ATMega168PA is a low-power, CMOS, 8-bit microcontroller, which has embedded analog to digital converters (ADC). This microcontroller is based on the AVR enhanced RISC architecture. By implementing instructions in a single clock cycle, the ATmega168PA attains throughputs approaching 1 MIPS per MHz, tolerating the system designers to optimize power consumption with respect to processing speed. The device core combines a rich instruction set with 32 general purpose working registers. All the 32 registers are directly connected to the Arithmetic

Logic Unit (ALU), allowing two independent registers to be accessed by one single instruction performed in one clock cycle. The architecture of the utilized microcontroller is code efficient and achieves throughputs up to ten times faster than conventional microcontrollers. The operation of this microcontroller in power-save mode continues running the asynchronous timer which allows the user to maintain a timer base while the rest of the device is sleeping. To have a very fast start-up with low power consumption, the crystal/resonator oscillator is running while the rest of the device is sleeping. According to the reliability qualification test results, provided by Atmel Company, the projected data retention failure rate is much less than 1 PPM over 20 years at 85°C or 100 years at 25°C.

4.5.2 Analog Switches

In the proposed structure, two switch devices are used to control the capacitance value of the capacitor bank. Each device has four internal switches, controllable with four control pins. Each switch has an on-resistance of 4Ω and can be sustained on +/- 15V of analog signal. This device has the advantage of LC²MOS fabrication process which enables the low power operation capability. Its fast switching speed and low cross coupling with high signal bandwidth makes the switch suitable for the tunable WPT application.

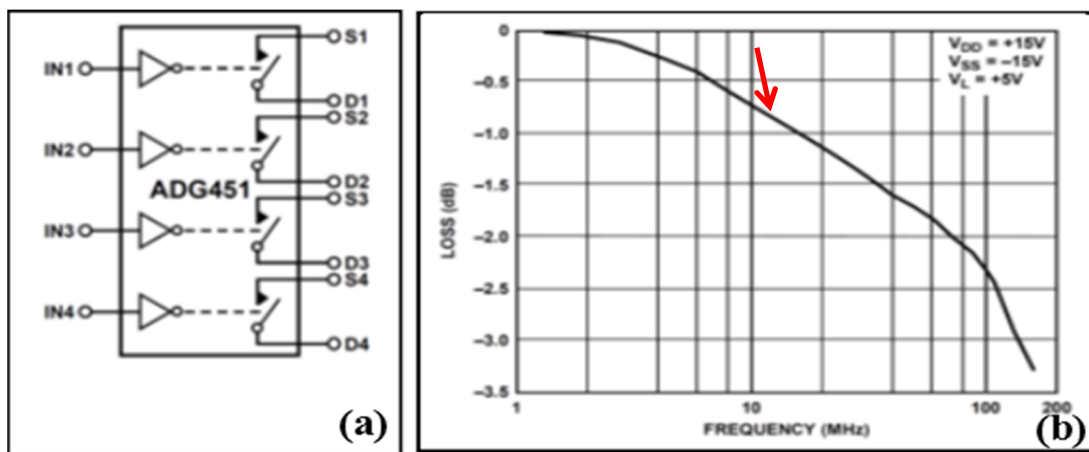


Figure 4.21 : Analog switch schematic with the loss vs. analog signal frequency, provided from datasheet

Figure 4.21a shows the schematic of the analog switch used in the reported system. Loss versus operation frequency is presented in **Figure 4.21b**, which demonstrates less than -0.75 dB loss at the targeted operational frequency of this work ($f=13.56$ MHz).

4.6 Circuit implementation and Fabrication of the dynamic matching technique for WPT system

The floor plan of the final design for the controller circuit is presented in **Figure 4.22a**. The PCB of the system is designed and Gerber file is extracted for PCB board fabrication. The final circuit is fabricated on FR-4 substrate, which is a glass-reinforced epoxy laminate printed circuit board. It has a dielectric permittivity of 4.1 and loss factor of 0.014 at 1MHz. the board implementation is performed in the University of Alberta's facilities using CNC milling machine. The power supply for the control system is provided using a lithium 3.3V coin shape battery.

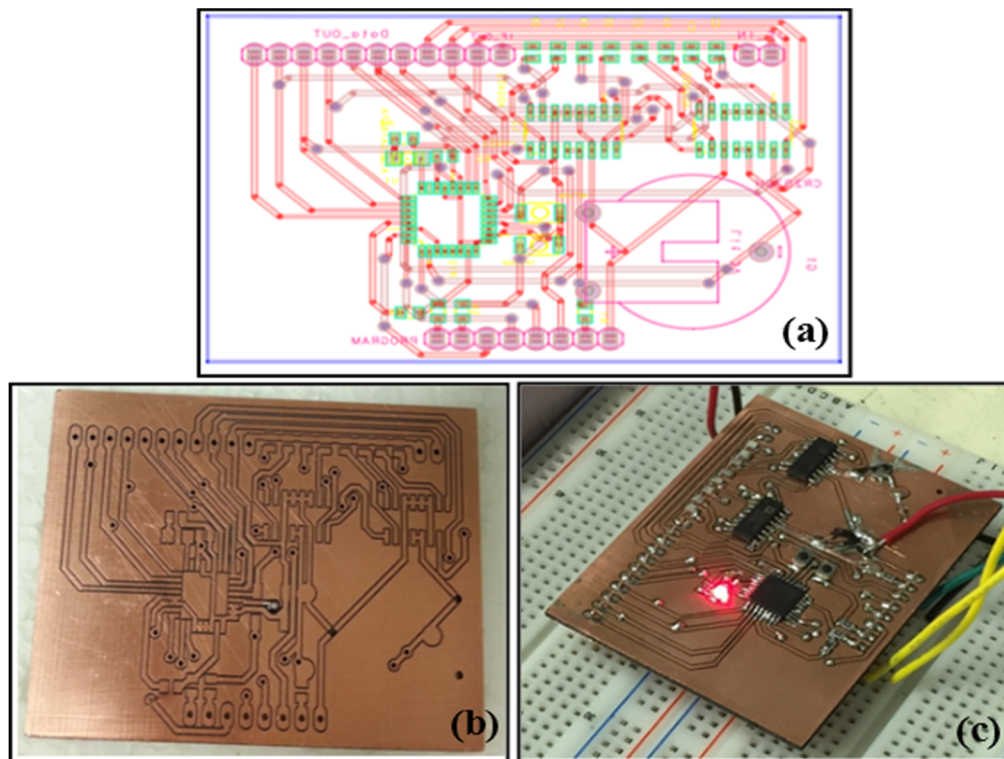


Figure 4.22 : (a) PCB layout of the controller circuit which is designed using top and bottom layer of the board, (b) fabricated circuit board and (c) implemented controller board operating in the system.

The application of the dynamic matching network with GA is studied in a WPT system for the receiver coil. The experimental setup of the final system is shown in **Figure 4.23**. A signal generator with signal amplitude of 7 Vp-p is used to provide the power to the Tx coil. Tx coil has initially matched to the standard impedance of 50 Ω at 13.56 MHz. At the receiver side a constant coil is connected to capacitor bank in parallel and a 3-stage rectifier is used to convert the RF signal to DC signal. A feedback loop is established between the rectifier output to capacitor bank using the microcontroller and analog switches.

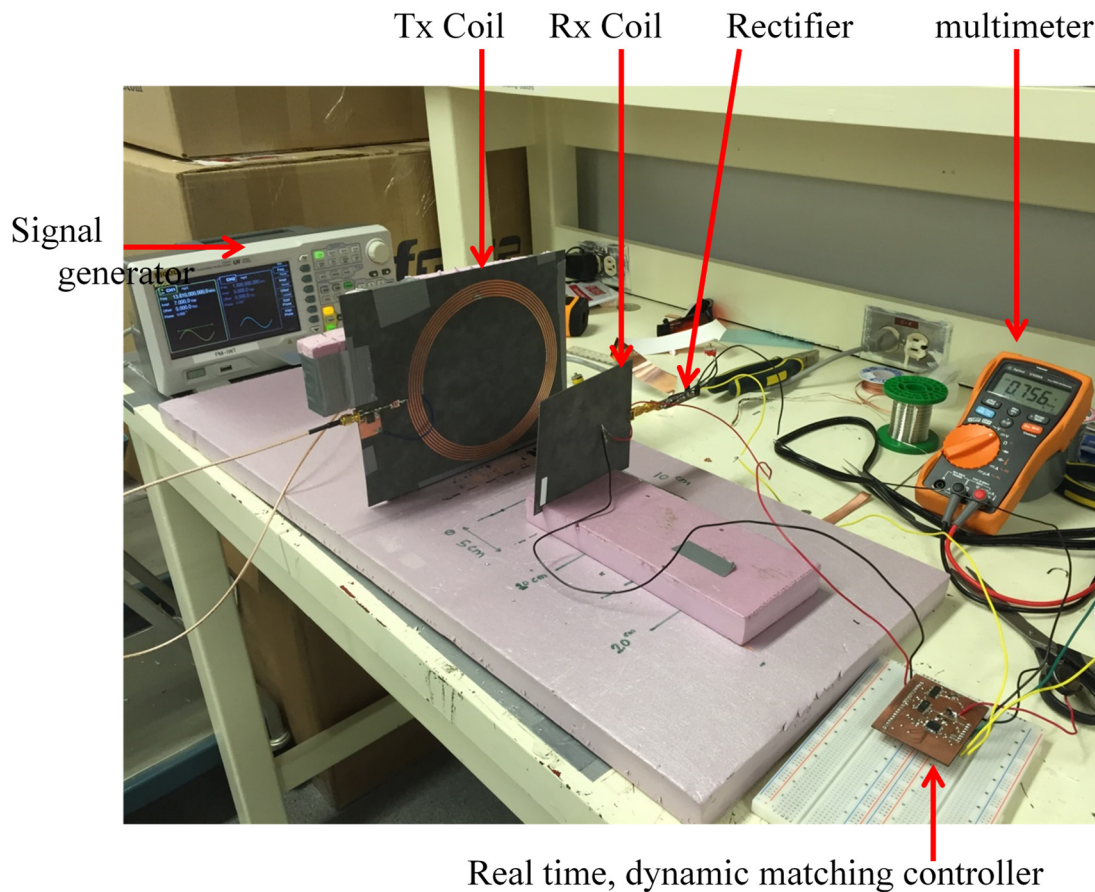


Figure 4.23 : Experimental setup for WPT using dynamic, real-time matching network, the processor utilizes intelligent algorithm for fast and assured convergence.

The distance between the transmitter and receiver is initially considered as 10 cm but the effect of distance variation is studied on this structure from 3 cm to 25 cm. The delay in the control system can be controlled by user. It has a minimum of 1 msec, since the capacitor bank and analog switches

should be stabilized for each control signal. Measurement results for this structure are presented in **Figure 4.24**. To record the data, the delay between each control signal is set to 200 msec.

Measurement results for output DC voltage of the rectifier demonstrates, for a constant output load, changing the distances between coils affects the coupling factor and transferred wireless power to the receiver side. However, performing the real-time dynamic tuning or matching (post-matching) enhances the DC voltage and improves the power, which is delivered to the load (**Figure 4.24a**). Next experiment is to change the input frequency of the sinusoidal signal with constant amplitude of $1V_{p-p}$ and study its effect before and after post matching for a constant load. **Figure 4.24b** shows at 13.56 MHz the output voltage has maximum value and post matching has significantly improved the output DC voltage amplitude.

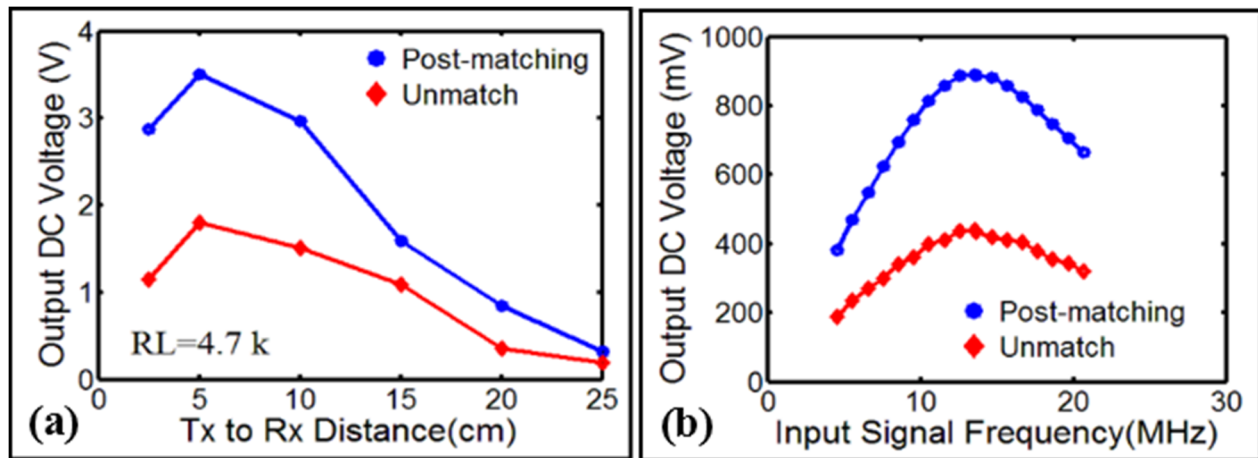


Figure 4.24 : (a) Measured results of output DC voltage versus different distance between Tx and Rx coils before and after real-time matching, (b) Measured output DC voltage for a sinusoidal signal with a constant amplitude of 1 V at different frequencies for unmatched and post-matched states.

4.7 Conclusion

Changing the distance between the transmitter or receiver coils has significantly corrupted the maximum power transfer efficiency, measured between the resonant coils of the transmitter and the receiver in traditional wireless power transfer systems. This degradation on the efficiency is mostly related to the impedance mismatch, which originates from the coupling variation between the coils. In the presented work, an adaptive real-time matching method based on genetic algorithm is presented for dynamic impedance matching performance. The reconfigurable matching network

is enabled by using analog switches to change and establish different capacitive values with different configuration. In order to have a fast and reliable capacitor selection which achieves the maximum power transfer efficiency, GA based search algorithm is proposed. The WPT system reinforced by adaptive matching network works with up to 91% power transfer efficiency improvement for variant distances between coils.

Chapter 5

Conclusion and Future Directions

5.1 Conclusions

This thesis addressed the power efficiency enhancement techniques in the context of RIC wireless power transmission systems utilizing real-time impedance matching network. The major contributions of this thesis are summarized as follows:

- A non-grounded metallic structures was proposed to be used as electric power and signal propagation medium to deliver electric power locally to the receiver nodes when they were in vicinity of the metallic structure. In contrast to, the conventional WPT systems, which required two double-ended resonant coils coupled together, this novel technique required one double-ended coil coupled to an open-ended coil which was locally fed by a metallic structure. A comprehensive study on open-ended coil structure demonstrated the dependency of transmitted power efficiency on ground-plane size and distance from the coil. According to the presented results, impedance matching networks were necessary to achieve the highest power efficiency in open-ended coils. Therefore, an impedance matching technique using virtual ground was presented for open-ended resonant coils to maintain an efficient power delivery, where no actual ground signal was accessible.

- Implementation of a multistage voltage rectifier-multiplier was studied to rectify and multiply the received input RF signal to DC voltage at its output. It has been clearly shown that the loading effect of the rectifier-multiplier on the input matching network can be eliminated using several number of rectifier stages. A three stage multiplier was shown to allow the rectifier to maintain a matching efficiency of better than 90% over a load resistance variation from 1k Ω to 10k Ω . The multistage device was thus able to provide a wider range of DC voltages to a wider range of load impedances for applications that had less-loading requirements.
- Distance variation between the transmitter and receiver coils could potentially corrupt the maximum power transfer efficiency in traditional wireless power transfer systems. This degradation on efficiency was mostly related to the impedance mismatch, which was originated by the coupling effect between the coils. As a new approach, an adaptive real-time matching method based on genetic algorithm was presented for dynamic impedance matching performance. Analog switches along with capacitor bank and a processing unit enabled the realization of the reconfigurable impedance matching network. GA based search algorithm was proposed to enable a fast dynamic impedance matching network in the receiver node. The WPT system reinforced by adaptive matching network worked with up to 91% power transfer efficiency improvement for variant distances between coils. Additionally, it has been demonstrated in the measured and simulated results that for a multi-receiver node from a single transmitter coil system, dynamic impedance matching network is preferred on the receiver node than the transmitter node in order to guarantee the maximum and equal delivered power to the receiver nodes.

5.2 Directions for future Research

A potential future work can be the investigation on the coil structure for open-ended coils and improvement of its operation in power and data communication systems. As discussed on the open-ended coil structures, internal capacitor in between the traces significantly degraded the efficiency of the coil and introduce loss in transferred power. One potential solution can be utilizing a 3D printed coil and changing the isolation material between the traces while using non-planar structure.

Conclusion and Future Directions

Moreover, effect of repeater coils in the open-ended coil structure can be studied to achieve the maximum power transfer efficiency in larger distances from the transmitter coil.

More future works can be performed on dynamic matching of the system. In this work, GA was considered as the search algorithm since its implementation was simple and low cost. However, other evolutionary techniques can be investigated to reach a WPT system with dynamic matching system with fast response. Progress on search techniques improvement on software can be combined with hardware study. This work utilized capacitive bank which in some applications such as biomedical implantable devices where the size of the system is critical, is challenging. Considering varactor capacitors in combination with capacitor bank can be the potential alternative solution. Employing the backscattering techniques for real-time monitoring of the delivered power amplitude is another road map for the future works. In this technique variation of the DC voltage at the rectifier output can be transferred to a frequency shift using a ring voltage controlled oscillator. An analog switch in parallel with a receiver coil can create considerable impedance variation by shortening the input coil terminals in the receiver. This effect can be translated as reflected power variation in the transmitter node. Using the backscattered signal in the transmitter, dynamic variations in the receiver node can be continuously monitored. Additionally, the transmitted power level and efficiency can be controlled by changing the amplitude of the power source or by altering the impedance matching network in the transmitter node.

An attractive application and future plan for this work is utilizing the received power level in the receiver or reflected power signal in the transmitter as a sensing parameter for study of environmental parameter variation. In RIC systems, each coil in the transmitter or receiver side is associated with capacitor array to establish the resonant condition. These capacitors can be a fixed capacitor or variable capacitor where its value can be adjusted by environmental and physical parameters such as humidity or materials permittivity. The variation in the capacitor of the resonant coils can be translated to power level variation and be used in sensing applications consequently. If the sensing potential of this device is proven with respect to the sensitivity and selectivity parameters, a broad range of applications can be considered as a future work using the WPT systems.

Bibliography

- [1] http://batteryuniversity.com/learn/article/the_future_battery
- [2] http://batteryuniversity.com/learn/article/battery_statistics
- [3] <https://www.ec.gc.ca/mercure-mercury/default.asp?lang=En&n=8E1CA841-1>
- [4] Dick, Christian Peter, Christian Polak, and Eberhard Waffenschmidt. "Proposal of a figure of merit for the characterization of soft-magnetic shielding material used in inductive wireless power transmission systems." *Emerging and Selected Topics in Power Electronics, IEEE Journal of* 3, no. 1 (2015): 272-279.
- [5] Ishida, Hiroto, and Hiroshi Furukawa. "Wireless Power Transmission Through Concrete Using Circuits Resonating at Utility Frequency of 60 Hz." *Power Electronics, IEEE Transactions on* 30, no. 3 (2015): 1220-1229.
- [6] Occupational Safety and Health Administration, Cincinnati Technical Center (May 20, 1990). "Electromagnetic Radiation and How It Affects Your Instruments. Near field vs. Far field." (Department of Labor – Public Domain content. Most of the content referenced by this work in this article is copied from a public domain document. In addition, this paper has provided references.). U.S. Dept of Labor. Retrieved 2010-05-09.
- [7] Rappaport, Theodore S. *Wireless communications: principles and practice*. Vol. 2. New Jersey: prentice hall PTR, 1996.
- [8] Dargie, Walteneus W., and Christian Poellabauer. *Fundamentals of wireless sensor networks: theory and practice*. John Wiley & Sons, 2010.
- [9] Brown, W.C. The history of power transmission by radio waves. *IEEE Trans. Microw. Theory Tech.* 1984, 32, 1230–1242.
- [10] Brown, W. Experiments in the Transportation of Energy by Microwave Beam. In *Proceedings of the IRE International Convention Record*, New York, NY, USA, 21–25 March 1966; pp. 8–17.
- [11] Glaser, P.E. Power from the sun: Its future. *Science* 1968, 162, 857–861.
- [12] https://en.wikipedia.org/wiki/Resonant_inductive_coupling
- [13] Li, Weilai. "High efficiency wireless power transmission at low frequency using permanent magnet coupling." (2009).
- [14] Dilip Chaurasia, Santosh Ahirwar, "A Review on Wireless Electricity Transmission Techniques".
- [15] wikipedia. [Online] http://en.wikipedia.org/wiki/Near_and_far_field.
- [16] M. Zargham and P. Gulak, "Maximum Achievable Efficiency in Near-Field Coupled Power-Transfer Systems," *IEEE Transactions on Biomedical Circuits and Systems*, 6, 3, June 2012, pp. 228-245.
- [17] C. Chen, T. Chu, C. Lin, and Z. Jou, "A Study of Loosely Coupled Coils for Wireless Power Transfer," *IEEE Transactions on Circuits and Systems II: Express Briefs*, 57, 7 July 2010, pp. 536-540.
- [18] K. E. Koh, T. C. Beh, T. Imara, and Y. Hori, "Multi-Receiver and Repeater Wireless Power Transfer via Magnetic Resonance Coupling – Impedance Matching and Power Division Utilizing Impedance Inverter," 15th International Conference on Electrical Machines and Systems (ICEMS), October 2012, pp. 1,6,21-24.
- [19] D. Liang, H. T. Hui, and T. S. Yeo, "A Phased Coil Array for Efficient Wireless Power Transmission," *IEEE International Symposium on Antennas and Propagation*, July 2012, pp. 1-2.
- [20] D. Huang, Y. Urzhumov, D. Smith, K. H. Teo, and J. Zhang, "Magnetic Superlens-Enhanced Inductive Coupling for Wireless Power Transfer," *Journal of Applied Physics*, 111, 6, March 2012, pp. 064902-8.
- [21] A. P. Sample, D. T. Meyer, and J. R. Smith, "Analysis, Experimental Results, and Range Adaptation of Magnetically Coupled Resonators for Wireless Power Transfer," *IEEE Transactions on Industrial Electronics*, 58, 2, February 2011, pp. 544-554.
- [22] J. Park, Y. Tak, Y. Kim, and S. Nam, "Investigation of Adaptive Matching by the Frequency Tracking Method for Near Field Wireless Power Transfer," *IEEE Transactions on Antennas and Propagation*, AP-59, 5, May 2011, pp. 1769-
- [23] Sazonov, Edward, and Michael R. Neuman, eds. *Wearable Sensors: Fundamentals, implementation and applications*. Elsevier, 2014.
- [24] <http://powerelectronics.com/alternative-energy>
- [25] Dixon, Juan, Luis Moran, Jose Rodriguez, and Ricardo Domke. "Reactive power compensation technologies: State-of-the-art review." *Proceedings of the IEEE* 93, no. 12 (2005): 2144-2164.
- [26] Cheon, Sanghoon, Yong-Hae Kim, Seung-Youl Kang, Myung Lae Lee, Jong-Moo Lee, and Taehyoung Zyung. "Circuit-model-based analysis of a wireless energy-transfer system via coupled magnetic resonances." *Industrial Electronics, IEEE Transactions on* 58, no. 7 (2011): 2906-2914.

Conclusion and Future Directions

- [27] Ahn, Dukju, and Songcheol Hong. "A study on magnetic field repeater in wireless power transfer." *Industrial Electronics, IEEE Transactions on* 60, no. 1 (2013): 360-371..
- [28] <http://powerelectronics.com/alternative-energy/witricity-demonstration-system-features-high-frequency-egan-fets>
- [29] <http://www.expertsmind.com/questions/classification-of-inductors-3016287.aspx>
- [30] <http://www.radio-electronics.com/info/data/inductors/inductor-types.php>
- [31] http://info.ee.surrey.ac.uk/Workshop/advice/coils/air_coils.html
- [32] <https://www.google.com/patents/US4441498>
- [33] <https://www.google.com/patents/US5541399>
- [34] Liu, Jia-Qi, Long Wang, Yu-Qian Pu, Joshua Lw Li, and Kai Kang. "A magnetically resonant coupling system for wireless power transmission." In *Antennas, Propagation & EM Theory (ISAPE), 2012 10th International Symposium on*, pp. 1205-1209. IEEE, 2012.
- [35] "AN2866 Application note," *ReVision*, no. January 2009, pp. 1–24.
- [36] C. W. Van Neste*, Richard Hull, Tinu Abraham, J.E. Hawk, Arindam Phani, Thomas Thundat." *Wireless Single Contact Power Delivery*", 978-1-4673-7447-7/15/©2015 IEEE.
- [37] Tianjia Sun, Xiang Xie, Guolin Li, Yingke Gu, Xiaomeng Li, Zhihua Wang." *A Wireless Energy Link for Endoscopy with End-Fire Helix Emitter and Load-Adaptive Power Converter*". ©2010 IEEE
- [38] Macnamara, Thereza, *Introduction to Antenna Placement and Installation*. USA: John Wiley and Sons. p. 145. ISBN 0-470-01981-6 (2010).
- [39] Gray, Paul R., Paul Hurst, Robert G. Meyer, and Stephen Lewis. *Analysis and design of analog integrated circuits*. Wiley, 2001.
- [40] Visintini, R. "Elettra Synchrotron Light Laboratory, Sincrotrone Trieste, Trieste, ITALIA."
- [41] Heljo, Petri, Kaisa E. Lilja, Himadri S. Majumdar, and Donald Lupo. "High rectifier output voltages with printed organic charge pump circuit." *Organic Electronics* 15, no. 1 (2014): 306-310.
- [42] Takhedmit, H., H. Kilani, L. Cirio, P. Basset, and O. Picon. "Design and experiments of a 2.4-GHz voltage multiplier for RF energy harvesting." *Proc. PowerMEMS* (2012): 448-51.
- [43] Takhedmit, H., L. Cirio, S. Bellal, D. Delcroix, and O. Picon. "Compact and efficient 2.45 GHz circularly polarised shorted ring-slot rectenna." *Electronics letters* 48, no. 5 (2012): 253-254.
- [44] Nintanavongsa, Prusayon, Ufuk Muncuk, David Richard Lewis, and Kaushik Roy Chowdhury. "Design optimization and implementation for RF energy harvesting circuits." *Emerging and Selected Topics in Circuits and Systems, IEEE Journal on* 2, no. 1 (2012): 24-33.
- [45] Park, Hyejin, Hwiwon Kang, Yonggil Lee, Yongsu Park, Jinsoo Noh, and Gyoujin Cho. "Fully roll-to-roll gravure printed rectenna on plastic foils for wireless power transmission at 13.56 MHz." *Nanotechnology* 23, no. 34 (2012): 344006.
- [46] Devi, Kavuri Kasi Annapurna, Norashidah Md Din, and Chandan Kumar Chakrabarty. "Optimization of the voltage doubler stages in an RF-DC convertor module for energy harvesting." (2012).
- [47] AVAGO Technologies, "Surface Mount RF Schottky Barrier Diodes," HSMS-282x datasheet, November 26, 2014.
- [48] Beck, Joseph M. "Using Rectifiers in Voltage Multiplier Circuits." *Application Note. Vishay Semiconductor* (2002).
- [49] Agilent Technologies, "Large-Signal S-Parameter Simulation," September, 2006.
- [50] Pozar, David M. *Microwave engineering*. John Wiley & Sons, 2009.
- [51] Barnett, Raymond E., Jin Liu, and Steve Lazar. "A RF to DC voltage conversion model for multi-stage rectifiers in UHF RFID transponders." *Solid-State Circuits, IEEE Journal of* 44, no. 2 (2009): 354-370.
- [52] U. Joe and M. Hgovanloo, "Design and optimization of printed spiral coils for efficient transcutaneous inductive power transmission," *IEEE Trans Biomed. Circuits Syst.*, vol. 1, no. 3, pp. 193–202, Sep. 2007.
- [53] X. Liu and S. Y. R. Hui, "An analysis of a double-layer electromagnetic shield for a universal contactless battery charging platform," in *Proc. 36th IEEE Power Electron. Spec. Conf.*, Jun. 16, 2005, pp. 1767–1772.
- [54] Z. N. Low, R. A. Chinga, R. Tseng, and J. Lin, "Design and test of a highpower high-efficiency loosely coupled planar wireless power transfer system," *IEEE Trans. Ind. Electron.*, vol. 56, no. 5, pp. 1801–1812, May 2009.
- [55] D. Ahn and S. Hong, "A transmitter or a receiver consisting of two strongly coupled resonators for enhanced resonant coupling in wireless power transfer," *IEEE Trans. Ind. Electron.*, vol. 61, no. 3, pp. 1193–1203, Mar. 2014.
- [56] L. Chen, S. Liu, Y. Zhou, and T. Cui, "An optimizable circuit structure for high-efficiency wireless power transfer," *IEEE Trans. Ind. Electron.*, vol. 60, no. 1, pp. 339–349, Jan. 2013.

- [57] D. Ahn and S. Hong, "A study on magnetic field repeater in wireless power transfer," *IEEE Trans. Ind. Electron.*, vol. 60, no. 1, pp. 360–371, Jan. 2013.
- [58] T. Beh, M. Kato, T. Imura, S. Oh, and Y. Hori, "Automated impedance matching system for robust wireless power transfer via magnetic resonance coupling," *IEEE Trans. Ind. Electron.*, vol. 60, no. 9, pp. 3689–3698, Sep. 2013.
- [59] Y. Lim, H. Tang, S. Lim, and J. Park, "An adaptive impedance-matching network based on a novel capacitor matrix for wireless power transfer," *IEEE Trans. Power Electron.*, vol. 29, no. 8, pp. 4403–4413, Aug. 2014.
- [60] Han, Junghoon, Young Kim, and Noh-Hoon Myung. "Efficient performance optimisation of wireless power transmission using genetic algorithm." *Electronics Letters* 50, no. 6 (2014): 462-464.
- [61] Mehri, Sondos, J. Ben Hadj Slama, Ahmed C. Ammari, and Hatem Rmili. "Genetic algorithm based geometry optimization of inductively coupled printed spiral coils for remote powering of electronic implantable devices." In *Computer & Information Technology (GSCIT), 2014 Global Summit on*, pp. 1-6. IEEE, 2014.
- [62] Versloot, Thijs Willem, Duncan James Barker, and Xurxo Otero One. "Optimization of Near-Field Wireless Power Transfer Using Evolutionary Strategies."
- [63] Fogel, David B. "An introduction to genetic algorithms: Melanie Mitchell. MIT Press, Cambridge MA, 1996. \$30.00 (cloth), 270 pp." (1997): 199-204.
- [64] Syswerda, Gilbert. "Uniform crossover in genetic algorithms." (1989): 2-9.
- [65] De Jong, Kenneth A., and William M. Spears. "A formal analysis of the role of multi-point crossover in genetic algorithms." *Annals of mathematics and Artificial intelligence* 5, no. 1 (1992): 1-26.